The Engineering and Development of pH-Responsive Biopolymers for Drug Delivery Applications

Alexander Chen

Trinity Hall College

Supervisor
Prof. Nigel Slater

A dissertation submitted for the degree of Doctor of Philosophy at the University of Cambridge

December 2018

Declaration

This thesis is the result of my own work and includes nothing which is the outcome of work done in collaboration except as declared in the Preface and specified in the text. It is not substantially the same as any that I have submitted, or, is being concurrently submitted for a degree or diploma or other qualification at the University of Cambridge or any other University or similar institution except as declared in the Preface and specified in the text. I further state that no substantial part of my thesis has already been submitted, or, is being concurrently submitted for any such degree, diploma or other qualification at the University of Cambridge or any other University or similar institution except as declared in the Preface and specified in the text. It does not exceed the prescribed word limit for the relevant Degree Committee

PREFACE

This thesis is submitted for the degree of Doctor of Philosophy at the University of Cambridge. The research reported herein was carried out under the supervision of Professor Nigel Slater at the Department of Chemical Engineering and Biotechnology between October 2014 and October 2018.

This thesis contains 70 figures, 11 Tables, and 48,025 words in total including appendices, tables, figure captions and references.

Some of the work in the thesis has been published in the following papers:

- Chen, A., Mercado, S.A., and N. K. H. Slater. "Antioxidant modified amphiphilic polymer improves intracellular cryoprotectant delivery and alleviates oxidative stress in HeLa cells." Advanced Material Science Vol 2: 1-7. doi: 10.15761/AMS.1000131

- Mercado, S. A., Orellana-Tavra, C., Chen A., and N. K. H. Slater. "The intracellular fate of an amphipathic pH-responsive polymer: key characteristics towards drug delivery." Materials Science and Engineering C 69 (2016): 1051-1057.

SUMMARY of dissertation by Alexander Chen entitled: The Engineering and Development of pH-Responsive Biopolymers for Drug Delivery Applications

This dissertation describes experimental studies to understand the structure of biocompatible pH responsive polymers and their interaction with the biological system in order to design more effective entities for biomedical applications. A systemic approach was used to study the structure and biological interaction of pH responsive biocompatible poly (L-lysine iso-phthalamide) (PLP) polymer and its derivatives.

Poly (L-lysine isophalamide) is a unique polymer that contains pendant carboxylate group and modification with phenylalanine was able to enhance the intracellular delivery efficiency of the polymer. However, the exact structure and mechanism of action remains mostly unknown. In this study, a variety of modifiers was used to synthesise new PLP derivatives in order to elucidate their effect on the polymer structure and other functional characteristics. New characterisation methods including circular dichroism and small angle neutron scattering were introduced to provide more detailed information on the polymer structure and evidence to explain the polymer-membrane interaction. It was determined that PLP adopted a helical structure in solution and that the ability of the PLP- derivative to from a lamellar structure in solution would lead to enhanced intracellular delivery effectiveness.

Chirality of the PLP components and modifiers were also examined. Three PLP enantiomers and four phenylalanine modified PLP were synthesised and characterised. The polymers were determined to be chemically identical and had comparable functionalities. However, it was proven again that the ability for polymer to form lamellar structure would result in enhanced intracellular delivery efficiency. The structural and functional information was later used to better design a drug delivery system for the cryopreservation of mammalian cells. The approach was successful, as the resulting vitamin E modified polymer was able to achieve similar cryosurvival rate with trehalose as cryoprotectant compared the gold standard DMSO protocol. The success marked the importance of application-specific design and understanding of drug delivery systems.

Acknowledgements

I would like to express my sincere gratitude to my supervisor and mentor Prof Nigel Slater for his constant support, guidance, and inspiration throughout my PhD.

Past and present members of the Bioscience and Engineering group and the Department of Chemical Engineering had contributed greatly to my studies and research. I would like to thank Krish, JJ, Amanda, Ning, Tian, Christian, Claudia, Sam, Michelle, Andy, Maggie, all the technical staff members, and all the administration staff members of the department for their support. I am especially grateful to have met three amazing friends, Arthur, Radu, and Sergio during my PhD.

I would like to acknowledge my funding body the European Commission (through the Marie Skłodowska-Curie Actions), for the financial support and providing an interdisciplinary academic network. Special thanks to Dr. Ian Tucker who was part of the network and provided me with the opportunity to conduct SANS experiments and guided me throughout the process.

My studies would not have been possible without the love and support of my friends and family. I would like to thank my parents Sue-Ching and Dung-Sheng for always having faith in me and providing me unconditional support throughout my life. There are truly no words to describe how grateful and proud I am to be their son. I would like to thank my brother, Benjamin, for his understanding and keeping our parents accompanied for the past 11 years since I left home. Additionally, I would like to thank my in-laws, Polen and Caroline for raising an amazing daughter and embracing me as part of their family.

Finally, I would like to thank my wife, Ava, for accompanying me through all the good and the bad times I had during our time in Cambridge. “Thank you, my love, for your devotion, understanding, and all the adventures we had and will have together.”

TABLE OF CONTENTS

List of Abbreviations

AAV	Adeno-Associated Virus
AFM	Atomic Force Microscopy
AMP	Antimicrobial Peptides
ANOVA	Analysis of Variance
ATR-FTIR	Attenuated Total Reflectance Fourier Transform Infrared Spectroscopy
C9	Complement Component 9
CD	Circular Dichroism
CME	Clathrin-Mediated Endocytosis
CPP	Cell Penetrating Peptides
CRA	Cryoprotective Agent
Da	Dalton
DCC	N,N'-Dicyclohexylcarbodiimide
DCHF-DA	2',7'- dichlorofluorescin diacetate
DDS	Drug Delivery System
DLS	Dynamic Light Scattering
DMAP	4-Dimethylaminopyridine
DMF	N,N-Dimethylformamide
DMSO	Dimethyl Sulfoxide
DOPC	1,2-Di(cis-9-octadecenoyl)-Sn-Glycero-3-Phosphocholine
E. coli	Escherichia coli
EDC	N-(3-Dimethylaminopropyl)-N'-Ethylcarbodiimide Hydrochloride
EDTA	Ethylene diamine tetraacetic acid
EMA	European Medicines Agency
ER	Endoplasmic Reticulum
FBS	Fetal Bovine Serum
FDA	Food and Drug Administration
FITC	Fluorescein Isothiocyanate
FTIR	Fourier-Transform Infrared Spectroscopy
GPC	Gel Permeation Chromatography
GPCR	G-protein Coupled Receptors
GPI	Glycosylphosphatidylinositol
GUV	Giant Unilamellar Vesicles
HA	Hemagglutinin
HAP	Hydroxyapatite
HeLa	Human Immortal Cell Line Derived from Cervical Cancer
HPMA	N-(2-hydroxypropyl) Methacrylamide
kb	kilobase
kDa	Kilodalton
LDH	Lactate Dehydrogenase
MALDI-TOF	Matrix-Assisted Laser Desorption/Ionization Time-of-Flight Mass Spectroscopy
Mn	Number Average Molecular Weight

MRE	Mean Residual Ellipticities
MW	Molecular Weight
Mw	Weight Average Molecular Weight
NHL	Non-Hodgkin's Lymphoma
NMP	N-Methyl-2-Pyrrolidone
NMR	Nuclear Magnetic Resonance
NS	Not Significant
PB	Phosphate Buffer
PBS	Phosphate Buffer Saline
PEG	Polyehtylene Glycol
PEI	Polyethyleneimine
Pen	Penicillin
PF-50	Phenylalanine Modified Poly (L-Lysine Iso-Fumaride)
PFP	Pore-Forming Protein
PG-50	Glycine Modified Poly (L-Lysine Iso-Phthalamide)
PI	Propidium Iodide
PLF	Poly (L-Lysine Fumaride)
PLP	Poly (L-Lysine Iso-Phthalamide)
PLP	Poly (L-Lysine Iso-Phthalamide)
PLP-D	Poly (D-Lysine Iso-Phthalamide)
PLP-L	Poly (L-Lysine Iso-Phthalamide)
PLP-L-D	Poly (L-Lysine and D-Lysine Iso-Phthalamide)
PP-50	Phenylalanine Modified Poly (L-Lysine Iso-Phthalamide)
PP-50-D-D	D-Phenylalanine Modified Poly (D-Lysine Iso-Phthalamide)
PP-50-D-L	D-Phenylalanine Modified Poly (L-Lysine Iso-Phthalamide)
PP-50-L-D	L-Phenylalanine Modified Poly (D-Lysine Iso-Phthalamide)
PP-50-L-L	L-Phenylalanine Modified Poly (L-Lysine Iso-Phthalamide)
PS	Polystyrene
PVA	Polyvinyl Alcohol
PVitE-25	Vitamin E modified Poly (L-Lysine Iso-Phthalamide)
ROS	Reactive Oxygen Species
SA	Sialic Acid
SANS	Small Angle Neutron Scattering
SAP	Sweet Arrow Peptide
SEC	Size Exclusion Chromatography
siRNA	Small Interfering RNA
SLD	Scattering Length Density
Strep	Streptavidin
Sulfo-NHS	N-Hydroxysulfosuccinimide
TFA	Trifluoroacetic Acid
UV	Ultraviolet

List of Figures

List of Tables

Chapter 1 LITERATURE REVIEW AND RESEARCH AIMS

1.1 Introduction

This section explores the motivation of using pH-responsive biocompatible poly (*L*-lysine *iso*-phthalamide)-based polymers as a delivery platform for therapeutic agents. The chapter begins with an overview of biocompatible polymers and how they advanced the field of medicine. Followed by background on pathophysiology of cells and transportation machineries that interact with polymers. Subsequently, a summary of poly (*L*-lysine *iso*-phthalamide)-based polymers and their successful applications. The section concludes with a brief description of the specific aims of this report and the outline of the thesis.

1.2 Overview of Synthetic Materials in Biomedical Applications

1.2.1 Synthetic Materials for Biomedical Application

The field of medicine had been extremely successful in drug development and controlling diseases in the past century. These developments partially contributed to the increase of approximately 30 years in life expectancy in western Europe, the US, Canada, and New Zealand (Christensen *et al.*, 2009). However, the need for more efficient and effective treatments is ever-expanding, especially with the rapidly increasing world population with prolonged lifespans (Christensen *et al.*, 2009). New materials and disciplines have been created to satisfy these needs in forms such as drug delivery system (DDS) and biocompatible scaffolds for regenerative medicine as the field of polymer chemistry continued to advance throughout the past decade (Wilczewska *et al.*, 2012; Mura, Nicolas and Couvreur, 2013). Biopolymer-based drug delivery systems developed in the later 1990's alone, were responsible for over $10 billion of annual sales (Langer, 1998). Which did not even account for the rising demand in synthetic replacement for biological tissues, smart medicine and advance diagnostics.

Biocompatible polymers are macromolecules that, when in contact with the biological system, do not elicit adverse effects such as immune or necrotic responses. These materials can be either naturally occurring or artificial. Artificial polymers are more structurally diverse and versatile compared to their naturally occurring counterparts (Duncan, 2003). Early synthetic polymers were commonly taken from areas of science and technology outside of medicine. The lack of understanding for the pathophysiology of the biological system when exposed to these materials created inherent problems such as polyetherurethanes used in artificial hearts causing thrombogenesis or polysaccharide such as arginate causing inflammatory responses (Bernacca and Wheatley, 1998; Langer and Tirrell, 2004; Jones, 2008). Therefore, for synthetic materials to achieve their full potential in medical applications, the biological parameters similar to the effectiveness should be integrated in the initial design. The applications and development of biocompatible polymers will be further discussed in the following sections.

1.2.2 Selected Biomedical Applications of Biopolymers

Biopolymers were the basis of a wide range of biomedical applications including drug delivery, polymer therapeutics, diagnostics and regenerative medicine (Langer and Tirrell, 2004). The main focus of this review will be on drug delivery and polymer therapeutics due to the scope of this thesis.

Polymers can be used as an active delivery vehicle or an inert linker between active therapeutics and targeting agents depending on their functionality. In many cases, polymers were incorporated to favorably modify the solubility, systemic toxicity, pharmacokinetics, and promote targeted delivery (Duncan, 2003; Swierczewska, Lee and Lee, 2015). For example, polyethylene glycol (PEG) is one of the most commonly used polymers to increase protein solubility, prolong plasma half-life and reduce immunogenicity (Delgado, Francis and Fisher, 1992; Lee, Na and Bae, 2005; Swierczewska, Lee and Lee, 2015). PEGylation has become the most established half-life extension technology with over 20 PEGylated therapies approved for different medical indications in the US and Europe (Swierczewska, Lee and Lee, 2015).

Another well-established polymer that has been applied for biomedical use is N-(2-hydroxypropyl) methacrylamide (HPMA). The biodegradable polymer was first synthesised in 1973 and reported to be an effective modifier for insulin and chymotrypsin in 1977 (Johnson, Kopečková and Kopeček, 2009; Yang and Kopeček, 2017). The polymer was later conjugated to doxorubicin and further modified to produce a series of derivatives. The strategy was proven advantageous as it increased the maximum tolerated dose of doxorubicin (expressed in drug equivalent) (Lee, Na and Bae, 2005; Kopeček, 2013; Wu *et al.*, 2017). Additional modifications of the polymer-drug conjugate were made by incorporating short peptide targeting sequences or antibodies to construct target specific therapeutics (Shiah *et al.*, 2001; Lu *et al.*, 2003). HPMA-drug conjugate demonstrated anti-cancer activity *in vivo* and reached clinical development with a second generation of these constructs in development (Yang and Kopeček, 2017).

In addition to using polymer as a carrier for traditional therapeutics, drug-free macromolecular therapeutic applications of biopolymer conjugates are becoming an emerging field. Johnson *et al.* designed a HPMA co-polymer with fragments of anti-CD20 antibody that crosslinked CD20 receptors to induce receptor clustering effect in B cells (Johnson, Kopečková and Kopeček, 2009; Johnson, Kopečková and Kopeček, 2012). The construct was able to induce apoptosis in five different CD20-expressing cells and it was effective against human non-Hodgkin's lymphoma (NHL) Raji B cells (Chu, Yang and Kopeček, 2012). These cases demonstrated the promising future of biopolymers propelling the field of medicine as drug delivery systems and more significantly, novel therapeutics.

1.3 Cell Membrane Structure and Intracellular Delivery

The mammalian cell is the basic structure of a functional organism (Figure 1-1). The interior content of the cell is separated by the cell membrane which is a lipid bilayer incorporating various molecules and proteins. The phospholipids in the cell membrane create a hydrophobic barrier for hydrophilic molecules preventing most molecules from

freely diffusing through the membrane. Channels spanning across the cell membrane constitute of membrane proteins allow selected molecules to enter the cell regardless of their hydrophobicity. Additionally, cells have transportation mechanisms for macromolecules and membrane impermeable particles. Why these structures are important, how cells transport foreign molecules and how they interact with amphiphilic macromolecules will be discussed in this section (Tortora and Nielsen, 2012).

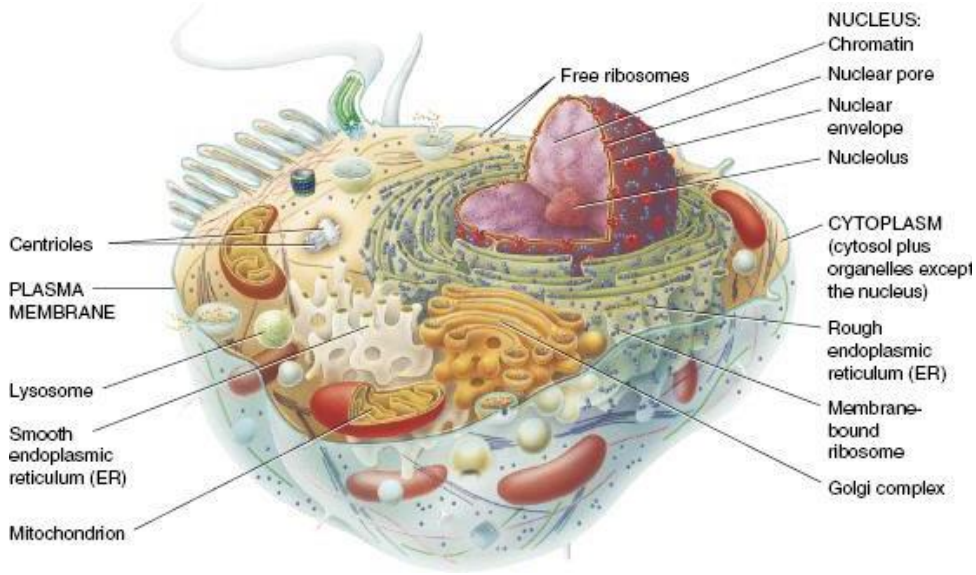

Figure 1-1: Illustration of cell structures and cytosolic organelles, reproduced from Tortora and Nielson, 2012.

1.3.1 Cell Membrane Structure

Phospholipids are molecules containing hydrophilic, commonly charged, head groups and hydrophobic fatty acid tails. These lipids self-assemble into an enclosed bilayer structure, where the hydrophobic groups were stacked towards each other, in physiological conditions, separating the exterior environment from the interior component (Figure 1-2). As mentioned in the previous section, the hydrophobic core of the bilayer

membrane structure prevents hydrophilic molecules from crossing. Larger molecules, such as proteins or nucleic acids, are also impermeable to the plasma membrane.

Typical plasma membranes are simple bilayer in nature, however, membranes in the biological systems are composed of hundreds of different phospholipids, polysaccharides, and membrane proteins (van Meer, Voelker and Feigenson, 2008; Sampaio *et al.*, 2011). In fact, 50% by weight of the membrane in a typical mammalian cell is consist of protein (Holthuis and Menon, 2014). The lipids are in a disordered liquid state which enables movement of membrane components, but the lateral mixing is highly non- uniform (Singer, S.J.; Nicolson, 1972; Spector and Yorek, 1985). The fluidity and non-homogeneous structure have important implications for many crucial cellular processes such as protein trafficking, membrane fusion, and signalling transduction (Helmreich, 2002; Holthuis and Menon, 2014).

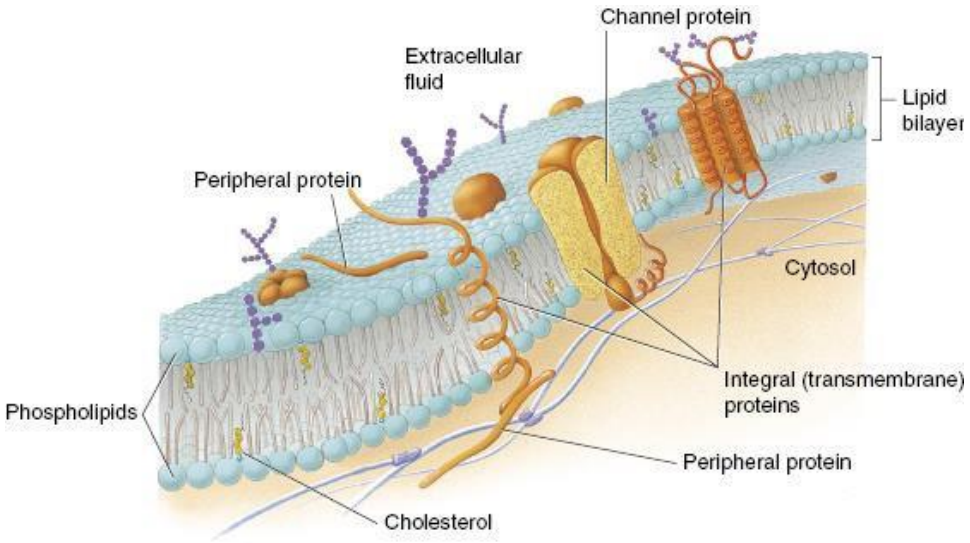

Figure 1-2: Illustration of cell membrane structure and membrane components, reproduced from Totora and Nielson, 2011.

In fact, certain lipids along with certain functional proteins to form ‘lipid rafts’ or ‘micro functional domains’ with increased cholesterol and sphingolipid concentration that are segregated from membrane (Pralle *et al.*, 2000; Allen, Halverson-Tamboli and Rasenick, 2007). Common proteins found on lipid rafts include

glycosylphosphatidylinositol (GPI)-anchored proteins, doubly acylated proteins, such as G-proteins, cholesterol-linked and palmitoylated proteins such as the Hedgehog signaling proteins, and transmembrane proteins (Brown and London, 1998; Hooper, 1999; Resh, 1999; Rietveld *et al.*, 1999). These proteins play major roles in cell signaling as they transmit information from the extracellular space such as hormones or cytokines and modify the cell behaviour. For example, histamine could act by binding to G-protein coupled receptors (GPCR) and induce cells to exhibit inflammatory responses. Other cell functions involving membrane proteins, specifically, transportation of foreign molecules into the cell and how the pathway affected the field of medicine will be discussed in the following section.

1.3.2 The Role of Intracellular Delivery

In nature, cells have mechanisms to transport molecules across the cell membrane to acquire essential nutrients and communicate across cells and organs. For example, glucose, the essential fuel for cells to produce energy and maintain cell function, could diffuse through sugar-specific membrane channels without being blocked by the cell membrane. For larger molecules or molecules without membrane channels, cells utilise a process called endocytosis, where cells internalise molecules from the extracellular environment. Endocytosis can be further categorised into four groups defined by the volume or membrane proteins involved (Figure 1-3).

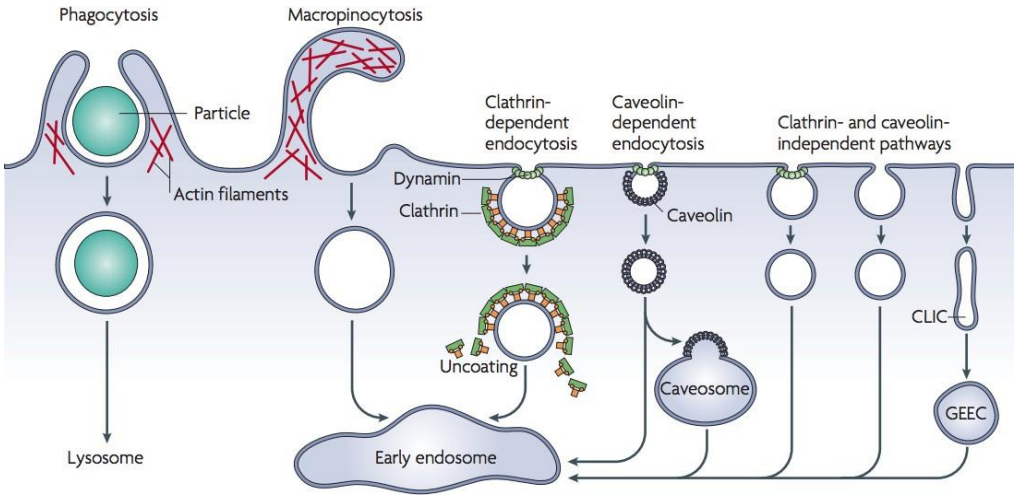

Figure 1-3: A schematic Illustration of different endocytosis pathways, reproduced from Mayor and Pagano, 2007.

The first category involves active engulfment of large unselected volumes. Some examples are phagocytosis and marcopinocytosis observed in macrophages, a type of mobile white blood cell, scavenging apoptotic cells and foreign pathogens (Swanson, 2008). The second type is clathrin-mediated endocytosis (CME), which utilises the triskelion-shaped scaffold clathrin protein to form transport vesicles. It is a selective process involving receptor-mediated recruitment of clathrin and formation of membrane-bound vesicles that detach from the cell membrane. This process is highly conservative across mammalian cell types and utilised to internalise many well-studied ligands such as transferrin (Mousavi *et al.*, 2004). The third type, caveolin- mediated endocytosis, depends on flask-shape caveolin-lipid membrane complexes namely caveolae. Caveolae, believed to be important in endocytosis and signal transduction, are typically 50-80 nm in diameter and are co-localised with high cholesterol, sphingolipid, and signalling protein membrane regions (Anderson, 1998). The fourth type is the general cell internalisation process of small molecules without the facilitation of either clathrin or caveolin (Mayor and Pagano, 2007).

The categorisations at times could be difficult to define as different types of endocytosis can be used to internalise the same ligand in different cells (Jones, Gumbleton and Duncan, 2003; Singh *et al.*, 2003; Damm *et al.*, 2005). Thus, it is crucial to determine the targeted cell type and recruit the correct internalisation motif for delivery systems that aim to utilise these native pathways (Varga *et al.*, 2005).

Additionally, the fate of each pathway can be relatively different. Endocytosis vesicles can be recycled back to the cell surface or further develop into late endosomes. The latter development will result in the acidification of the vesicle lumen and subsequently result in the fusion with lysosomes. The pH in the vesicle lumen of early endosomes and late endosomes are 7 to 6 and 6 to 5 respectively. The fusion of late endosome with lysosome will lead to further decrease the pH to below 5.5 along with the introduction of degradative enzymes (Mukherjee, Ghosh and Maxfield, 1997). This process is similar to the human digestive system, where larger molecules are broken down and absorbed while ensuring foreign agents are neutralised. How the understanding of these native internalisation pathways is relevant to intracellular delivery would be discussed in the following section.

1.3.2.1 Applications and Current Challenges in Intracellular Delivery

The interest for intracellular delivery was sparked by the discovery that cell physiology could be manipulated by synthetic nucleic acid sequences (Seeman, Cheng and Iles, 1973; Subbarao *et al.*, 1987; Timothy E. McKnight *et al.*, 2004; Villalobos *et al.*, 2006; Wang *et al.*, 2009). Transfection, which refers to the delivery of DNA or RNA into the cytosolic place, has nearly become synonymous with intracellular delivery in the past decade as is one of most studied and arguably the most important applications (Midoux and Monsigny, 1999; Han *et al.*, 2007; Martin and Rice, 2007; Yue *et al.*, 2011). Transfection was the core technology that enabled nucleic acid synthesis in bacteria, therapeutic protein production in immortalised cell lines, and selective inhibition/expression of proteins in cells for biomedical research. However, as previously discussed, macromolecules including nucleic acid were unable to cross the cell membrane intact. An array of techniques has been developed to transport molecules across the cell membrane. These techniques can generally be categorised into ones that utilise the previously discussed endocytosis pathways and other methods that do not involve endocytosis. The two types of intracellular delivery would be discussed in the following sections.

1.3.2.2 Endocytosis-Dependent Intracellular Delivery

As introduced in the earlier section, the uptake of molecules through membrane-bound vesicles is broadly defined as endocytosis (Christie and Grainger, 2003). It was discovered as early as 1974 that cells selectively internalised lysosomotropic agents through lysosomes and this transportation mechanisms could be utilised as a solution to overcome the cell membrane barrier (de Duve, 1974). Viruses and bacteria which replicate within cells are perhaps the first entities to exploit the endocytosis pathway to introduce pathogenic materials into the intracellular space. Influenza virus, an enveloped RNA virus, contains surface viral protein hemagglutinin (HA) which contains a terminal sialic acid (SA) binding site (Weis *et al.*, 1988). The virus initiates the infection process by attaching HA to cell surface receptors that contains terminal SA residues. Although these receptors are currently unknown, studies suggest that the binding of HA to these receptors trigger the endocytosis of the virion (Dou *et al.*, 2018). The endocytosis can either occur through the clathrin-dependent process or micropinocytosis (Roy *et al.*, 2000; Rust *et al.*, 2004; Chen and Zhuang, 2008). After the virus is transported to the endosome where the pH decreases, HA will go through a large conformational change and expose a fusion peptide domain (White, Helenius and Gething, 1982). As the fusion peptide would enable the viral membrane to merge with the endosomal membrane which resulted in the release of viral genome (Figure 1-4). The entry and membrane fusion are rapid processes and could occur in approximately 10 minutes (Dou et al., 2017). The viral entry of endocytosis pathway became the inspiration and basis of many intracellular delivery systems in the past decade.

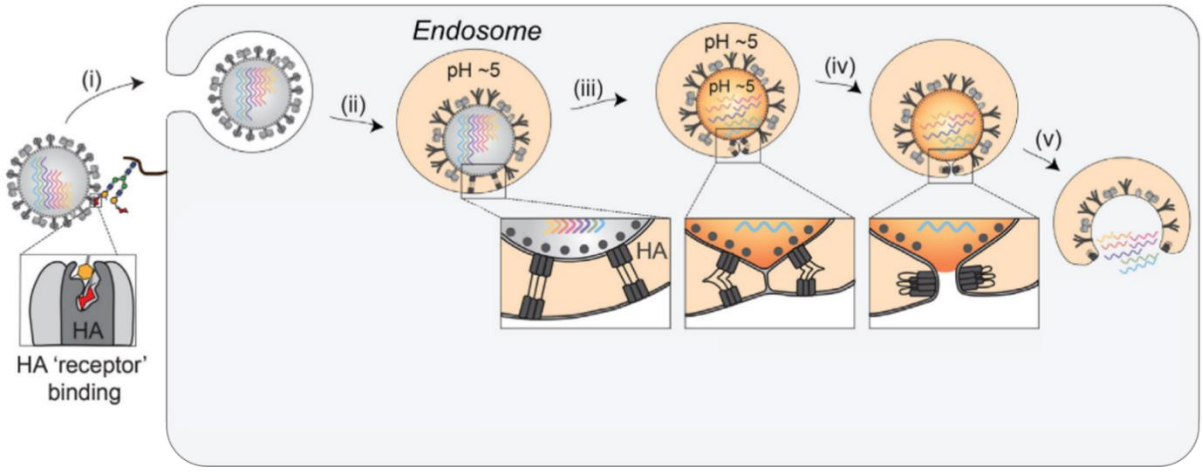

Figure 1-4: A schematic Illustration of influenza virus entry into mammalian cell through endocytosis and the HA protein performing pH-dependent membrane fusion activity, reproduced and modified from Dou *et al.*, 2018.

One obvious intracellular delivery system is modified viruses that carry nucleic acid encoding the desired protein constructs. For example, adeno-associated virus (AAV), a non-pathogenic small (~4.7 kb) single strand DNA virus, is a commonly used vector to deliver specially designed genome sequences for the generation of T-cell therapies (Mays and Wilson, 2011; Maeder and Gersbach, 2016). The viral vectors are still considered one of the most effective and efficient intracellular delivery systems.

Synthetic transfecting agent, such as polyethyleneimine (PEI), also mediates the delivery of DNA by utilising the endocytosis pathway. The polymer first forms complexes with DNA, internalised by cells into the endosome, and disrupts the lysosome through the "proton sponge effect" (Boussif *et al.*, 1995; Forrest and Pack, 2002). The amine groups on PEI have buffering effect in acidic endosomes and induce osmotic imbalance and passively rupture the membrane vesicle (Boussif *et al.*, 1995; Behr, 1997). This process enables the payload to be released from the lysosome into the cytosol.

The two above-mentioned examples demonstrated the importance of the endocytosis pathway as a route for intracellular delivery systems. Systems or techniques that are

independent of endocytosis were also well developed and contributed to the advancement of various advancement in the medical field. These developments would be discussed in the following section.

1.3.2.3 Endocytosis-Independent Intracellular Delivery

Intracellular delivery techniques that do not involve the endocytosis pathway generally target the cell membrane directly by causing holes, pores or defects to enable the passage of certain agents. These techniques could be physical or biochemical and can be categorised as membrane penetration or permeabilization (Stewart, Langer and Jensen, 2018).

Membrane penetration strategies use conduits or vehicles to puncture the cell membrane and create passages for the cargo. Techniques including microinjection, ballistic particles, and nanoneedles are common examples. Microinjection was the first method to be invented as a direct penetration intracellular strategy (Korzh and Strähle, 2002). This technique disrupts the cell membrane with a miniaturised pipette-like element, which subsequently injects the payload directly into cells in a controlled manner. It could, however, be limited by the size of the injection needle, the precision of the pump that ejects the payload, and number of experiments at a given time. Nanoneedles utilise a similar penetration principle except that they typically consist of finer fabricated structures for penetration and are more modifiable (Melechko *et al.*, 2003; Shalek *et al.*, 2010). The payloads are usually loaded on the nanoneedle structures and designed to be released after they came into contact with the cytosolic space. All these delivery techniques would cause puncture of the cell membrane and the target cells would require repair of the cell membrane and other cellular structures.

Membrane permeabilisation, on the other hand, makes the plasma membrane temporarily permeable to cargo present in the extracellular environment. The permeability of the membrane for the cargo would depend on the size and the duration of the transient

channels. Thus, depending on the property of the cargo, the permeabilisation strategy would have to be designed accordingly. The membrane disruptive events could be achieved physically or biochemically (Stewart, Langer and Jensen, 2018). Physical methods could range from mechanical, electrical, thermal, and laser-based. These techniques usually allow better control over the intensity and duration of membrane disruptive events (Hapala, 1997; Meacham *et al.*, 2014). However, these techniques would not be further discussed as it is out of the scope of this study.

Biochemical agents that could disrupt the cell membrane includes detergents, surfactants, organic solvents, peptides, and numerous proteins. As an example, detergents and organic solvents are commonly used to disrupt the cell membrane and extract certain lipophilic components (Karande *et al.*, 2005). Various peptides and proteins created by organisms ranging from bacteria to mammals has the ability to impact the membrane integrity. Pore-forming proteins (PFPs) including colicins produced by *E. coli* and the C9 protein of the human immune system are one example (Bischofberger, Iacovache and van der Goot, 2012). An array of membrane-active peptides has been known to be able to interact with and disrupt the plasma membrane (Sun, Forsman and Woodward, 2015). One type of membrane-active peptides is antimicrobial peptides (AMP), which are usually amphiphilic and cationic with the ability to induce pore formation at critical concentration (Zasloff, 2002; Brogden, 2005). Although only a small amount of the over 5,000 AMPs were studied for their mechanism of action, a universal feature of these peptides is the ability to adopt different conformations when it came into contact with lipid bilayers (Zasloff, 2002). More specifically, the peptides are able to form two distinctive peptide-lipid states. The peptide initially forms an inactive surface-bound state that adsorbs onto the lipid membrane outer surface and then rearranges into formation that supports stable pores across the lipid bilayer (Sengupta *et al.*, 2008). Of note that these peptides, such as melittin, often adopt α-helix secondary structure in their active state. Although there are currently many theories attempt to characterise the exact mechanism of how AMPs disrupt the cell membrane, the overall prerequisites for AMP-mediated formation appears to be a critical concentration of peptides in solution and the ability to aggregate in the lipid Layer (Sengupta *et al.*, 2008). The understanding of how AMP and related cell-

penetrating peptides could disrupt the plasma membrane forms the basis of intracellular delivery applications. One such synthetic polymer delivery system will be discussed in the following section.

1.4 pH-Responsive Polymers as a Drug Delivery System

Poly (L-lysine iso-phthalamide) was developed by Eccleston *et al.* in the late 1990's (Figure 1-5). Inspired by the influenza hemagglutinin protein, the polymer was designed to be biodegradable, easily synthesised and amphiphilic (Eccleston, Slater and Tighe, 1999). Eccleston synthesised a range of pH-responsive polymers with iso-phthalic acid and diamines of various carbon chain lengths to develop intracellular delivery systems *in vitro* (Eccleston *et al.*, 2000). After extensive experimentation, PLP was determined to be the most suitable polymer for intracellular delivery application.

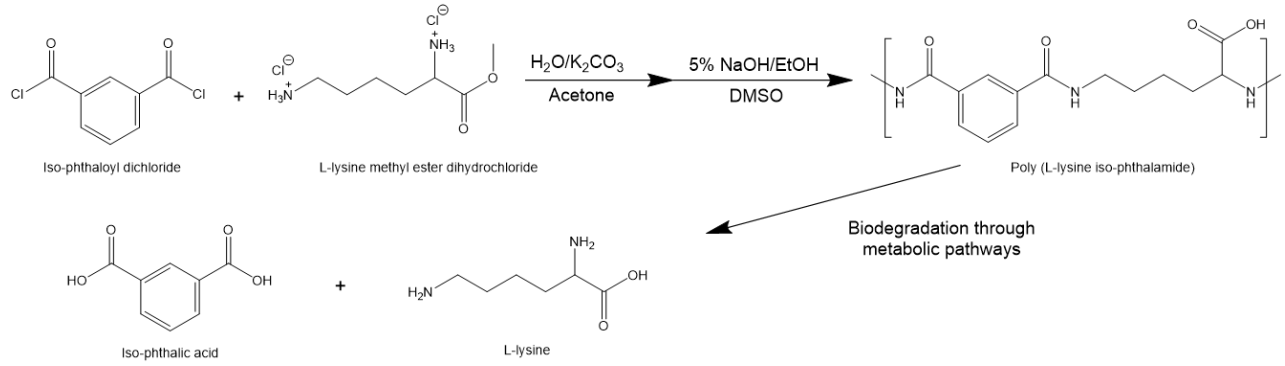

Figure 1-5: Illustration of reaction scheme for PLP synthesis and systemic metabolic breakdown. The chemical structure of PLP is shown on the upper right-hand corner. PLP can be broken down into biocompatible metabolic products L-lysine and iso-phthalic acid.

The linear polymer has a free carboxylic acid group in each subunit that can be ionised at physiological pH range. It is believed that while the carboxylic acid is at physiological

pH, it holds a negative charge which cause each subunit to be expanded. As the pH decreases, the polymer loses the negative charges and hydrophobic interaction between the subunits becomes the dominant force. Subsequently, PLP forms hydrophobic globular structures and aggregate in aqueous solution (Chen, 2007). To note, these were hypotheses from previous studies intended to explain the pH-responsive and polymer-membrane interaction of PLP. The pendant carboxylic acid groups are not only an important part of the pH responsive character of PLP. The reactive carboxylic acid groups are suitable for conjugation and modification. The modifier and amount of grafting can be easily controlled to produce various derivatives (Chen *et al.*, 2009; Khormaee *et al.*, 2010). How these modifications were achieved and how modifications affect PLP characteristics would be discussed in the following section.

1.4.1 Modification of PLP

Hydrophobic amino acids including L-valine, L-leucine, and L-phenylalanine were first used to modify the PLP property and successfully enhanced the intracellular delivery efficiency of membrane impermeable molecules in mammalian cells (Chen *et al.*, 2009). It was previously shown that incorporating L-phenylalanine at 75% molar ratio to carboxylic acid groups resulted in the most effective PLP-based intracellular delivery (Chen *et al.*, 2009). This result led to the belief that hydrophobicity of the modifying amino acid would determine the intracellular delivery efficiency of the resulting polymer.

However, the positive relationship of hydrophobicity of the modifying amino acid and delivery efficiency of the polymer came into question when Khormaee *et al.* compared L-phenylalanine grafted PLP to L-tyrosine grafted PLP and found the effectiveness of the two polymers are comparable. The overall hydrophobicity of phenylalanine and tyrosine are significantly different, but the study concluded that aromatic structure may be the key for the improved intracellular delivery efficiency of the modified PLP polymers (Khormaee *et al.*, 2010). Identifying the key factors that are crucial to enhance membrane interaction and disruption are important as the overall effectiveness and solubility of PLP-based polymers are heavily affected by the hydrophobic modifier.

Inspired by the idea of membrane affinity and polymer therapeutics proposed by Langer *et al.* that polymers could have dual function as a drug carrier and active agent, modifiers beyond amino acids were further explored in this study (Langer and Tirrell, 2004). Biologically active hydrophobic molecules such as cholesterol, sphingolipids and hydrophobic vitamins, were studied as potential hydrophobic modifiers in this study. These modifications may provide PLP with enhanced membrane interactive property, at the same time, biological function to improve the overall effectiveness of the polymer drug delivery system.

1.4.2 Biomedical Applications of PLP-based Polymers and Future Developments

The post-genomic era has enhanced our understanding in the pathophysiology of the biological system. Macromolecules such as antibodies and nucleotides are often applied as therapeutics. The target of a large portion of these drugs is within the cell, therefore, carriers enabling these therapeutics to access the intracellular component are of crucial importance. Small interfering RNA (siRNA) was discovered as an effective way to achieve protein knockout. However, the commonly used PEI and lipofectamine based delivery systems for nucleotide were immunogenic and toxic at higher doses. In a study, Khormaee *et al.* showed that PP-75 was biocompatible and a suitable delivery system for siRNAs. Stathmin siRNA-conjugated PP-75 was able to supress stathmin expression in U-251 human glioblastoma cell line *in vitro* at a comparable level to stathmin siRNA delivered by lipofectamine. Additionally, stathmin siRNA-conjugated PP-75 was able to suppress U-251a tumor growth *in vivo* by suppressing tumor stathmin level which subsequently reduced the tumor drug resistance towards chemotherapeutic treatment (Khormaee *et al.*, 2013). In addition to the delivery of nucleic acid, PP-75 was also proven to be a suitable and effective delivery system for the membrane impermeable trehalose, a naturally occurring cryoprotectant. Lynch et al. showed that co-incubation of PP-75 and trehalose in erythrocytes mediated the uptake and increased the intracellular concentration of trehalose to 123 ±16 mM. The increase in intracellular trehalose concentration would translate into approximately 20% higher erythorocyte cryosurvival (Lynch *et al.*, 2010).

The two examples proved that PLP-based polymers are effective intracellular drug delivery systems that are biocompatible and highly modifiable. As the PLP polymer is extremely versatile, further improvement and modifications could be made to enhance the delivery efficiency not only as a drug delivery system but also as a potential polymer therapeutics. How to increase the understanding of this polymer system and use the knowledge for a more intelligent design of the polymer would be explored in this thesis.

1.5 Research Aims

The aim of research conducted in this study was to investigate ways improve the intracellular delivery efficiency and effectiveness of pH-responsive polymers for the appropriate biological application. This was achieved by using various chemical modifications and synthesis of new pH responsive polymers to create a spectrum of similar polymers for comparison. The polymers were characterised by different techniques to determine the molecular composition, secondary structure,

1.5.1 Understand the structure of PLP-based polymers

1.5.2 Systemically study the effect of pendant group modifications on PLP

1.5.3 Use amino acids with different chirality in PLP polymer backbone or as a modifier to study polymer structure and biological activities

1.5.4 Explore other modifications and additional biomedical applications

1.5.5 Discover potential replacement materials

1.6 Thesis Outline

CHAPTER 1, LITERATURE REVIEW AND RESEARCH AIMS, explores the current landscape of functional polymers and intracellular delivery systems with specific focus on pH-responsive biocompatible polymers.

CHAPTER 3, SYNTHESIS AND CHARACTERISATION OF PLP-BASED POLYMERS, outlines the syntheses and development of pH responsive and biocompatible polymer, PLP. The chapter further discussed new techniques used to unveil additional structural and functional insights of PLP.

CHAPTER 3, THE EFFECTS OF CHIRALITY ON THE STRUCTURE AND FUNCTIONALITY OF PH-RESPONSIVE DELIVERY POLYMERS, describes how the chirality of the component for the syntheses of PLP-based polymers would affect the structure and functionality of the resulting polymer. Amino acids of different chirality were used to synthesis an array of PLP-based polymers and characterised by physical and biological assays.

CHAPTER 4, THE SYNTHESES AND CHARATERISATION OF SECOND GENERATION PLP-LIKE POLYMERS, discusses whether using a different di-acid could result in a more biocompatible polymer while retaining the intracellular delivery capability of PLP. The chapter further explores whether modification with hydrophobic amino acids could successfully enhance the second-generation pH-responsive polymer.

CHAPTER 5, SYNTHESIS AND CRYOPRESERVATION APPLICATION OF AN ANTIOXIDANT GRAFTED PLP, describes a new application-specific design using functional modifier to increase PLP delivery efficiency and introduce anti-oxidative function. The chapter outlines the rationale for the design of the polymer for cryopreservation and how it ultimately improved the survival of cells undergone cryopreservation.

CHAPTER 6, CONCLUSION AND FUTURE WORKS, presents the main finding of this work and outlines future studies that could lead to the further improvement of PLP as a drug delivery system.

Chapter 2 SYNTHESIS AND CHARACTERISATION OF PLP-BASED POLYMERS

2.1 Introduction

2.1.1 Development of poly (L-lysine iso-phthalamide)

Poly (L-lysine *iso*-phthalamide) (PLP), an amphiphilic polyamide with hydrophobic groups and pendant hydrophobic carboxylate groups, was first synthesised and characterised by Eccleston *et al.* as an intracellular delivery system (Eccleston *et al.*, 2000). The development of PLP was inspired by the viral fusogenic peptide hemagglutinin (HA) that has membrane disruptive activity below physiological pH. It was previously suggested that PLP is membrane neutral at physiological pH and undergoes a conformation change once the carboxylate groups are protonated (Figure 2-1). The membrane lytic activity of PLP was measured by release of hemoglobin from red blood cells which was determined to lyse 20% of red blood cells at pH 4.5 (Eccleston *et al.*, 2000). It was thought that the PLP polymer could facilitate the endosomal escape through enhanced membrane interaction and the proton sponge effect, where the positively charged protons absorbed onto the amine group of polymer result in osmic imbalance and eventual rupture of the endosomes, at a slightly acidic endosome environment in HeLa cells due to the formation of hydrophobic micro-domains and the carboxylate groups of the polymer (Chen *et al.*, 2009) .

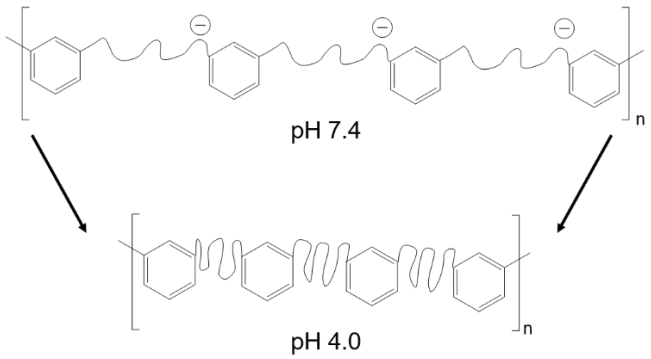

Figure 2-1: Conformational change of poly (L-lysine iso-phthalamide) in solution at pH 7.4 and pH 4.0. Simplified cartoon to depict PLP and negative charges arose from the carboxylate pendant group on the polymer at pH 7.4.

PLP was initially assumed to be a flexible random coil in solution at pH 7.4, similar to typical polymer such as polystyrene (PS) in solution. The carboxylate group on the side chain generates ionic repulsion between the negatively charged groups making it an extended structure. As the pH decreases, the carboxylate groups are protonated and the ionic repulsion weakens so the polymer can adopt a more compact globular structure driven by hydrophobic association of the benzene rings on the polymer backbone (Chen, 2007; Khormaee, 2009). It was suggested that the globular form of PLP at low pH is membrane active and constitutes part of the membrane disruptive activity like the helical HA protein which adopts a more compact structure when protonated to facilitate membrane fusion. Additionally, the “proton sponge effect” was proposed to be the second mechanism for PLP to cause membrane disruptive activity. The proton sponge effect was first proposed by Behr *et al.* in 1997, where macromolecules with proton receiving functional groups can buffer the hydrogen ions pumped into the endosome and lead to transportation of additional protons and ions causing an osmotic imbalance of the endosome causing it to break (Behr, 1997; Benjaminsen *et al.*, 2013). Both mechanisms were thought to be an important way PLP could escape the endosomal pathway.

Despite PLP having membrane lytic activities and intracellular delivery capabilities, two main issues prevented PLP from becoming an efficient drug delivery system. First, the pH at which PLP is membrane active is considerably lower than the physiological pH of

7.4. The pK_a of PLP occurs in the pH range of 4.5 to 5 and such values of pH only occur in the biological system in the late endosomal pathway. Any therapeutic material could be digested or destroyed that late into the endosomal process. Second, the hemolysis assay showed that the membrane disruption ability of PLP is weaker than natural occurring cell penetrating peptides (CPPs) (Eccleston *et al.*, 2000).

How different chemical modifications of PLP affect membrane disruption has been studied, however, direct evidence of the structure different pH environments and the exact delivery mechanism is yet to be unveiled. More extensive studies would enhance clarity on what factors would contribute to increasing the delivery efficiency and could further improve the effectiveness of this economical and biocompatible poly-anion drug delivery system.

2.1.2 PLP Sidechain Modification

Chen *et al.* first discovered that by grafting hydrophobic amino acids to the pendant carboxylate of PLP at different molar ratios through N,N'-Dicyclohexylcarbodiimide (DCC)-mediated amide formation, the polymer membrane disruptive activity could be significantly enhanced while raising the transition pH of the polymer (Chen, 2007). The amino acids used include valine (Val), leucine (Leu), and phenylalanine (Phe) to generate PV, PL and PP polymers respectively. It was initially thought that hydrophobicity of the polymer modifying amino acids was the sole factor for the improved delivery efficiency until Khormaee *et al*. reported that modification with an aromatic amino acid tyrosine (Tyr), an amino acid less hydrophobic than Phe, increased the intracellular delivery efficiency of PLP to a similar level to the Phe modification. Her paper suggested that the aromatic structure of the modifier was also an important factor that affects the overall polymer delivery efficiency (Khormaee *et al.*, 2010). Various cell penetrating peptides have increased effectiveness after adding amino acids containing aromatic side chains such as tryptophan (Nakano and Okamoto, 2001). Aromatic amino acids are also commonly observed in transmembrane proteins such as G-protein coupled receptors (GPCR) that play crucial roles in physiological response like

muscle movement or mood regulation (Kroeze, Sheffler and Roth, 2003). These findings indicated that multiple characteristics of how the modifier affects the overall membrane interactive and disruptive activity of PLP-derivatives. Thus, it is important to systematically identify the influence of modifiers to improve the overall effectiveness of PLP-based polymers. Additional amino acids were used to modify PLP and the resulting polymers were compared to PLP and Phenylalanine modified PLP.

2.1.3 Polymer Characterisation Methods

PLP-based polymers were previously characterised by standard physical methods including NMR, FTIR, GPC, and dynamic light scattering (DLS) (Chen, 2007). The results provided convincing evidence of the primary chemical structure of the polymer and the chemical modifications. Additionally, the transition pHs of polymers were characterised using UV spectroscopy and previously with pyrene-based assay at a range of pHs with phosphate and citrate buffers. The results indicated that the precipitation of PLP-based polymers at below physiological pH, or transition pH, is correlated with the formation of hydrophobic micro- domains and membrane disruptive activity. The intracellular delivery characteristic of the polymers was further evaluated by quantifying membrane impermeable fluorophore calcein in mammalian cells after incubation. It was determined that the closer the transition pH is to the endosomal pH of 5.5, the higher the intracellular delivery efficiency in the calcein delivery assay. However, the overall conformational change and the mechanism of membrane disruption is yet to be fully elucidated.

Attempts were made to capture the transition of the polymer using characterisation techniques such as DLS or atomic force microscopy (AFM). The challenge lies in the resolution and the experimental condition of methods such as DLS and AFM. DLS was commonly accepted as a good method to characterise polymer molecules in solution. However, it provides information on the theoretical hydrodynamic diameter of the molecule assuming it is globular. Additionally, the resolution is limited to around the 10

nm range. AFM on the other hand, provides a higher resolution, but a more complicated setup and lengthy data collection process. Only liquid AFM could provide information of polymers in solution. It will however, require a flat surface such as mica to deposit the sample, and a liquid chamber for polymer solution. With the advancement in characterisation methods, more detailed structural information could be obtained to further study of the PLP-based polymers. This includes secondary structures through characterising the optical activity of polymers by polarised light source and high-resolution structural data in solution using small angle neutron scattering (SANS).

Circular dichroism (CD) is the difference between the absorbance of left- and right-handed circular polarised light and can more broadly refer to the spectroscopy of recording this difference (Langeveld-Voss *et al.*, 1996). This method was commonly used to characterise natural and synthetic macromolecules that are optically active. Proteins and polypeptides, for example, are often determined through CD spectra by comparing the result with semi-empirical models to predict secondary structures such as α helices or β sheets. The most abundant optically active functional groups are amide bonds that generate CD signal in the far UV region. These signals are often affected by the secondary structure and, thus used to identify unique peptide formations. Other optically active groups including aromatic rings on the amino acid side chains with CD spectra in the near UV region. Since structurally, PLP is also a polyamide containing aromatic groups, CD could be applied to extract information on the overall orientation of optical active amide groups and aromatic group to gather information on the overall structure.

Synthetic helical polymers were commonly characterized by CD to confirm their helical orientation after the 1950s. For example, optically active helical poly(phenylacetylene) bearing an L-alanine (L-Ala) residue with a long n-decyl chain as pendants was determined to adopt a helical structure by AFM while the sense of the helix formed by the polymer was determined by CD (Yashima *et al.*, 2009). This method, however, has limitations on projecting the exact structure as models are mostly established semi-empirically and without a comprehensive data base for synthetic polymers it is nearly impossible to predict the secondary structure with this method (Langeveld-Voss *et al.*,

1996; Pasternack, 2003). Complementary methods such as X-ray diffraction are commonly used in parallel with CD to confirm the molecular structure for polymers with a defined crystal structure. In this study, CD was used to characterise PLP and its derivatives at different pHs in the presence or absence of lipid vesicles to study the polymer structure. X-ray diffraction data of PLP and its derivatives, however, could not be obtained with the experimental setup due to insufficient contrast.

Another powerful technique to characterise macromolecular structures is SANS which utilises the neutron scattering pattern after penetration of the tested sample. The technique is able to probe the 3D structure of a material from 1 nm up to a few hundred nm and describe the object in detail. Typical quantifiable data that can be extracted from SANS could include shape, volume, gyration radius, mass, and fractal dimension. Additionally, how objects in the sample are organised within the media and interact between them could also be studied by SANS. The scattering data recorded from the technique is a 2-dimensional plot with intensity in the y-axis and scattering vector (q) in the x-axis. Intensity is measured as the differential scattering cross section per unit volume while the scattering vector could be mathematically calculated as $4\pi\theta/\lambda$. The scattering angle (θ) is recorded during the experiment while the wavelength (λ) of the neutron beam, which is considered as a planar monochromatic wave, is selected for the experiment (Cousin, 2015). To summarise, the recorded scattering pattern could be used to calculate the macro- and micro-structures of the sample at high precision and resolution (Hammouda, 1995; Mondal Roy and Sarkar, 2011). Due to its non-destructive nature and rapid data collection, the method was able to provide high quality structural data of macromolecules in solutions and change in structure in different environments. In this study, various polymers at different pHs were tested to generate crucial information for unveiling the structure of PLP and PLP-based polymers at different pH environments for the first time.

In this chapter, new and existing PLP-based polymers were synthesised to study their overall structure, characteristics, and functionalities. CD and SANS were applied for the first time to characterise PLP and its derivatives at different pHs to supplement existing characterisation methods for portraying a more comprehensive picture of the polymer

structure and membrane interactive activity. The additional information would provide a more detailed structural and mechanistic understanding of the polymer and assist the improvement of PLP-based polymer or even more broadly, anionic polymers as a drug delivery agent.

2.2 Materials and Methods

2.2.1 Materials

Iso-phthaloyl chloride, potassium carbonate, N,N'-dicyclohexylcarbodiimide (DCC), concentrated hydrochloric acid, 4-dimethylaminopyridine (DMAP), N,N-dimethylformamide (DMF), L-tryptophan methyl ester dihydrochloride, glycine methyl ester hydrochloride, potassium hydroxide, di-tert-butyl dicarbonate, sodium borohydride, N-hydroxysulfosuccinimide (Sulfo-NHS), N-(3-dimethylaminopropyl)-N'-ethylcarbodiimide hydrochloride (EDC), sodium phosphate dibasic, sodium phosphate monobasic, phosphoric acid, deuterium hydroxide, dipotassium deuterium phosphate, potassium di-deuterium phosphate, phosphoric acid-d_3 solution, acetone, methanol, dichloromethane, ethylene diamine, trifluoroacetic acid (TFA), chloroform, ethyl alcohol, diethyl ether, triethylamine, and trypan blue stain (4%) were purchased from Sigma-Aldrich, Gillingham, UK. L-lysine methyl ester dihydrochloride was obtained from Acros. L-phenylalanine methyl ester hydrochloride was purchased from Alfa Aesar, Heysham, UK. Sodium hydroxide, sodium carbonate and DMSO were purchased from Fisher Scientific, Loughborough, UK. Dulbecco phosphate-buffered saline was purchased from Life Technologies, Paisley, UK. Florisil Mesh was purchased from Material Harvest, Cambridge, UK. Chemicals were chemical grade and used as received without modification unless otherwise stated.

2.2.2 Synthesis of poly (L-Lysine Iso-phthalamide)

Poly (L-lysine *iso*-phthalamide) was synthesised according to the method of Eccleston *et al.*, using single-phase polymerisation technique (Eccleston, Slater and Tighe, 1999). The reaction is depicted in Figure 2-2 below.

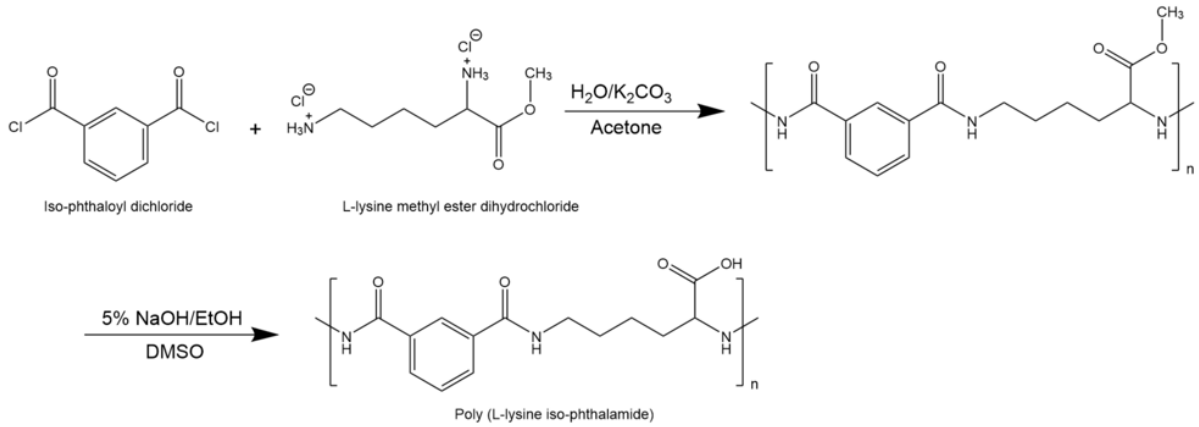

Figure 2-2: Reaction scheme for the synthesis poly (L-lysine iso-phthalamide). The synthesis is a polycondensation of L-lysine methyl ester dihydrochloride and iso-phthaloyl chloride in Acetone/Water solution.

In a typical reaction, *L*-lysine methyl ester·2HCl (0.15 mol, 0.2 M) and an acid acceptor, potassium carbonate (K_2CO_3 0.6 mol, 0.8 M), were dissolved in deionised water (750 mL). The aqueous solution was placed in an ice bath and stirred with a Teflon-coated magnetic stir bar. A pre-cooled dry acetone (750 mL) solution containing *iso*-phthaloyl chloride (0.15 mol, 0.2 M) was added rapidly to the water solution. The reaction was allowed to proceed for 30 minutes, during which poly (L-lysine methyl ester *iso*-phthalamide) precipitated out of the solution. The polymer was transferred to a beaker containing deionised water (DI water) soaked for 3 hours. Fresh DI water was changed every hour while the polymer was gently massaged for 5 minutes during each water change. The raw material was dried overnight in a vacuum oven at 55 ºC. Dried poly (*L*-lysine methyl ester *iso*-phthalamide) was broken down and dissolved in DMSO. Same volume of 5 wt% NaOH solution in ethanol (2.5 molar equivalents to each poly (*L*-lysine methyl ester *iso*-phthalamide) subunit [MW = 276.3 Da], 1.25 M) was added slowly to the polymer solution. The hydrolysed polymer precipitated out in 2-3 minutes, and was collected by vacuum filtration and re-dissolved in DI water.

The crude polymer solution was dialysed in Visking tubing membrane (MW cut-off 12 - 14 kDa) against deionised water for 1 week to remove inorganic salts, residual organic solvents, and low molecular weight oligomers. Fresh DI water (3 L) was changed daily for the during the 1-week purification period. Solid impurities were removed by vacuum filtration. The pH of the clear solution was adjusted to 7.4 using 1M NaOH and lyophilised to yield the sodium form of poly (*L*-lysine *iso*-phthalamide).

To prepare the neutral form, the purified sodium form polymer was acidified to pH 3.0 with 1 M HCl. The precipitate was collected by vacuum filtration, washed 3 times with DI water and lyophilised to yield a fine white powder.

The neutral form of the polymer was used for the structural characterisation and modification while the sodium salt form was used to prepare aqueous polymer solutions for other the physiochemical and biological property studies.

2.2.3 Synthesis of Amino Acid-Modified Poly (L-lysine Iso-phthalamide)

The derivative of poly (*L*-lysine *iso*-phthalamide) grafted with amino acids includes, *L*-glycine, *L*-tryptophan and *L*-phenylalanine, were formed using standard DCC promoted amide-coupling chemistry as depicted in Figure 2-3 below (Haslam, 1980).

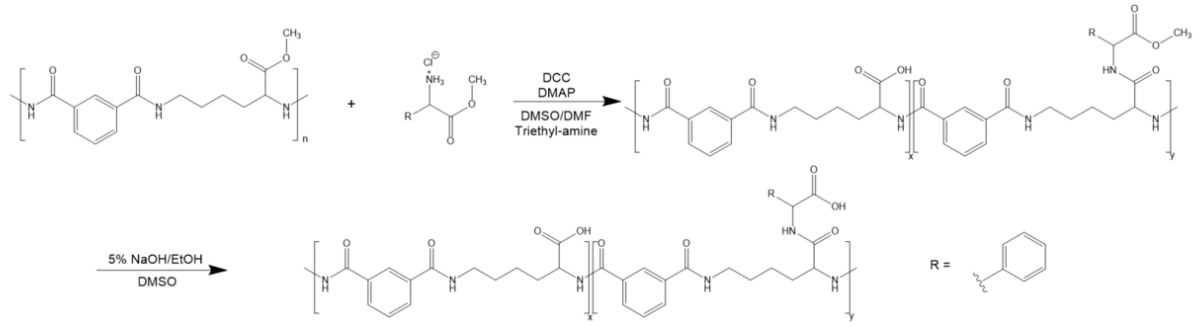

Figure 2-3: Reaction scheme for the synthesis of Phenylalanine grafted poly (L-lysine iso-phthalamide). The reaction was achieved through standard DCC/DMAP coupling. The phenyl group is denoted as R and y varies by grafting percentage.

In a typical synthesis for 50% amino acid grafted-PLP, poly (*L*-lysine *iso*-phthalamide) (3 g, 10.87 mmole [COOH]), appropriate amount of *L*-glycine methyl ester·HCl, triethyl amine as an acid acceptor (1.2 molar equivalent to *L*-glycine methyl ester·HCl), and DMAP as a catalyst (0.6 g, 20 wt% of the polymer) were dissolved in a pre-cooled and anhydrous binary DMSO/DMF (1:3 V:V, 60 mL) solvent. A separate solution of DCC (3 molar equivalent of *L*-glycine methyl ester·HCl) in DMF (20 mL) was prepared and added dropwise to the polymer solution. The reaction was allowed to proceed at room temperature for 60 hours.

Solid impurities and side product dicyclohexylurea were removed by vacuum filtration and a 5 w/v NaOH in anhydrous ethanol solution (2.5 molar equivalent of each polymer subunit) was added to hydrolyse ester groups. Polymers with low grafting percentage (< 25%) precipitated out directly in 2-3 minutes. For polymers with higher degree of grafting, the reaction was allowed for 3 hours and added rapidly to 5 volume of diethyl ether. The precipitate was collected by vacuum filtration and re-dissolved in DI water. The polymer was dialysed in Visking tubing membrane (Medicell, MW cut-off 12-14 kDa) against DI water for 1 week. Fresh DI water (1 L) was changed daily for the during the 1-week

purification period. The pH of the solution was adjusted to ~7.4 and lyophilised to produce a white powder. For the preparation of the neutral form, the dialysed solution was acidified to pH ~3 with 1 M HCl. The precipitation was collected by vacuum filtration, washed 3 times with DI water, and lyophilised to a fine white powder.

The derivatives grafted with *L*-phenylalanine or *L*-tryptophan was prepared analogously except doubling the amount of triethyl amine for the starting material contains 2 molar equivalents of HCl instead of one. The degree of grafting was controlled by varying the molar ratio of $[NH_2]$/[COOH] on amino acid methyl ester and polymer subunit respectively.

2.2.4 Polymer Characterisation

2.2.4.1 Nuclear Magnetic Resonance (NMR)

Polymers were dissolved in DMSO-D_6 and characterised by Bucker Advance 500 MHz NMR spectroscopy (Bruker Biospin GmbH, Germany). The H NMR spectrum were processed through peak picking and integration with MNova software (Mestrelab Research, Spain). The data was used to confirm polymer structure and calculate grafting percentage of modified PLP polymers.

2.2.4.2 Fourier Transform Infrared Spectroscopy (FTIR)

Attenuated total reflectance Fourier transform infrared spectroscopy (ATR-FTIR) was used to determine the presence of benzene ring, amide group, and carboxylate group. Similar to other absorption spectroscopy techniques, FTIR uses a light source to excite chemical functional groups and extract unique emission patterns. FTIR shines polychromatic light of different frequencies to acquire absorption data and which can then Fourier transformed into an absorption spectrum. The advantage of this method is the higher signal-to-noise ratio that could be obtained.

Absorption spectra of PLP-based polymers were collected using a Thermo Nicolet Nexus 870 spectrometer (Waltham, MA, USA) as the average of 32 scans with a wavenumber resolution of 4 cm^{-1} in the 600-4000 cm^{-1} range. As a control, unmodified PLP was used to be compared to modified polymers.

2.2.4.3 Size Exclusion Chromatography (SEC)

The SEC measurements were performed in collaboration with Ms. Shiqi Wang at the Department of Chemical Engineering, Imperial College London. The experiment was performed according to Dabai *et al*. using polystyrene (PS) as a standard using a 300 mm long, 7.5 mm i.d., PS/polydivinylbenzene-packed, Mixed D size exclusion column (Polymer Laboratories, UK) with 1-methyl-2-pyrrolidinone (NMP) as the mobile phase at flow rate of 0.5 mL/min and 80 ºC. Signal detection was measured by a Knauer diode array Smartline 2600 detector with UV absorbance at 270, 300, 350, and 370 nm (Herod *et al.*, 2000; Dabai *et al.*, 2014). The standard curve was constructed using PS at molecular weight (MW) ranging from 580 to $5x10^6$ Da. A linear relationship between the log of MW and elution time was established for estimating the sample molecular weight.

2.2.4.4 Measuring Transition pH of Polymers Through Turbidity

Polymers were each dissolved in DI-water to make 10 mg/mL polymer stock solution. Phosaphase buffer (PB) at different pHs were prepared by first making 0.1 M PB with corresponding amount of phosphoric acid, sodium phosphate monobasic and sodium phosphate dibasic. The pHs of the stock solutions were measured by a pH meter (n=3). The polymer solutions were added to PB buffer at various pH in a 1:10 dilution to make 1 mg/mL final concentration in clear Eppendorf semi-micro Vis cuvettes (Eppendorf, UK). The UV spectra of the solutions were measured at 460 nm with a BMG Labtech SPECTROStar Nano (Allmendgruen, Germany).

2.2.4.5 Circular Dichroism (CD) of PLP-based polymers

Circular dichroism is the spectrum generated by recording the absorbance of polarised light at various wavelength of a chiral molecule. The method is commonly used to characterise chiral molecules and secondary structure of chiral macromolecules. In the case of polypeptides and proteins, the near UV region of CD spectra in proteins often arise from the aromatic amino acids. Each aromatic amino acid has a unique wavelength profile and spectrum arises from the vibronic transitions of different excitation level (Langeveld-Voss *et al.*, 1996; Greenfield, 2006). The shape and magnitude of the near UV spectrum heavily depends on the type of aromatic amino acid present, their mobility, their environment (H-bond, polar group and polarisability) and their spatial disposition in the protein. Even though the understanding for the near UV CD spectra is currently not advanced enough to provide concrete structural information, it is still a useful tool to unveil the changes of proteins with exposure to different environments or site directed mutagenesis (Kelly, Jess and Price, 2005; Miyahara, Nakatsuji and Sugiyama, 2013). In the case of PLP and PLP-based polymers, data from the near UV region could unveil some important changes in different pH environments relating to the aromatic groups of the polymers (Freskgaard *et al.*, 1994).

Stock solution of the polymers were prepared by dissolving lyophilised polymers in their sodium form in DI water at 1 mg/mL. PB at different pHs were prepared by first making stock solution of 0.1 M PB with corresponding amount of phosphoric acid, sodium phosphate monobasic, and sodium phosphate dibasic. The pHs of the stock solutions were measured by a pH meter (n=3) before diluted with DI water into 10 mM PB solution. Stock polymer solution were added to 10 mM PB at the corresponding pH for CD measurements with a final polymer concentration of 0.1 mg/mL. Spectra were recorded at 25^{o}C on an Aviv model 410 circular dichroism spectrophotometer (Aviv Instruments, Lakewood, NJ, USA). Far UV-spectra were scanned from 185 nm to 260 nm while near UV-spectra were scanned from 260 nm to 320 nm. Data was collected for every 1-nm interval and averaged for 5 seconds. Each of the final spectra was the result of averaging three scans. All spectra were baseline corrected and smoothed with Aviv 540 software

(Aviv Instruments, Lakewood, NJ, USA). 10 mM PB of the tested pH were measured and used as blank for baseline correction. Mean Residual Ellipticities (MRS) were calculated with Function 2-1.

$$[\theta]_{MRW,\lambda} = N \times MRW \times \theta_\lambda / 10 \times c \times d \qquad \textbf{Function 2-1}$$

The θ_λ is the ellipticity measured in millidegrees at a given wavelength, *d* is the length of the cell in centimeters, *c* is the polymer concentration in grams per liter. The Mean Residue Weight (MRW) is the polymer subunit molecular weight. N is the number of peptide bonds in the PLP or PLP-based polymer per subunit. Grafting percentages were taken into account for modified PLP polymers (Kelly et al., 2005; Redmann & Rhodes, 1979).

2.2.4.6 Small Angle Neutron Scattering (SANS)

SANS experiments were performed at ISIS, Science & Technology Facilities Council (STFC), Didcot, UK under the supervision of Dr. Ian Tucker from Unilever and Dr. Robert Dalgliesh from the STFC. The scattering studies were carried out using the Larmor beamline using the white beam time of flight method. The geometry and neutronics were set up so as to collect data from 0.005 to 0.5 reciprocal angstroms in Q. Samples were prepared in D_2O and using appropriate phosphoric acid-d_3, potassium dideuterium phosphate, and potassium deuterium phosphate salts so as to maintain the pH at either 4.1, 6.1 or 7.4. Samples were placed into clean cylindrical 2 mm quartz spectrophotometer cells and data were collected for a period of 60 minutes, followed by 10 minutes for the sample transmission. Time of flight data were reduced, regrouped into 1-D radial averaged data using the Mantid data reduction suite. The scattering length density (SLD) was calculated as discussed later in this section and was fed into the models. SLD calculator Web (https://sld-calculator.appspot.com/) was used to determine the SLD of the 0.1 M deuterated PB used in the experiment. A 550:1 of D_2O and Na_2DPO_4 was used as input for Compound Formula from the calculated molar ratio. Density of D_2O of 1.1 g/mL was used in place of 0.1 M deuterated PB as the density of

0.1 M PB is 0.2% greater than H_2O and the difference can be considered trivial in this experiment.

Data were processed using Igor 7 (Wavemetrics inc., OR, USA) with the NIST Center for Neutron Research (NCNR) Analysis Macro extension (Kline, 2006). Primary analyses on the slope of the Intermediate region (0.01 $Å^{-1}$ < q < 0.1 $Å^{-1}$), which measures the size and compactness of the objects at a scale of approximately 100 to 1,000 Å, was performed to determine the microscopic shape of the individual objects in the samples using the slope of the SANS spectra. After selecting the most probable shapes, the corresponding models from an existing library in the Igor software (Wavemetrics inc., OR, USA) were selected. The fit function of the software then automatically projects a SANS spectrum and compares it to the experimental spectrum. Different models will provide prediction on different dimensional characters of an object. For example, a model for cylinders would predict the length and the radius while a model for spheres would provide only the radius. Depending on the number of outputs, this would determine the degree of freedom the model would have to generate a best-fitting model to describe the sample. How well the model fit would be described as reduced Chi-square value which would depend on the degree of freedom of the model and how the projected spectrum and experimental spectrum deviate. Reduced Chi-square value is commonly used commonly to measure the goodness of fit and is defined as chi-square per degree of freedom (Andrae, Schulze-Hartung and Melchior, 2010). Models selected as the best fit reported in this study had a reduced Chi-square value closest to 1.

2.2.5 Biological Assays

2.2.5.1 Cell Culture

All tissue culture experiments were conducted in sterile laminar flow cabinets (Microflow Class 2), using sterile disposable plasticware, to minimise contamination. Material or chemical introduced to cell culture vessels was sterilised by autoclave (121 ˚C for 20 minutes) or filtered through 0.22 µm-filters (Millex-Fisher Scientific, Paisely, UK).

HeLa adherent epithelial cells (human cervical cancer cells) were grown in DMEM media supplemented with 10% (v/v) fetal bovine serum (FBS), 2 mM L-glutamine, 100 U/mL penicillin/streptomycin (Pen-Strep) unless specified otherwise. HeLa cells were trypsinised using trypsin-EDTA and maintained in a humidified incubator with 5% CO_2 at 37 ºC.

Cell concentration was determined by manual counting with a haemocytometer (Sigma, UK). The cell suspension was stained with trypan blue, to discriminates between live and dead cells. Cell suspensions (10 µL) were introduced to the haemocytometer and covered with a glass slip and counted under an Olympus CK2 microscope. The four corner squares of cells on the heamocytometer were averaged and converted to a cell count by multiplying the dilution factor times and the area of a standard haemocytometer square.

2.2.5.2 Intracellular Delivery of Membrane Impermeable Calcein

2.2.5.2.1 Flow Cytometry for Fluorescence Measurement

Calcein (a membrane impermeable fluorophore) was used as a tracer molecule to monitor the effect of polymer intracellular delivery efficiency. Disodium calcein salt was dissolved in phosphate buffer saline (PBS) at pH 7.4 to make 200 mM stock solution. HeLa cells were seeded in 24-well plates at $5x10^4$ cells/mL in 0.5 mL supplemented DMEM to full confluence in 24 hours followed by incubation with 0.22 µm filter-sterilised supplemented media and 2 mM calcein in the presence or absence of polymers. Cells were washed twice with PBS, trypsinised and resuspended in phenol red-free DMEM supplemented with FBS spun down at 0.2 g for 5 minutes. The supernatant was removed and the cell pellets were resuspended in phenol red- and FBS-free DMEM and transferred into a Titertube 1 mL micro test tube (Bio-Rad, UK). Cells were analysed by Cytek DxP8 cell sorter (Cytek Bioscience, USA) with 10,000 event count measuring side scattering and fluorescent intensity at various emission wavelengths. The results were processed by FlowJo software (Cytek Bioscience, USA) by quantifying fluorescent intensity of the gated cells. All experiments were conducted in triplicates.

2.2.5.3 Structure Transformation of PLP Polymers in the Presence of Lipid Vesicles

2.2.5.3.1 Preparation of DOPC Giant Unilamellar Vesicles (GUV)

GUV used in this study was synthesised by Mr. Mattia Morandi of Institut Charles Sadron, Strasbourg, France. GUVs were prepared using a variation of the gel-assisted formation method introduced by Weinberger (Weinberger *et al.*, 2013). Simply a polyvinyl alcohol (PVA) gel formed with a 5% volume fraction of PVA in PBS at pH 7.4 was deposited on a borosilicate glass and placed at 80°C for 2 hours to form a homogenous gel substrate. 10 μL of 1,2-Di(cis-9-octadecenoyl)-sn-glycero-3-phosphocholine (DOPC) in chloroform (2 mg/mL) were deposited on the gel substrate and kept in vacuum for 30 min to ensure complete solvent evaporation. The resulting lipid film was hydrated with a polymer solution in 10 mM PB for at least 1 hour to the appropriate concentration. The liposome suspension solutions were then collected by pipettes for experiment.

2.2.5.3.2 CD Measurement of polymer in the presence of GUV

GUV solutions prepared as mentioned in the previous section were used for the CD experiment. Spectra were recorded at 25 ºC on an Aviv model 410 circular dichroism spectrophotometer (Aviv Instruments, Lakewood, NJ, USA). Far UV-spectra were scanned from 185 nm to 260 nm. Data was collected and treated as mentioned in the previous CD section. GUV in 10 mM PB was used as blank for baseline correction.

PLP or PP-75 aqueous solution was diluted in 10 mM PB at different pHs to make 0.1 mg/mL in 10 mM solution at various pHs. Solutions with 0.2 mg/mL GUV in the presence of 0.1 mg/mL PLP or PP-75 in 10 mM PB at different pHs were also measured by CD. All spectra were baseline corrected and smoothed with Aviv 540 software (Aviv Instruments, Lakewood, NJ, USA).

2.2.6 Statistical Analyses

All data are reported as the mean ± standard deviation from at least three independent measurements. The statistical significance in mean values between two groups was

analysed using a one-way ANOVA followed by a Tukey's test for multiple comparisons. The tests were analysed using GraphPad Prism (GraphPad Software, US). A p-value of <0.05 was taken as statistically significant and noted as * ($p< 0.05$), ** ($p< 0.005$); and **** ($p < 0.0001$). The same statistical analyses were conducted in all the remaining chapters.

2.3 Results and Discussion

2.3.1 PLP synthesis and characterisation

After synthesis and purification, the polymer was a white solid in both its sodium and acidic forms. Structural characterisation was performed via ^{1}H-NMR, FTIR and Gel Permeation Chromatography (GPC). The acidic form of PLP in DMSO-d_6 was used for NMR to confirm the chemical structure. The ^{1}H-NMR spectrum and the chemical structure of PLP are depicted in Figure 2-4 with the appropriate proton assignment as the following δ 1.28-1.62 (g, -CH_2-), 3.26 (f, -CH2-), 4.38 (h, -CH-), 7.5 (c, bezene-H), 7.9 – 8.02 (b, d, H-benzene-H), 8.32 (a, benzene-H), 8.56 -8.76 (e, i, -NH-). The ^{1}H-NMR spectrum agreed with the chemical shifts reported (Eccleston *et al.*, 2000; Chen *et al.*, 2009). Of note, the peak at 12.3 is assigned to the proton on the COOH group as it has a high chemical shift typical the functional group. However, the presence of this peak at approximately 12 ppm for PLP and its derivative will depend on the purity of the sample and may not be observed in all NMR spectra.

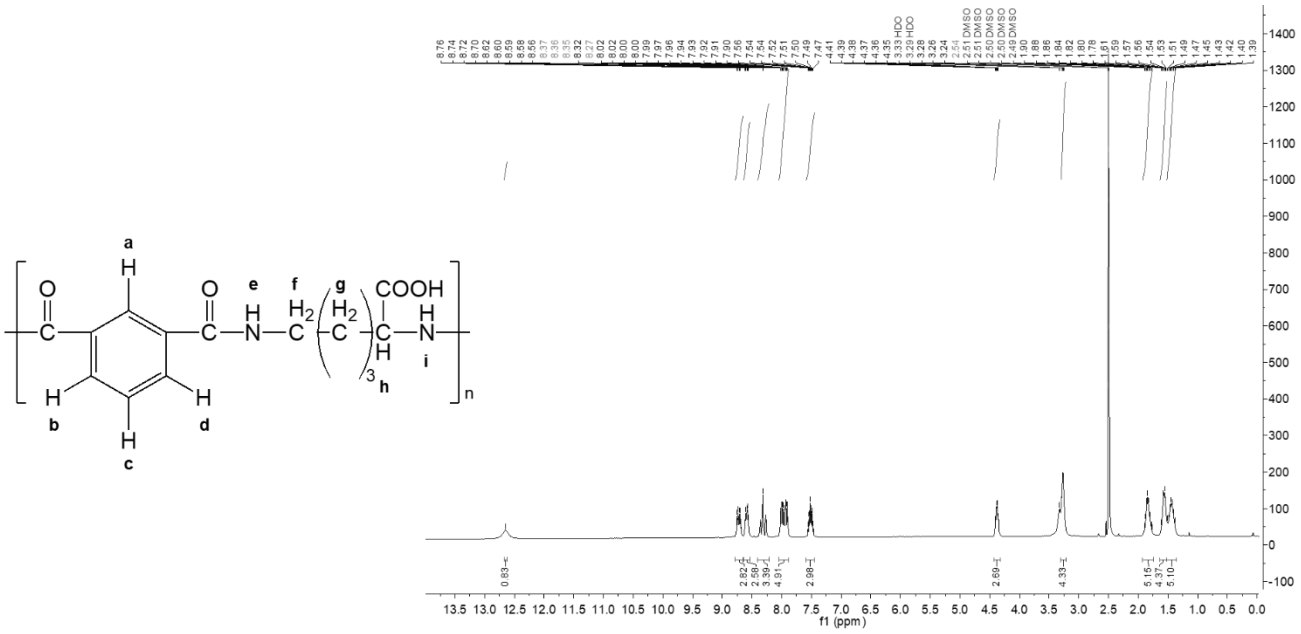

Figure 2-4: Chemical structure and 1H-NMR Spectrum of poly (L-lysine iso-phthalamide) in DMSO-D_6. The protons on the chemical structure of PLP were each assigned to a legend and labelled on the ^{1}H-NMR spectrum. The peak at 2.5 ppm was due to water residue and can be ignored.

Further confirmation of the PLP chemical formulation could be observed in the FTIR spectrum with the appropriate chemical functional group assignment in Figure 2-5. The absorption peaks include N-H and O-H stretch (3300 cm^{-1}), carboxylic acid C=O stretch (1710 cm^{-1}), amide band I (1630 cm^{-1}), amide band II (1530 cm^{-1}), and C-O stretch (1270 cm^{-1}), which agreed with what was previously reported (Chen, 2007).

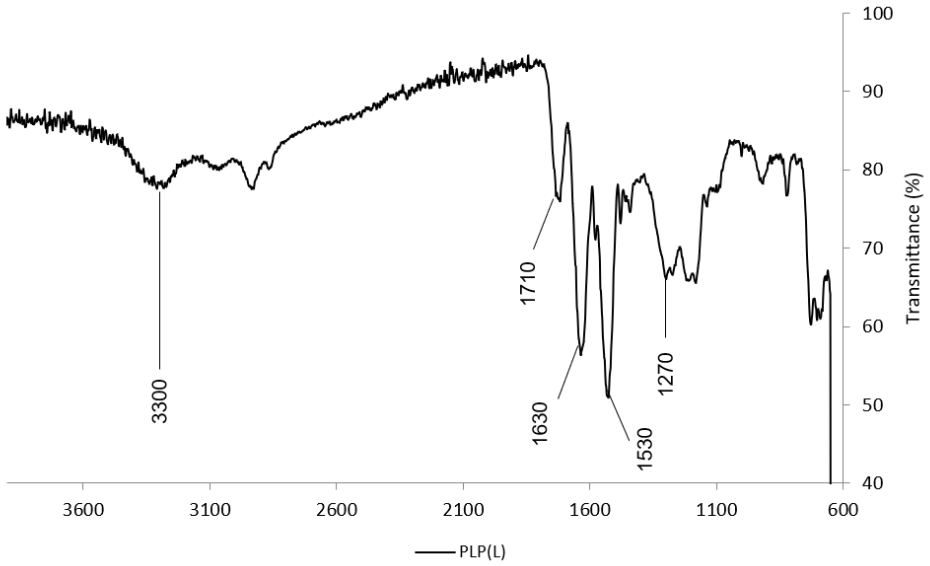

Figure 2-5: FTIR spectrum of poly (L-lysine iso-phthalamide). Peaks labelled were assigned to the appropriate functional groups of PLP.

SEC result of PLP obtained with the method used in this study method suggested a Mn of 472.39 kDa and Mw of 882.24 kDa (Figure 2-6). The result was different from the Mw of 23820 Da and Mw of 5894 Da previously reported by Chen and Khormaee using gel permeability chromatography (GPC) and matrix-assisted laser desorption/ionization time-of-flight mass spectroscopy (MALDI-TOF) respectively (Chen, 2007; Khormaee, 2009). The molecular weight obtained was different from the previous results as the polymers in this study were dissolved in an organic solvent, N-Methyl-2-pyrrolidone (NMP), rather than an aqueous solution like the two previously reported methods. Additionally, the standard polymer, PS, used in this experiment is an extremely flexible polymer without polar amide groups compared to PLP that contains amphiphilic functional groups and could adopt an organised structure. Therefore, the PLP molecular weight determined by the PS standard would not be an accurate representation of the true molecular weight. This GPC method could however, be a useful alternative to compare the molecular weight of PLP and PLP- based polymer.

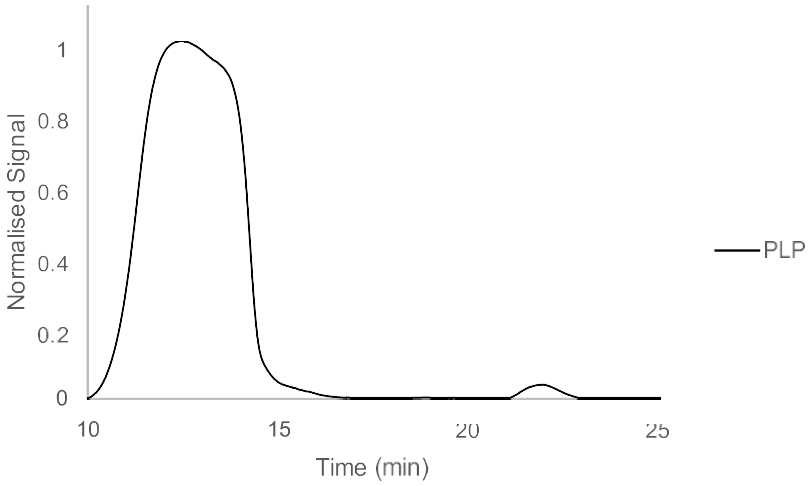

	Mn (kDa)	Mw (kDa)	PDI
PLP	472.39	882.24	1.87

Figure 2-6: Size exclusive chromatography spectrum of poly (L-lysine iso-phthalamide). Molecular weight and polydispersity of PLP were determined by comparing to a standard curve constructed by PS and results are presented in the table below the spectrum.

2.3.2 Amino acid-grafted PLP synthesis and characterization

Phenylalanine (Phe) grafted PLP (PP) is the most effective form of delivery polymer of the modified PLP. PP-50 and PP-75 were synthesised using the same DCC/DMAP protocol developed by Chen *et al.* to yield white solids. ^{1}H-NMR showed that the PP polymer had comparable chemical composition compared to that previously reported (Figure 2-7) (Chen, 2007). The peak at 7.3 ppm corresponds to the five hydrogens on the phenyl group of Phe and was used to calculate the grafting percentage. The grafting percentage calculated by ^{1}H-NMR was 46.0 % and 60.8% for PP-50 and PP- 75 respectively. The results were comparable to what was previously reported (Chen, 2007).

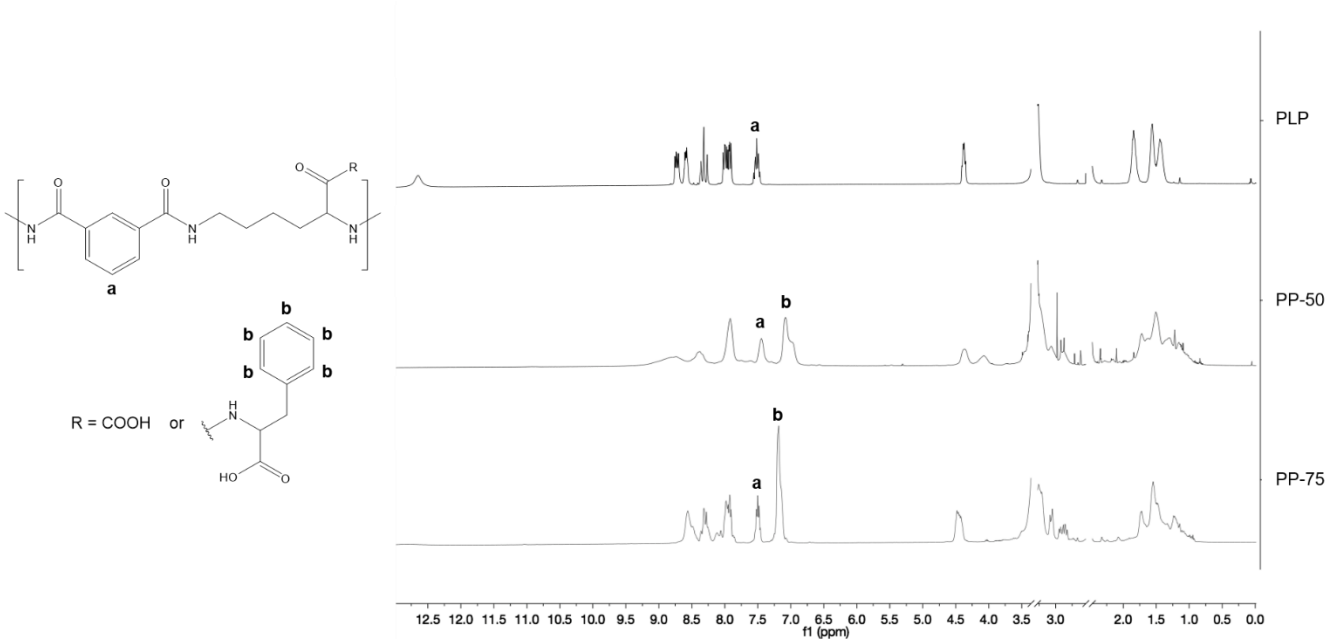

Figure 2-7: Chemical structure and ^{1}H-NMR Spectra of PLP, PP-50, and PP-75. The unique proton on the backbone benzene was denoted as **a** and assigned to the according peak on the NMR spectra. Five protons on the phenyl group were denoted as **b** and assigned to the peak on the NMR spectra of PP-50 and PP-75. DMSO and water peaks at 2.5 and 3.5 ppm were removed for better visualisation of the spectra.

In order to better understand how amino acid modifications affected PLP and how efficient were the reactions, the simplest form of amino acid, glycine (Gly), was used for modification of PLP. After reaction and purification, a white PG-50 solid was yielded. The polymer was characterised by ^{1}H-NMR with a grafting percentage of 49.0% (Figure 2-8). The overall reaction efficiency was 98.0% for PLP glycine grafting compare to 92.0 % of PP-50 and 81.1 % for PP-75. This could be due to the fact that there was no steric hindrance effect for glycine methyl ester compared to L-phenylalanine ethyl ester that contains a benzene ring on the side chain. Therefore, the amine group on the glycine has a higher chance to react with the free carboxylate group on the PLP side chains. The reaction efficiency could also be affected by the solubility of L-phenylalanine methyl ester in DMSO/DMF.

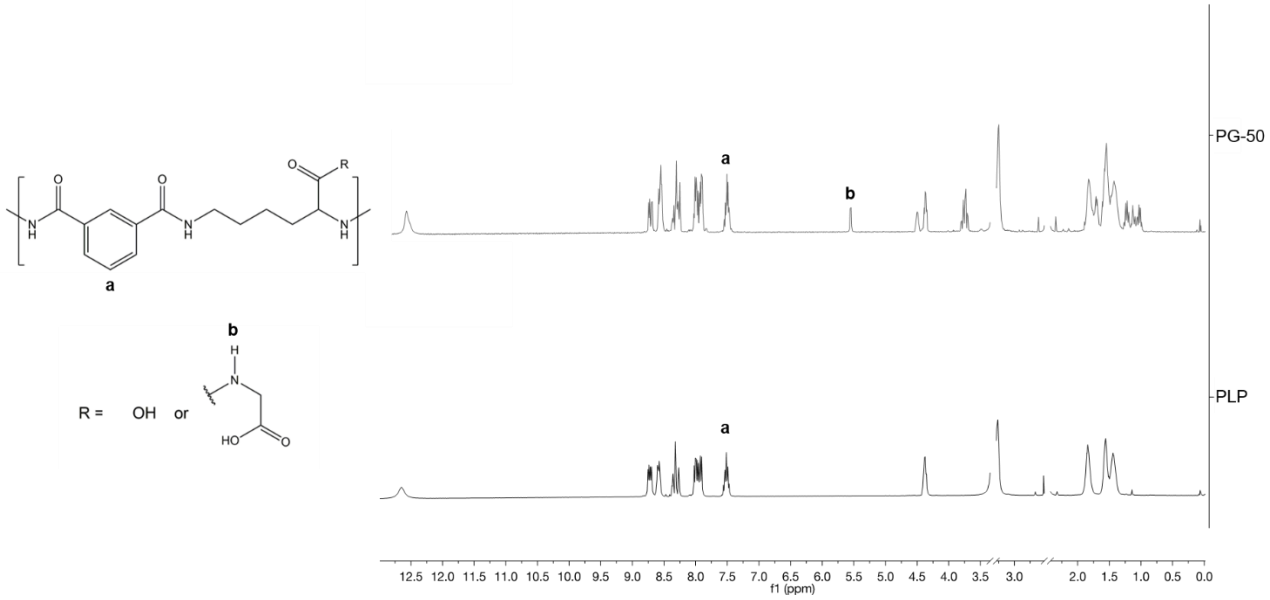

Figure 2-8: Chemical structure and ^{1}H-NMR Spectra of PG-50 and PLP. The unique proton on the backbone benzene was denoted as **a** and assigned to the according peak on the NMR spectra. The unique proton on the amine group of the grafted glycine was denoted as **b** and assigned to the peak on the NMR spectrum of PG-50. DMSO and water peaks at 2.5 and 3.5 ppm were removed for better visualisation of the spectra.

The chemical structures of the polymers were further confirmed through FTIR and the PP polymers' spectra agreed with what were previous reported by Chen *et al*. (Chen *et al.*, 2009). The transition pHs of PLP, PG-50 and PP-50 were shown in Figure 2-9, where PP-50 had the highest transition pH at pH 4.9. Surprisingly, glycine modification slightly increased the transition pH by approximately 0.6 while transition pH of PLP and PP-50 were determined to be 3.67 and 4.90. The transition pH of both PLP and PP-50 were lower than what was previously reported 4.7 and 5.5 at 1 mg/mL (Chen, 2007). The main reason for the difference could be due to the buffer system that was used in this study. The higher transition pH values were determined using a phosphate citrate system while phosphate buffer was used in this study.

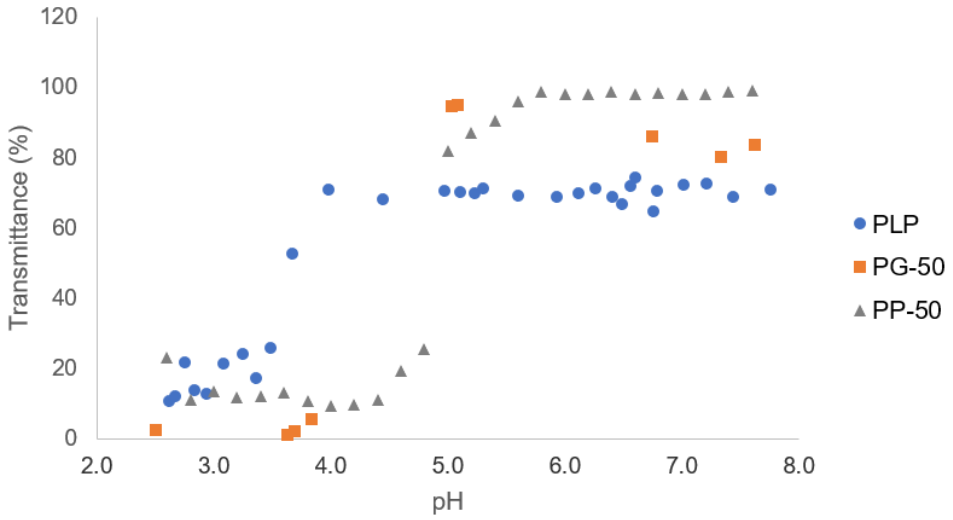

Figure 2-9: Variation of the turbidity of PLP, PG-50, and PP50 in different pH conditions. The turbidity of polymers in phosphate buffer at pH between 2.5 and 7.8 were measured at λ = 460 nm.

The buffer range for phosphate buffer is between pH 5.8 and 8.0 while citrate buffer's between pH 3.0 and 6.2. In the experiments previously conducted used a mix of phosphate and citrate buffer was used to determine the transition pH (Chen, 2007). In this study, phosphate buffer was used and that could cause the difference in transition pH. Citrate could not be used in CD experiments because it absorbs strongly in the far UV region that could interfere with the spectrum of PLP polymers. For consistency and because PB has the capacity to make the desired pH, it was used throughout the experiment. The pH of each solution was measured by a pH meter (n=3) and determined to be the desired pH in agreement with what was listed on the Sigma website. No titration experiments were involved, therefore, buffering capacity would not have a major impact on the result.

As Phe and Tyr were both used to modify PLP, to completely test the hypothesis that the aromatic side chain was a main factor to increase membrane disruptive activity, L-tryptophan (Trp) was used to modify PLP polymer to yield a water insoluble yellow solid PW-50. ^{1}H-NMR was used to characterise the polymer and the six hydrogens on the aromatic group of Trp were assigned to the peaks between 6.8 and 7.3 ppm as shown on Figure 2-10. The assignment was based on comparing the spectrum of PW-50 and PLP side by side. There was methanol residue in the PW-50 sample which resulted in additional peaks between 1.0 to 1.4 ppm and a single peak at 4.3 ppm. The ethanol

residue was from the hydroxylation of ethyl ester PW-50. The grafting percentage of PW-50 was determined to be 30.8 % by ^{1}H-NMR (Figure 2-10). The grafting efficiency was rather low (61.6 %) compare to other modifications such as Phe (92.0%) and Gly (98.0%). What might had affected the reaction efficiency could be the lower solubility of Trp in DMSO/DMF and the solubility of PW-50 in polar solvents which may cause the polymer to crash out before reaching higher grafting percentage. Even at this lower grafting percentage PW-50 was insoluble in water and PB and exhibited a surfactant effect. Various methods such as sonication or increasing temperature to 60 ºC did not increase the solubility of PW-50, making the polymer unsuitable for any further experimentation.

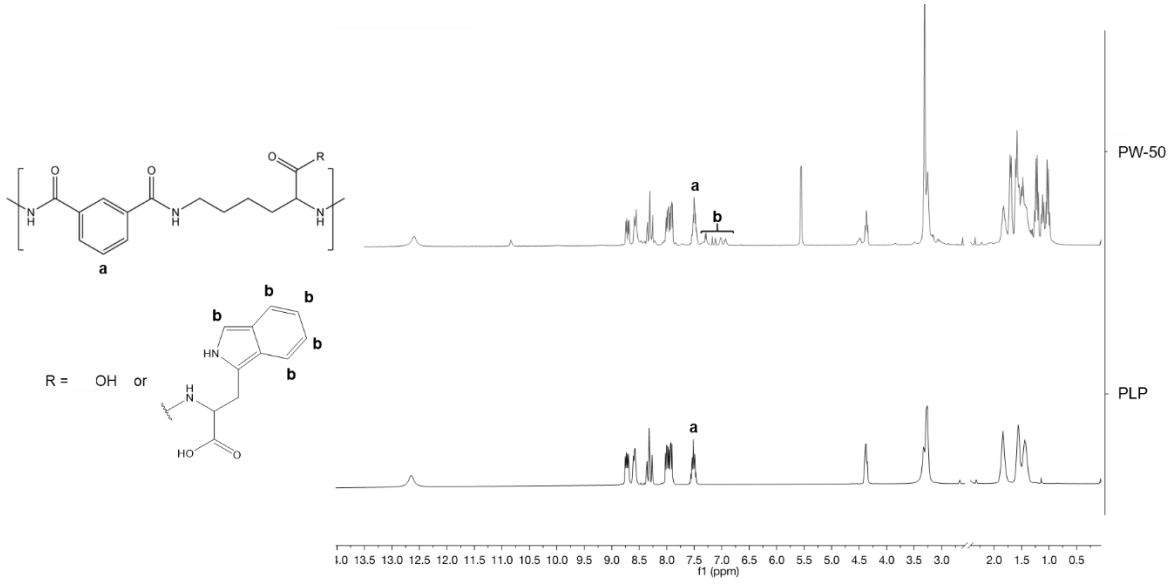

Figure 2-10: Chemical structure and ^{1}H-NMR Spectra of PW-50 and PLP. The unique proton on the backbone benzene was denoted as **a** and assigned to the according peak on the NMR spectra. The five protons on the aromatic group excluding the one on the secondary amine of the grafted tryptophan were denoted as **b** and assigned to the peaks accordingly on the NMR spectrum of PW-50. DMSO peaks at 2.5 ppm were removed for better visualisation of the spectra.

As PW-50 was determined to be insoluble in water, replacement of half of the Trp with Phe in the reaction on a molar basis was an attempt to create a soluble hybrid polymer. A cream colored solid PPW-50 was obtained after purification and lyophilisation. The polymers were characterised by ^{1}H-NMR and calculated to have a total grafting percentage of 37.6 % for PPW-50 (Figure 2-11). Phe and Trp individual grafting percentage were 21.6 % and 15.8 % respectively. In other words, the reaction efficiency

for Phe and Trp in the reaction were 87.2 % and 47.2 %. The result was interesting as the hybrid grafting reaction efficiency of Phe and Typ grafting were both lower compared to using a single amino acid. Even comparing the two amino acids in the same reaction, Phe had a much higher efficiency. This could be explained by the different in solubility of Phe and Trp in the reaction condition as mentioned before. Additionally, the nitrogen on the aromatic sidechain of Trp might have hindered its efficiency on forming reactive complex with the DCC catalyst, which in turn, decreased the overall reaction efficiency. The activity of PPW-50 will be discussed in a later section.

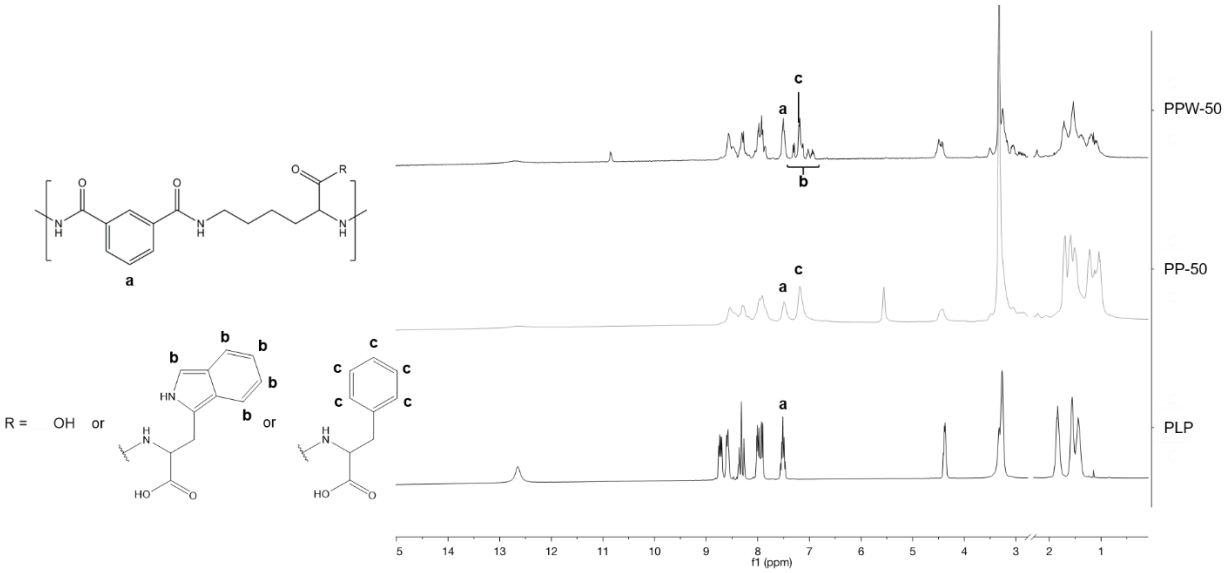

Figure 2-11: Chemical structure and ^{1}H-NMR Spectra of PPW-50. The ^{1}H-NMR spectra of PP-50 and PLP were included as references. The unique proton on the backbone benzene was denoted as **a**. The five protons on the aromatic group excluding the one on the secondary amine of the grafted tryptophan were denoted as **b** and assigned to the peaks accordingly on the NMR spectrum of PPW-50. The five protons on the phenyl group of the grafted phenylalanine were denoted as **c** and assigned to the peak at 7.2 ppm. DMSO peaks at 2.5 ppm were removed for better visualisation of the spectra.

2.3.3 Polymer Secondary Structure and Conformation Characterisation by CD

Each polymer was dissolved in 10 mM PB at various pHs and characterised by CD spectroscopy. PLP and PG-50 had very similar CD spectra at pH 7.4 while PP-50 had a distinct spectrum with a stronger absorption of both left- and right-circularly polarised light relatively to the two other polymers (Figure 2-12A). As shown in Figure 2-12B, PLP at physiological pH had negative CD at 215 nm. Increase in positive CD absorption was

observed as the pH decreased until pH 4.0 which was close to the transition pH 3.6 of PLP determined in this study. Further decrease in pH did not contribute to enhanced polarised light absorption. Instead, a decrease in CD was observed at pH 3.0. This observation could be due to the precipitation of PLP polymer that decreased the overall concentration of optically active groups in the solution. The spectra at pH 3.0 was still similar to the spectrum at pH 6.1 but with decreased strength. The increase in CD as the pH decreased to its transition pH is an evidence that that the overall polymer was forming into a more ordered structure. This phenomenon could be further verified by SANS discussed in the following section.

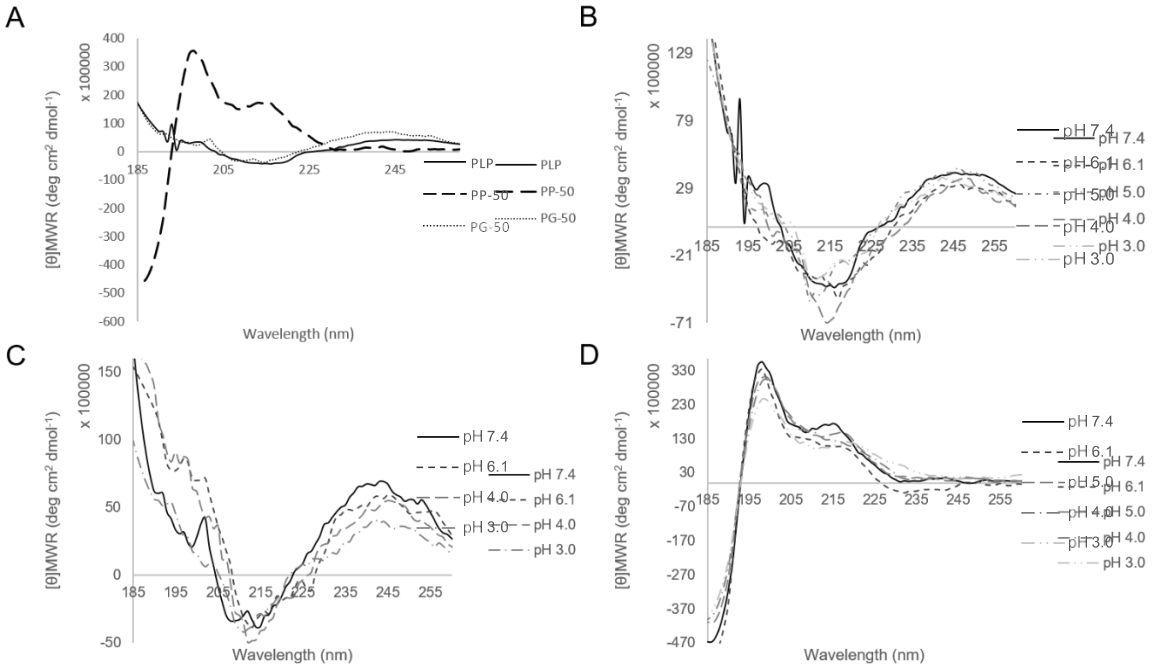

Figure 2-12: Circular Dichroism spectra of A) an overlay of PLP, PG-50, and PP-50 at pH 7.4. B) CD spectra of PLP C) PG-50, and D) PP-50at various pHs. Polymers were analysed at 0.1 mg/mL in phosphate buffer at the specified pH between 185 and 260 nm.

PG-50 was characterised by CD at four different pHs in 10 mM PB. The CD spectra of PG-50 was comparable to the PLP while PG-50 did not have a significant change in the CD at 215 nm as pH decreased (Figure 2-12C). This could be explained by the glycine modification on the pendant group of the PLP backbone. As glycine is not hydrophobic nor does it contain an aromatic group, therefore, it would disturb the packing of hydrophobic groups in PLP as pH decreases. Making it more difficult for PG-50 to

consolidate into a more compact macrostructure that PLP could potentially form.

PP-50 was characterised by CD spectroscopy in the same conditions as PLP and PG-50. The CD spectra of PP-50, unlike PG-50, had very different spectra compared to PLP. The broad positive peak between 225 and 255 nm could not be observed in PP-50's spectra. Instead having a local minimum at 215 nm, there were two maxima at 198 and 218 nm (Figure 2-12D). Similar to PLP, as the pH approached the transition pH, the CD became most prominent. In the case of PP-50, strongest signals could be observed at pH 6.1 and 5.0. Incidentally the two pHs were very close to the transition pH of PP-50 that was discussed in the previous section. The same observation was also observed in the case of PLP. The CD spectra of the polymers, however, suggested that the structure of the polymer might not shifted as dramatically as observed in typical fusogenic proteins. Never the less, the aggregation or formation of macrostructure might have contributed to the membrane disruptive activity of PLP-based polymers upon the change in response to environmental pH. Furthermore, the structural information was obtained in the absence of lipid membranes such as liposome or giant unilamellar vesicles (GUV). A more accurate structural information on the membrane-disruptive state could only be revealed with a more sophisticated study.

The near UV CD spectra of the three polymers at different pHs were also recorded between 260 and 320 nm in similar experimental conditions. For polypeptides, the near UV region reflects the environment where aromatic side chains and often change when the polypeptide changed conformation or was denatured (Freskgaard *et al.*, 1994; Kelly, Jess and Price, 2005). As shown in Figure 2-13A, the near UV spectrum of PLP changes as pH decreases. The change reflects that the aromatic benzene groups within the polymer experience different environment at different pH which may be result of changing intra- polymer conformation or inter-polymer interaction. A similar trend was observed in the near UV spectra of PG-50 and PP-50 shown in Figure 2-13B and Figure 2-13C respectively. Interestingly, the near UV spectrum of PP-50 at pH 7.4 was similar to the near UV spectrum of PLP at pH 7.4 while the spectrum of PG-50 at pH 7.4 was slightly different. As the pH decreases, the near UV spectrum of PG-50 seems to have less changes compared to the spectra of PLP and PP-50. This observation could imply that the packing of aromatic groups in PG-50 is slightly different from PLP.

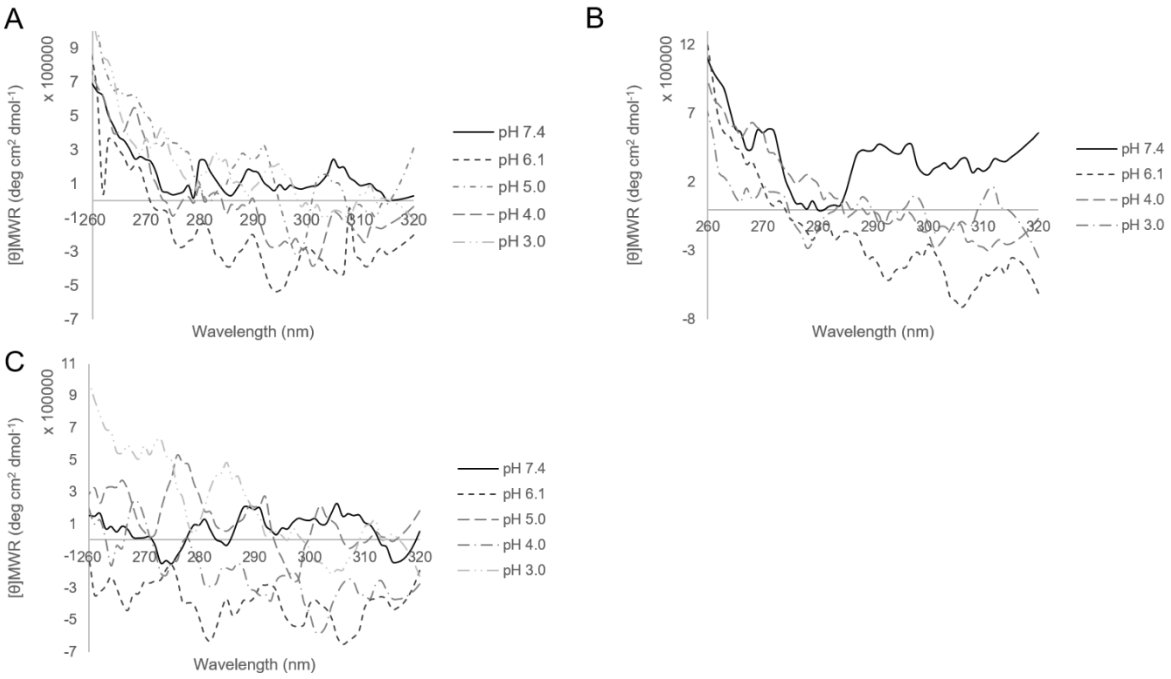

Figure 2-13: Circular Dichroism near UV spectra of A) PLP B) PG-50, and C) PP-50 at various pHs. Polymers were analysed at 0.1 mg/mL in 0.1 M phosphate buffer at the specified pH between 260 and 320 nm.

2.3.4 Small Angle Neutron Scattering

Neutron scattering has gained popularity as a method to characterise molecular structure especially for macromolecules in solution. The high resolution and non-destructive nature of the method enables the detection of even small changes in molecular structure while retaining the sample (Penfold and Thomas, 2014). In this study, SANS was used to characterise PLP and PP-50 polymer structures in deuterated 10 mM PB solution at different pHs. As shown in Figure 2-14, PLP was determined to have adopted a stiff rod structure with length of 200 Å and cylinder diameter at pH 7.4, 6.1 and 4.1. The diameter of the PLP increased as the pH decreased.

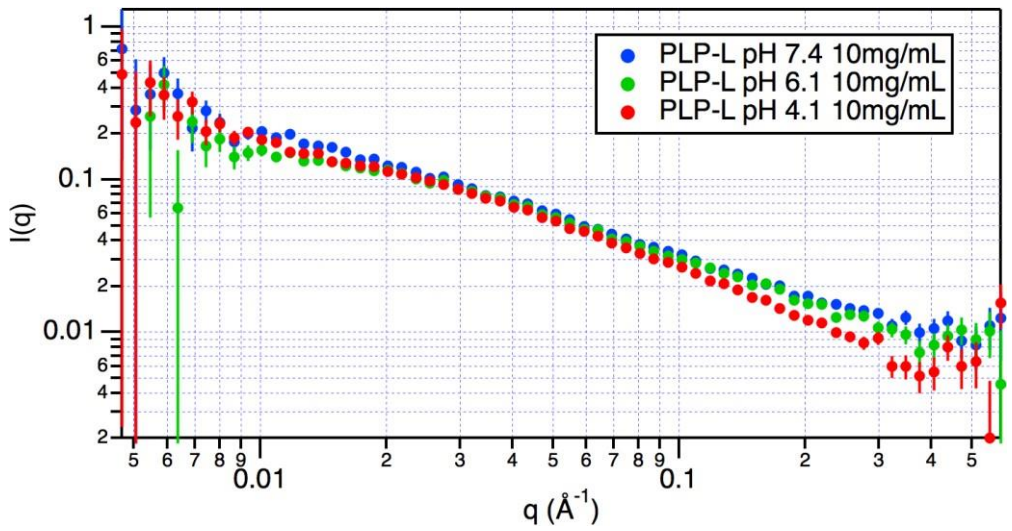

Figure 2-14: SANS spectra of PLP at pH 7.4, 6.1 and 4.1 in deuterated phosphate buffer solution. Deuterated phosphate buffer at selected pH was used as background. Spectra were fitted with the best matching models to determine the shape and dimensions of the polymer in solution. The simulated model and dimensions are presented in the Table 2-1.

pH	4.1	6.1	7.4
Form	Cylinder	Cylinder	Cylinder
Length (Å)	200	200	200
Diameter (Å)	21	16	14
Volume Fraction	0.0009	0.0015	0.002
SLD (10^{-6})	1	1	1

Table 2-1: The list of dimensions and projected structures of PLP at three pHs. The dimensions were derived from models that were simulated to best fit the SANS spectra shown in Figure 2-14.

Different from the previous hypothesis that PLP changes from an extended structure to a more compact globular structure upon lower pH, SANS data suggest that PLP is a rod structure between pH 7.4 and 4.1. From the increase in diameter and aggregation pattern of PLP, it is likely that the polymer is a thinner rod bundled into a larger structure. It is likely that the protonation affected the diameter of individual coils of PLP as well as the ability of PLP to aggregate into multi-coil bundles. The attenuated ionic repulsion intra-

molecularly induced a more compact coil of PLP, thus the slight decrease in diameter. Inter-molecularly, hydrophobic interaction was relatively strengthened and more PLP coils aggregated in PB buffer. As seen in Table 2-2, it is hypothesised that the diameter of individual PLP bundles would decrease as pH decreases while the number of PLP in each bundle increases. The projected diameter was calculated based on the perfect stacking of different number of identical cylinders (Figure 2-15). As shown in Table 2-2, the projected diameter agreed with the SANS data with only a small amount of difference. At pH 4.1, however, the projected diameter was 25.7 % larger than the data from SANS. This could be due to either underestimation of how much individual PLP diameter decreased or the false assumption of the individual PLP packing pattern. The hypothesis of PLP packing as a functioning multi-bundle rod was inspired by helical peptides with membrane disrupting properties, more specifically, celling penetrating peptides (CPP). For example, HA2 protein's fusion peptide subunit, X31, is most effective in membrane penetration when forming a triple helix structure. Another cell penetrating peptide, sweet arrow peptide (SAP), is an amphiphilic peptide with five helixes. According to a review, CPPs usually form a helical structure with hydrophobic and hydrophilic groups on two opposing sides (Lau *et al.*, 2004). This observation for CPPs that have similar membrane disruptive and amphiphilic characteristics forms the basis for the hypothesis that multiple helixes bundle into a rod with the hydrophilic side on the exterior. However, SANS does not have the resolution to confirm this theory and additional characterisation techniques such as X-ray crystallography would be required.

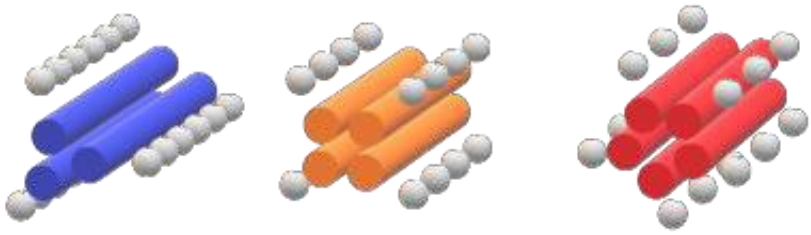

Figure 2-15: Proposed structure of PLP in solution at pH 7.4, pH 5.1, and pH 4.1. Each rod represents a PLP polymer chain and each grey sphere represent a negative charge. The bundle of rods depicts the hypothesised macrostructure of PLP in solution.

	pH 7.4	pH 6.1	pH 4.1
Hypothesised Individual PLP Diameter (Å)	6.8	6.4	6.0
Number of PLP Coils	3	4	5
Projected Diameter (Å)	14.65	15.45	26.4
Diameter Calculated by SANS (Å)	14	16	21
% Difference	4.64 %	3.44 %	25.71 %

Table 2-2: The list of proposed dimensions of PLP macrostructure at three pHs compared to SANS predicted dimensions. The dimensions were calculated by adding hypothesised individual PLP diameters which was derived from approximately the dimension of benzene ring.

PP-50 was also characterised by SANS at pH 7.4, 6.1, and 4.1. As shown in Figure 2-16, PP-50 resembles a barbell at pH 7.4 in PB buffer with length of 282 Å, diameter of 16.8 Å and an end cap diameter of 38.9 Å. The transition from a rod-like barbell object to a lamellar surface structure were derived from the best fitting model to the corresponding PP-50 SANS spectra and could be observed from the three PP-50 spectrum below.

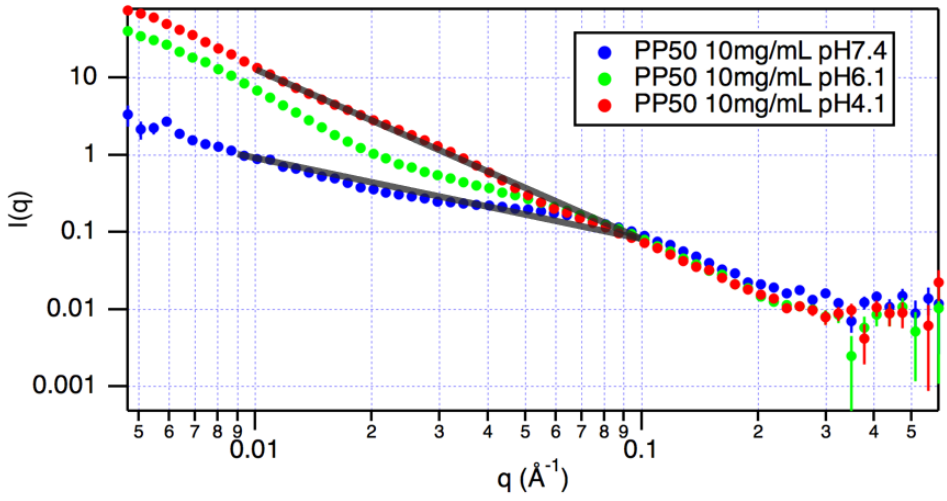

Figure 2-16: SANS spectra of PP-50 at pH 7.4, 6.1 and 4.1 in deuterated phosphate buffer solution. Deuterated phosphate buffer at selected pH was used as background. Spectra were fitted with the best matching models to determine the shape and dimensions of the polymer in solution.

Derived from models, PP-50 forms a fluid lamellar structure at pH 6.1, indicating that the polymer could aggregate and form organized macrostructure. At pH 4.1, PP-50 was observed to form a lamellar structure with 12 Å thickness. This observed self-assembly formation of lamellar structures could be of crucial importance to the enhanced membrane disruptive effectiveness of PP-50 compared to PLP. It was proven that forming high concentration of localized aggregation could significantly alter the membrane disruptive activity as shown in fusogenic X31 peptides. For X31 fusogenic peptide, the affinity towards lipid bilayer was not the most important factor for membrane disruptive activity but a “corporate effect” where coiled coil trimer was formed and is far more effective than the monomer. For PP-50, increase in amphiphilicity did decrease the membrane lysis tension [increase membrane vulnerability], but forming a localized structure or defect was a more effective mechanism to cause membrane lysis. The hydrophobic modification could indeed increase the interaction between the polymer and lipid bi-layer, however, the polymer intermolecular attraction contributed to the significant increase in the intracellular delivery efficiency.

2.3.5 Biological Activity of PLP-based polymers

2.3.5.1 Membrane activities of polymers determined by CD

Initial studies using the polymer with giant unilamellar vesicles (GUV) were conducted using PLP and PP-75 polymers. As shown in Figure 2-17A, the CD spectra of PLP with GUV at pH 7.4 is similar to PLP alone with a local maximum at 245 nm and minimum at approximately 215 nm. The circular light absorption was, however, less intense in the presence of GUV. This result suggested that PLP formed a less ordered structure in the presence of lipids indicating polymer-lipid interaction. The effect of pH responsiveness in the presence of lipid was further tested on PP-75 and studied by CD.

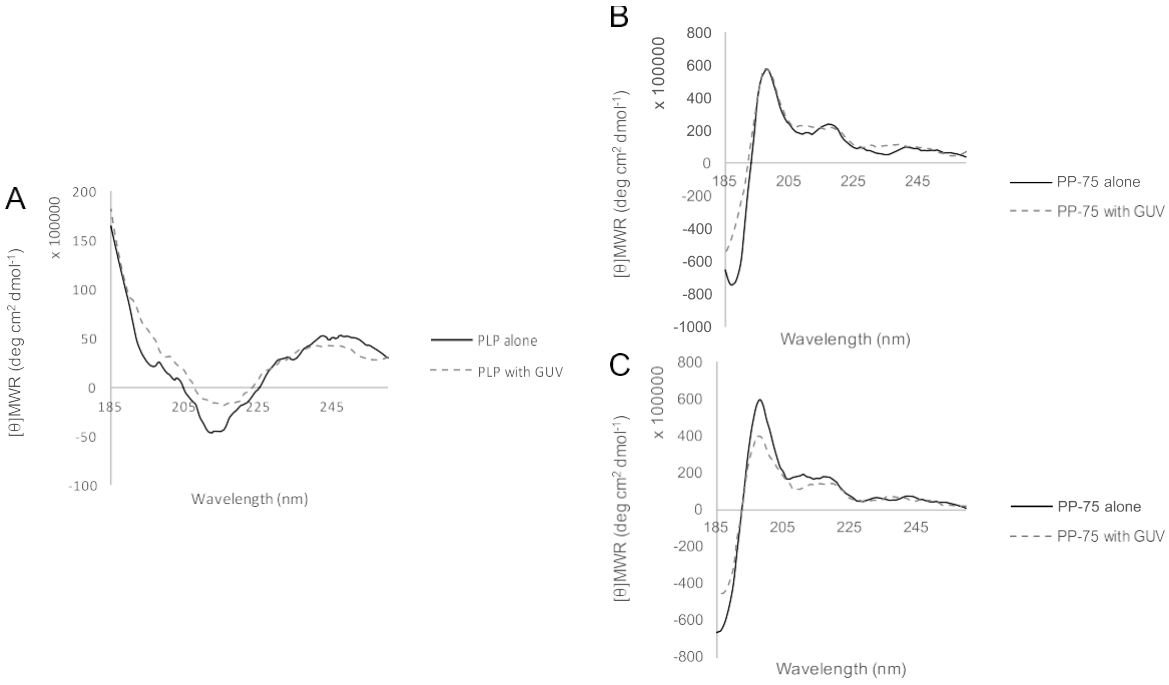

Figure 2-17: Circular dichroism spectra of A) PLP at 7.4 B) PP-75 at pH 7.4, and C) PP-75 at pH 5.1 in the absence or presence of giant unilamellar vesicle (GUV). Polymers were analysed in phosphate buffer at the specified pH. GUV in the phosphate buffer alone was used as background for the spectra with GUV.

As shown in Figure 2-17B, GUV did not affect the overall CD spectra of PP-75 compared to PLP. The far UV region of PP-75 in the presence of GUV was similar to PP-75 alone at pH 7.4 with a comparable maximum value at 198 nm. The reason of this result may be that at physiological pH, PP-75 forms an ordered structure that does not interact with lipid. However, as pH was dropped to 5.1, the absorbance of polarised light of PP-75 in the presence of GUV became less prominent at 198 nm (Figure 2-17C). This observation could be due to the enhanced membrane interaction of PP-75 at pH 5.1 where the polymer-membrane interaction became more prominent as the negative charge on PP-75 reduce. This interaction, in turn, affected the packing of PP-75 and made the optically active amide groups oriented in a less orderly fashion.

2.3.5.2 Intracellular Delivery of Membrane Impermeable Fluorophore

The intracellular delivery efficiency was measured by enhanced uptake of membrane impermeable fluorescent calcein dye in the presence of polymer. Flow cytometry was used to quantify the increase in fluorescent signal in HeLa cells. As shown in Figure 2-18, PLP increases calcein uptake slightly compared to control while PP-50 increases calcein uptake significantly. The results in HeLa cells were comparable to what was previous reported (Chen *et al.*, 2009). Interestingly, the hybrid polymer PPW-50 was as effective as PP-50 in enhancing intracellular delivery of calcein at 1 mg/mL and incubated for 24 hours in HeLa cells despite having a lower grafting percentage at 37.4% compared to 46.0% in PP-50 (Figure 2-18). It was previously reported by Chen et al., that the increase in grafting percentage of Phe positively corresponded to higher intracellular delivery efficiency in modified PLP. Therefore, the fact that PPW-50 at lower grafting percentage and a less hydrophobic amino acid modifier could achieve high calcein intracellular delivery efficiency further confirmed that aromatic side chains of the grafted amino acid had a major role in the intracellular delivery efficiency of the resulting polymer.

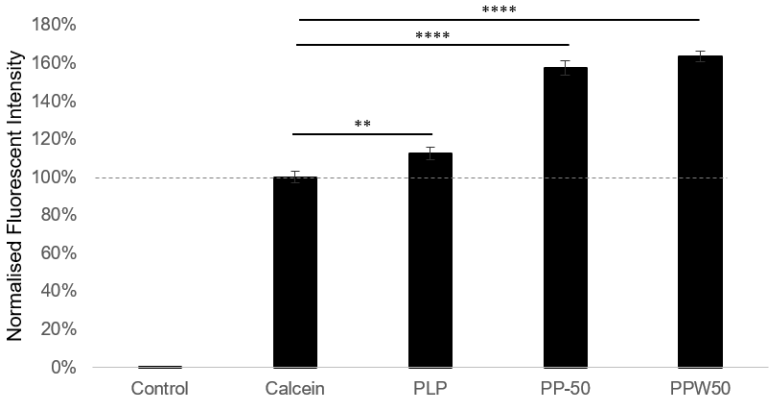

Figure 2-18: Intracelluar calcein concentration of HeLa cells determined by flow cytometry. HeLa cells were incubated with 2mM of calcein in the presence or absence of 1 mg/mL of polymer for 24 hours. Cells without calcein incubation were used as control. The fluorescent signal was normalised to calcein only without polymer (n=3). ** ($p = 0.0048$); **** ($p < 0.0001$).

2.4 Conclusion

PLP was confirmed by various characterisation methods to be similar to that previously reported (Chen, 2007; Khormaee, 2009). CD and SANS were new methods applied for the first time to characterise PLP. It was revealed that PLP forms an optically active helical secondary structure that is 200 Å by length. As pH decreases from physiological norm, the length of PLP remains the same while the macrostructure of the polymer changes. Based on the SANS data, a larger bundle rod structure as pH decrease was proposed. The proposed structure shown in Figure 2-15 did not deviate to much from the data collected. Therefore, it is likely that the previous hypothesis that PLP is a flexible polymer chain at pH 7.4 and condense into a globular structure at lower pH may not be accurate.

PG-50 studies provided evidence that steric hindrance of the amino acid side chain somewhat affects the grafting efficiency. Although Gly grafting did not significantly affect the polymer secondary structure, it does increase the transition pH slightly. As shown by SANS and CD data, PP-50 had a significant different secondary structure compared to PLP and it also forms a lamellar macrostructure. The formation of a larger lamellar macrostructure could potentially be an important factor for PP polymers to be a more effective membrane disruptive agent at its transition pH compared to PLP.

Hybrid PPW-50 polymer was the first time two amino acids were used simultaneously to modify PLP polymer. The grafting percentages of Phe and Trp were similar to if Phe and Trp were used individually. Despite having a lower overall grafting percentage PPW-50 had comparable intracellular delivery activity as PP-50 in HeLa cells. The result suggested that an aromatic amino acid has large impact on the effectiveness of modified PLP as an intracellular delivery agent.

This study did reveal new information on the structure of PLP and how modification could affect the resulting polymer. However, more in-depth studies are still warranted to reveal the exact structure of PLP and the mechanism of how PLP disrupts lipid membranes.

Chapter 3 THE EFFECTS OF CHIRALITY ON THE STRUCTURE AND FUNCTIONALITY OF PH-RESPONSIVE DELIVERY POLYMERS

3.1 Introduction

3.1.1 Chirality and Enantiomers

Nature consists of complex and sophisticated macromolecular structures for tasks such as information storage, support of tissue and localised chemical catalysis. Despite the large amount of resources and researchers devoted to achieving the same goal using synthetic systems, nucleic acid and proteins still outperform man-made materials. Nature utilises the self-assembly of both low- and high-molecular weight compounds as the building block for various biological architectures. The most common structural components relied on are the α-helix and β-sheets of peptides. These secondary structures along with steric, hydrophobic, electrostatic, and hydrogen bonding interactions give rise to the tertiary structure of proteins that provide the foundation of life. The smallest component, amino acids, contain different information through the form of chirality. In fact, the biological system relies heavily on chiral molecules such as L-amino acids and D-sugars (Hein and Blackmond, 2012).

A chiral molecule is a molecule that is non-superimposable on its mirror image. Chiral molecules consist of at least one chiral centre that is commonly induced by an asymmetrical carbon. The mirror image or images of a chiral molecule are called enantiomers. Enantiomers have the same chemical formula and the same functional groups but they all have a unique absolute configuration. The configuration of a chiral molecule could be described differently based on the entity's geometry or its ability to rotate plane-polarised light, which is a common technique to study chirality (Kelly and Price, 2000). Take the most common amino acid in the biological system, α-amino acid, as an example. The α-carbon of amino acids is the chiral centre except for glycine. The absolute configuration of amino acid could be defined by the Cahn-Ingold-Prelog system where the four groups attached to the α-carbon is described either clockwise (R) or counterclockwise (S) (Wang *et al.*, 2017). Amino acids could also be described by

relative configuration derived from Fischer's research in glyceraldehyde. The amino acid can be assigned the dextrorotatory (D)- or levorotatory (L)- configuration depending on how the chiral centre is arranged relative to chiral glyceraldehydes. Coincidentally, the assignment, D- and L-amino acids also rotated the polarised light clockwise and counterclockwise, respectively. Amino acids in the mammalian cells are almost exclusively the L enantiomers (Hein and Blackmond, 2012; Wang *et al.*, 2017).

The importance of using enantiomers to study macrostructures is that different enantiomers could result in different structure or activity. For example, only one enantiomer of a drug may be active because the cell receptors recognise distinct structure even when the molecules contain the same chemical composition (Nguyen, He and Pham-Huy, 2006). Using different enantiomers as starting material could provide additional insight in how synthetic polymers such as PLP and PP-50 form macrostructures and how that affect their interaction with the biological system. In this study L- and D-lysine were used to synthesise PLP while L- and D-phenylalanine were used to modify PLPs. The resulting polymers were characterised and studied *in vitro* to provide further insight for how PLP and PP-50 function.

3.2 Materials and Methods

3.2.1 Materials

Chemicals were purchased from Sigma Aldrich and biological reagents for cell culture were purchased from Thermo Fisher/Invitrogen if not otherwise specified.

3.2.2 Synthesis and Characterisation of PLP Enantiomers

Poly (lysine *iso*-phthalamide) (PLP) was synthesised as described in CHAPTER 2, section 2.2.2 Synthesis of Poly (L-Lysine Iso-phthalamide), except L-lysine was replaced

with D-lysine or equal amounts of L-lysine and D-lysine for poly (D-lysine iso-phthalamide) PLP-D and poly (L- and D-lysine *iso*-phthalamide) (PLP-L-D) respectively. Polymers were de-protected and purified as described in the previously and the characterisation methods are described below.

3.2.3 Synthesis and Characterisation of 50% Phenylalanine Modified Poly (Lysine Iso-phthalamide) Enantiomers

PLP-L and PLP-D were each used as the backbone to synthesise PP-50 polymers. The reaction was carried out as described in CHAPTER 2, section 2.2.3 Amino Acid Modified Poly (L-Lysine *Iso*-phthalamide) except the amount of PLP used was reduced to 1 g per reaction with all other chemicals and solvents reduced accordingly. Two enantiomers of Phenylalanine (Phe) were used separately in combination with PLP-L and PLP-D to yield four types of PP-50. The PP-50 were assigned as PP-50-L-L, PP-50-L-D, PP-50-D-L and PP-50-D-D where the first letter after PP-50 is the configuration of Phe and the second being the configuration of PLP backbone. Polymers were purified and treated as described in the previous chapter.

3.2.4 Characterisation of polymers

3.2.4.1 ^{1}H-NMR

Polymers in acidic form were dissolved in DMSO-d_6 and characterised by Bucker Advance 500 MHz NMR spectroscopy (Bruker Biospin GmbH, Germany). The ^{1}H-NMR spectra were processed through peak picking and integration with MNova software (Mestrelab Research, Spain).

3.2.4.2 Fourier Transform Infrared Spectroscopy (FTIR)

Absorption spectra of PLP polymers were collected using a Thermo Nicolet Nexus 870 spectrometer (Waltham, MA, USA) as the average of 32 scans with a wavenumber resolution of 4 cm^{-1} in the 600-4000 cm^{-1} range. As a control, unmodified PLPs were used to be compared to modified polymers.

3.2.4.3 Size exclusive chromatography (SEC)

The SEC experiment was performed according to Dabai *et al*. using polystyrene (PS) as a standard using a 300 mm long, 7.5 mm i.d., PS/polydivinylbenzene-packed, Mixed D size exclusion column (Polymer Laboratories, UK) with 1-mehtyl-2-pyrrolidinone (NMP) as the mobile phase at flow rate of 0.5 mL/min and 80 ºC. Signal detection was measured by a Knauer diode array Smartline 2600 detector with UV absorbance at 270, 300, 350, and 370 nm (Herod *et al.*, 2000; Dabai *et al.*, 2014). The standard curve was constructed using PS at molecular weight (MW) ranging from 580 to $5x10^6$ Da. A linear relationship between the log of MW and elution time was established.

3.2.4.4 Measuring Transition pH of Polymers Through Turbidity

Polymers were each dissolved in DI water to make 10 mg/mL polymer stock solution. PB at different pHs were prepared by first making 0.1 M PB with corresponding amount of phosphoric acid, sodium phosphate monobasic and sodium phosphate dibasic. The pHs of the stock solutions were measured by a pH meter (n=3). The polymer solutions were added to PB buffer at various pH in a 1:10 dilution to make 1 mg/mL final concentration in clear Eppendorf semi-micro Vis cuvette (Eppendorf, UK). The UV spectra of the solutions were measured at 460 nm with a BMG Labtech SPECTROStar Nano (BMG, Allmendgruen, Germany).

3.2.4.5 Circular Dichroism Spectroscopy

Circular dichroism (CD) is a powerful spectroscopic technique utilising left- and right-handed polarised light to determine asymmetrical structures in molecules. It was commonly used to determine the secondary structure of macromolecules such as proteins and the helical sense of synthetic polymers (Freskgaard *et al.*, 1994; Miyahara, Nakatsuji and Sugiyama, 2013; Zhang and Deng, 2016).

Stock solutions of polymers were prepared by dissolving lyophilised polymers in their sodium form in DI water at 1 mg/mL. PB at different pHs were prepared by first making stock solution of 0.1 M PB with corresponding amount of phosphoric acid, sodium phosphate monobasic and sodium phosphate dibasic. The pHs of the stock solutions were measured by a pH meter (n=3) before diluted with DI water into 10 mM PB solution. Stock polymer solution were added to 10 mM PB at the corresponding pH for CD measurements with a final polymer concentration of 0.1 mg/mL. Spectra were recorded at 25ºC on an Aviv model 410 circular dichroism spectrophotometer (Aviv Instruments, Lakewood, NJ, USA). Far UV-spectra were scanned from 185 nm to 260 nm while near UV-spectra were scanned from 260 nm to 320 nm. Data was collected for every 1-nm interval and averaged for 5 seconds. Each of the final spectra was the result of averaging three scans. All spectra were baseline corrected and smoothed with Aviv 540 software (Aviv Instruments, Lakewood, NJ, USA). 10 mM PB of the tested pH were measured and used as blank for baseline correction. Mean Residual Ellipticities (MRS) were calculated with the following formula.

$$[\theta]_{MRW,\lambda} = N \times MRW \times \theta_\lambda / 10 \times c \times d \qquad \textbf{Function 3-1}$$

The θ_λ is the ellipticity measured in millidegrees at a given wavelength, *d* is the length of the cell in centimeters, *c* is the polymer concentration in grams per liter. The Mean Residue Weight (MRW) is the polymer subunit molecular weight. N is the number of peptide bonds in the PLP or PLP-based polymer per subunit. Grafting percentages were taken into account for modified PLP polymers (Kelly, Jess and Price, 2005). Protein A, a protein with three alpha-helix residues commonly used to purify or detect immunoglobulins, was used at 0.1 mg/mL as a model to compare to PP-50 enantiomers

(Kessler, 1975). The average molecular weight of amino acid was used for MWR while N=1 were used as parameters to calculate the MRS for protein A. The calculated MRW spectrum of protein A was inversed while comparing to PP-50-L-L and PP-50-D-L.

3.2.4.6 Small Angle Neutron Scattering (SANS)

SANS experiments were conducted in the same condition as described in CHAPTER 2, section 2.4.6 Small Angle Neutron Scattering (SANS). Enantiomers of PLP and PP-50 were each conducted in the conditions same as PLP and PP-50.

3.2.4.7 Cell Culture

HeLa cells were handled, passaged and maintained as described in CHAPTER 2, using the same cell line, reagents, and conditions.

3.2.4.8 Biological Activities of Polymers

3.2.4.8.1 Flow Cytometry for Fluorescence Measurement

Calcein (a membrane impermeable fluorophore) was used as a tracer molecule to monitor the effect of polymer intracellular delivery efficiency. Disodium calcein salt was dissolved in PBS to make 200 mM stock solution. HeLa cells were seeded in 24-well plates at $5x10^4$ cells/mL in 0.5 mL supplemented DMEM to full confluence in 24 hours followed by incubation with 0.22 μm filter-sterilised supplemented media and 2 mM calcein in the presence or absence of polymers. Cells were washed twice with PBS, trypsinised and resuspended in phenol red-free DMEM supplemented with FBS spun down at 0.2 g for 5 minutes. The supernatant was removed and the cell pallets were resuspended in phenol red- and FBS-free DMEM and transferred into a Titertube 1 mL micro test tube (Bio-Rad,

UK). Cells were analysed by Cytek DxP8 cell sorter (Cytek Bioscience, USA) with 10,000 event count measuring side scattering and fluorescent intensity at various emission wavelengths. The results were processed by FlowJo software (Cytek Bioscience, USA) by quantifying fluorescent intensity of the gated cells. All experiments were conducted in triplicates.

3.2.4.8.2 Confocal Microscopy

HeLa cells were incubated in supplemented DMEM for 48 hours before the experiment in a 4-well 1.8 cm^2 chambered cover glass system (Nunc, UK) at $5x10^4$ cells/well and 500 μL/well. Cells were first washed twice with PBS and incubated with phenol red- and FBS-free DMEM in the presence or absence of 2 mM calcein for 24 hours with or without polymers. Cells were then washed twice with PBS and incubated with 5 μg/mL Hoecht 33342 and 5 μg/mL PI in phenol red- and FBS-free DMEM for 20 minutes. Subsequently, cells were washed again twice with PBS before phenol red-free DMEM was added to each well and imaged under confocal microscopy.

3.2.4.9 Measuring Cytotoxicity of Polymers

Cytotoxicity of polymer in HeLa cells was determined by commercially available MTS assays. The assay is a standard colorimetric method for determining the number of viable cells under proliferation. The active chemicals are a novel tetrazolium compound [3-(4,5-dimethylthiazol-2-yl)-5-(3-carboxymethoxyphenyl)-2-(4-sulfophenyl)-2H-tetrazolium; MTS] and an electron-coupling reagent (ohenazine ethosulfate; PES). The MTS tetrazolium compound is reduced by metabolically active cells to a colored formazan product that could be quantified at an absorbance of 490 nm by a spectrophotometer. The absorbance of the formazan product and viable cells within the range of the cell concentrations was a linear relationship. Therefore, the reduction of cellular metabolic activity of HeLa cells, followed by polymer or chemical exposures, was determined by MTS assay. The assay was performed according to the manufacturer's protocol.

Experiments were performed in six repeats. The spectra were recorded using a BMG Labtech SPECTROStar Nano plate reader (BMG, Allmendgruen, Germany).

3.3 Results and Discussion

3.3.1 PLP enantiomers

In this study, the effect of lysine enantiomers (L- or D-) has on the resulting polymer PLP-L, PLP-D, and PLP-L-D were studied (Figure 3-1). Polymers were synthesised and characterised with various methods to study how the PLP enantiomers differ and elucidate additional information on how the polymers interact with the biological system.

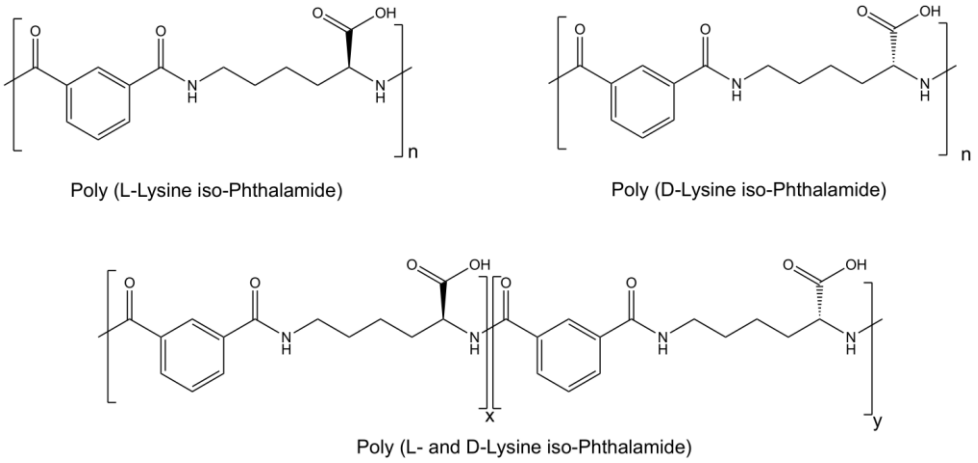

Figure 3-1: Chemical structure of PLP-L, PLP-D, and PLP-L-D. The Chiral centers on the α-carbon of lysine were specified and assigned either L or D. The total of x and y subunit in PLP-L-D is equal to n.

3.3.1.1 Synthesis of PLP enantiomers

L-lysine, D-lysine, or an equal molar amount of L-lysine and D-lysine were used separately to synthesise PLP-L, PLP-D and PLP-L-D. All three PLP enantiomers, PLP-L, PLP-D, and PLP-L-D, were synthesised, purified, and lyophilised in the same conditions as described in the materials and methods section to yield white solids. There were no observable differences in the color, texture, or yield of the three polymers throughout the syntheses and purification processes. Five characterisation methods including ^{1}H-NMR,

FTIR, SEC, CD, and SANS were applied to characterise the three polymers and the results would be reported in the sections below. In addition to the above-mentioned characterization methods, the three polymers were each tested *in vitro* with membrane impermeable fluorophore, calcein, for their intracellular delivery activities and biocompatibility with MTS metabolic assay.

3.3.1.2 Characterisation of PLP enantiomers

3.3.1.2.1 ^{1}H-NMR of PLPs

The three PLP enantiomers, PLP-L, PLP-D, and PLP-L-D, were each characterised by ^{1}H-NMR and shown to have identical peaks at δ 1.28-1.50 (g, -CH_2-), 3.26 (f, -CH2-), 4.38 (h, -CH-), 7.5 (c, bezene-H), 7.9 – 8.02 (b, d, H-benzene-H), 8.32 (a, benzene-H), 8.56 - 8.76 (e, i, -NH-) (Figure 3-2). The peaks agreed with what was previously reported by Ecclestion *et al.* and in Chapter 2 of this study. Integrated ratios of the peaks obtained through ^{1}H-NMR for the three polymers were calculated to be similar which proved further evidence that the three polymers have similar proton distributions and environments. There were two observable differences in the NMR spectra of the three PLPs which are peaks at 3.3 ppm and 12.7 ppm. The first peak at around 3.3 ppm corresponded to water residue in the polymer samples or solvent that are typical in H-NMR preparations. The peak should not be taken into account for determining polymer chemical structures in the case of PLP. The second peak at 12.7 ppm was the proton on the pendant carboxylate group of PLP that are commonly affected by hydrogen bonding and the pH environment. The peaks at the chemical shifts that high are usually weak and neglected for determining proton molar ratio due to its high variability.

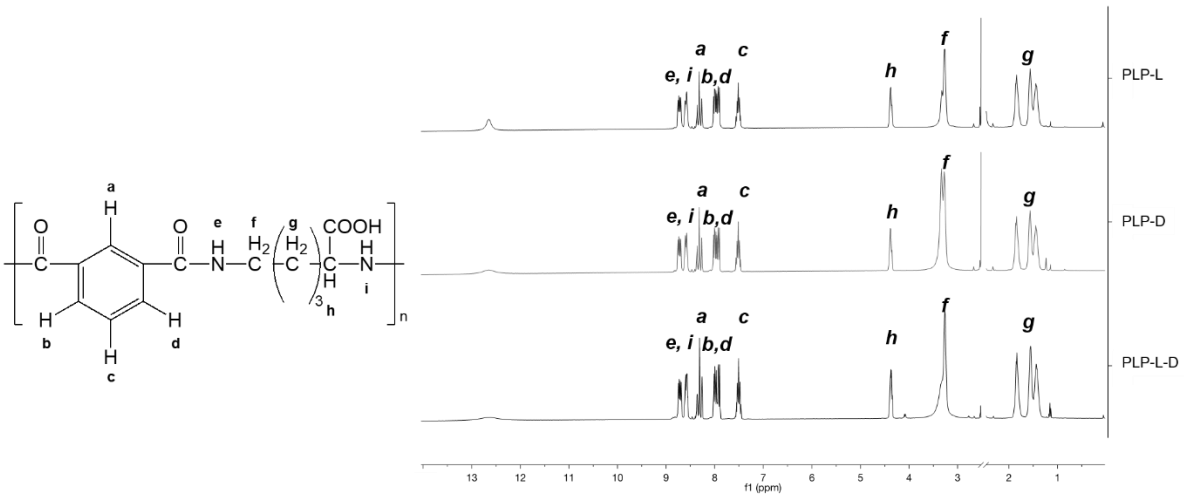

Figure 3-2: Chemical structure of PLP and ^{1}H-NMR Spectra of PLP-L, PLP-D, and PLP-L-D in DMSO-D_6. The protons on the chemical structure of PLP were each assigned to a legend and labelled on the ^{1}H-NMR spectrum. The DMSO peak at 2.5 ppm was removed for better visualisation.

3.3.1.2.2 FTIR of PLP enantiomers

FTIR was applied to characterise the three PLPs as additional evidence for their chemical structure. As shown in Figure 3-3, the three FTIR spectra of PLP-L, PLP-D, and PLP-L-D, in the respected order, all absorbed at key wavenumbers corresponding to N-H and O-H stretch (3300 cm^{-1}), carboxylic acid C=O stretch (1710 cm^{-1}), amide band I (1630 cm^{-1}), amide band II (1530 cm^{-1}), and C-O stretch (1270 cm^{-1}). The data suggested that all three polymers contain the above mentioned functional groups at the respected peaks assigned. Both ^{1}H-NMR and FTIR results strongly suggested that the three polymers have the same proton distribution and functional groups. Therefore, the three polymers could be concluded to have the same chemical formula. Note that NMR and FTIR both does not have the capability to distinguish enantiomers. To determine whether the three polymers are structurally different, CD and SANS were applied to elucidate further information about the three PLP polymers.

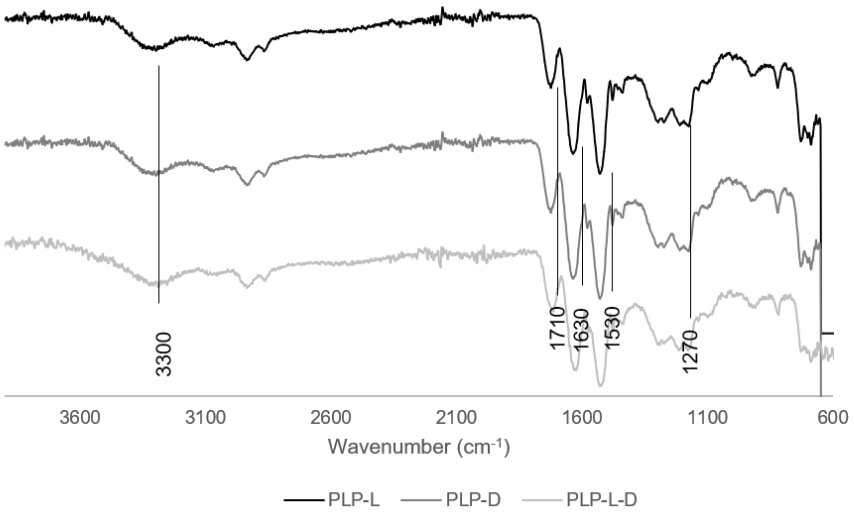

Figure 3-3: FTIR spectrum of PLP-L, PLP-D, and PLP-L-D. Peaks labelled were assigned to the appropriate functional groups of PLP. The spectrum of each polymer was color coded and listed below the horizontal axis label.

3.3.1.2.3 Size Exclusion Chromatography of PLP enantiomers

SEC was conducted to determine the molecular weight of all three polymers. As mentioned in the previous chapter, the SEC system used in this study was not the optimal system to characterise PLP and PLP-derived polymers. The SEC data could, however, be a useful reference to compare the size of the three PLP enantiomers and their poly dispersity. As shown in Figure 3-4, the three PLPs had very similar retention time with a large peak at approximately 12 minutes and a small peak at around 22 minutes. Based on the SEC data, PLP-L, PLP-D, and PLP-L-D had very similar size, distribution, and poly dispersity at 1.87, 1.85, and 1.99. respectively. This data suggested that the three PLPs adopt structures similar in size in the NMP solution. This data supported the theory that the three PLP enantiomers have similar size and macrostructures in solution.

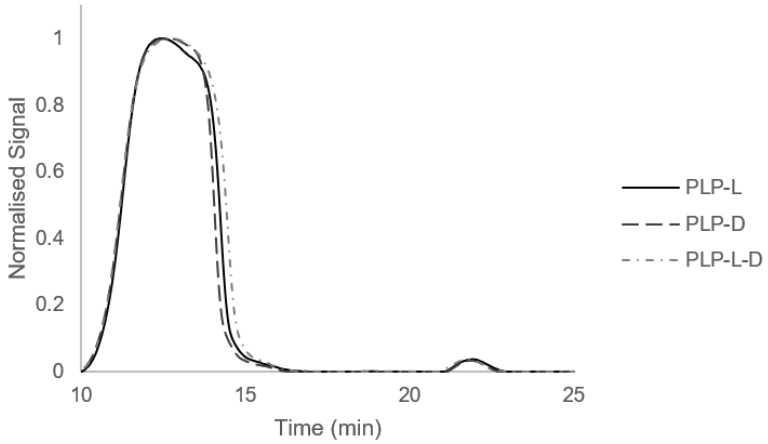

	Mn (kDa)	Mw (kDa)	PDI
PLP-L	472.39	882.24	1.87
PLP-D	503.89	931.85	1.85
PLP-L-D	462.86	919.90	1.99

Figure 3-4: Size exclusive chromatography spectrum of PLP-L, PLP-D, and PLP-L-D. Molecular weight and polydispersity for each of the three PLPs were determined by comparing to a standard curve constructed by PS and results are presented in the table below the spectra.

3.3.1.2.4 Measuring the Transition pH of PLPs by Turbidity

One of the important characters of PLP is its pH responsiveness. As determined in the previous chapter, PLP has a transition pH in PB at approximately 3.7. Using the same experimental setup, the transition of the three PLPs were determined. As shown in Figure 3-5, transition pHs of PLP-L, PLP-D, and PLP-L-D were determined to be 4.2, 4.0, and 3.6 respectively (n=3). This was surprising as the three PLPs were characterised to have the same chemical formulation, functional group and polydispersity. Transition pH of PLP-L was also previously determined to be 3.7, which is 0.5 apart from what was determined in this study. However, PLP-L and PLP-D had very close transition pH which was expected. PLP-L-D on the other hand, had a much lower transition pH. As previously mentioned, the aggregation of PLP is caused by the decrease in inter- and intra-molecular ionic repulsions. PLP-L-D might have similar structure to the other two PLPs, but because the alternating L- and D-lysine may cause the packing of PLP-L-D to require higher enthalpy compared to its two other enantiomers which resulted in the lower transition pH.

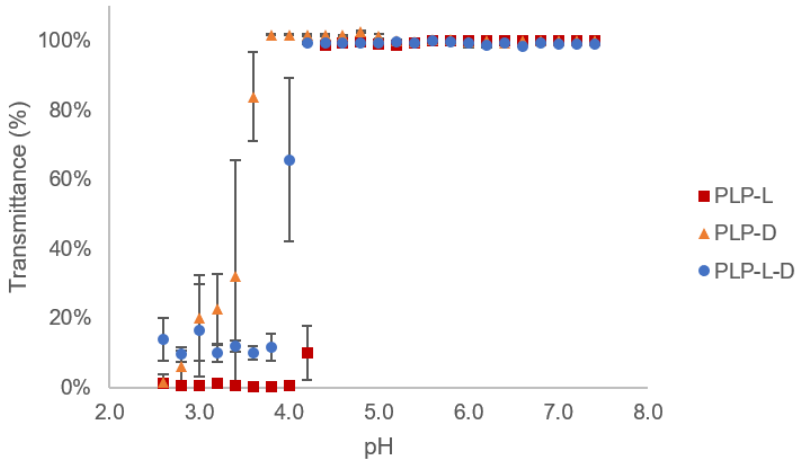

Figure 3-5: Variation of the turbidity of PLP-L, PLP-D, and PLP-L-D in different pH conditions. The turbidity of polymers in phosphate buffer at pH between 2.5 and 7.8 were measured at λ = 460 nm. Each data point was derived from three replicates. Error bars represent standard error.

3.3.1.2.5 Circular Dichroism

All three PLP enantiomers were characterised by CD spectroscopy at three different pHs between wavelength 185 nm to 320 nm. The spectra were separated into two different regions, the far- and near-UV regions, based on common methods used to analyse protein and peptide CD spectra. The far UV region (185 to 260 nm) is usually dominated by amide bonds and the near UV region (260 to 320 nm) by aromatic functional groups. As shown in Figure 3-6A, far-UV spectra of PLP-L and PLP-D were mirror images. This indicated that the two chemically identical polymers both have asymmetrical centres but with different chiralities. The structure of PLP-L was hypothesised to be a helical coil supported by CD and SANS discussed in Chapter 2. For coil structures, the direction, either clockwise or anti-clockwise, of which the coil is formed is defined as sense (Yashima *et al.*, 2009). And logically in PLP synthesis, using L-lysine would produce a helix of one sense while using D-lysine would produce a helix with the opposite sense since *iso*-phthalic acid linker contains no chiral centre. Therefore, the CD spectra provided strong evidence that PLP-D adopted a helical structure of opposite sense to PLP-L. On the other hand, PLP-L-D which was synthesised using equal molar ratio of L-lysine and D-lysine as starting material, had no prominent CD spectrum in the far UV region at pH 7.4, 6.0, and 4.0. There are two possible explanations for the lack of CD signal in the far

UV region for PLP-L-D. First, PLP-L-D may lack the secondary helical structure like the other two PLPS that is oriented to exhibit CD signal. This phenomenon could be observed in proteins that were denatured either by high temperature or detergent and lost their secondary structure (Kelly, Jess and Price, 2005; Greenfield, 2006). To parallel this lack of CD signal in proteins with PLP-L-D, the L- and D-lysine mixture might have induced the polymer to adopt a random coil formation. The second hypothesis is that the L- and D-lysine regions each form micro-domain of opposite sense within the polymer resulting in destructive interference of CD signal. This phenomenon was well documented in synthetic chirality- induced helical polymers such as polyacetylenes. The polymer backbone forms into helical domains with opposite sense in water but could be induced into a single sense by adding chiral solvents (Yashima and Katsuhiro, 2007). As the L- and D-lysines are chemically identical, there is no direct way to prove the lysine distribution in the PLP polymer. In other words, there is no simple method to determine whether L-lysine and D- lysine alternate in each subunit or form sub-regions where L-lysine-based subunits repeat for a number of times before a D-lysine sub-region occur in the PLP-L-D linear polymer.

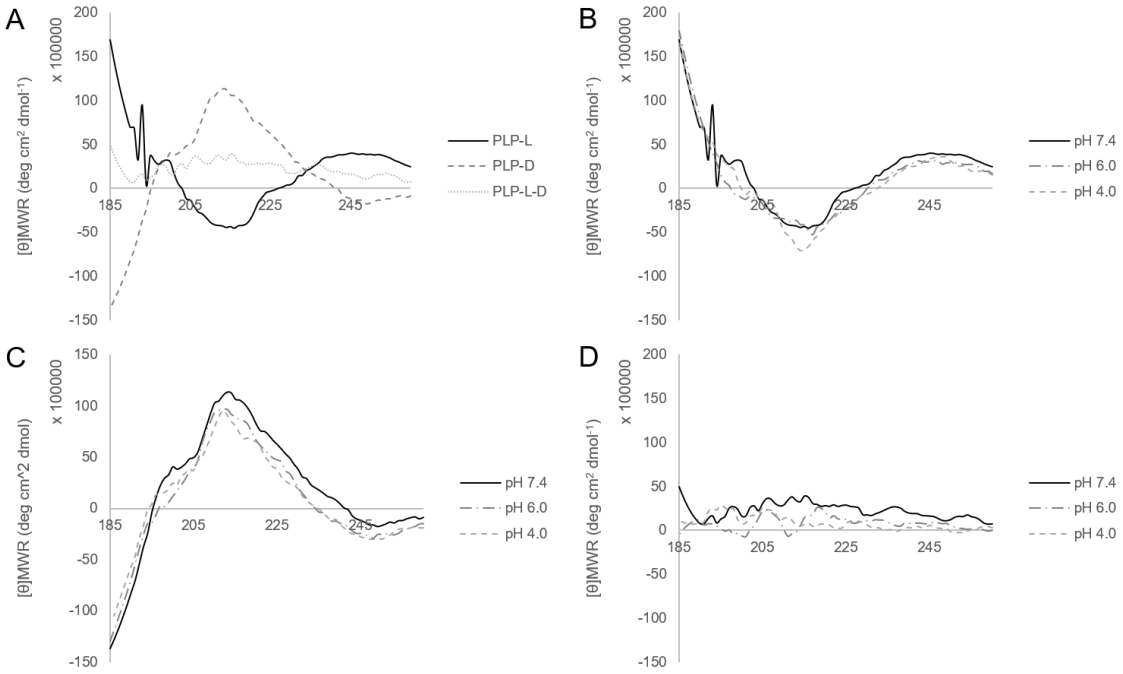

Figure 3-6: Far UV Circular Dichroism spectra of A) an overlay of PLP-L, PLP-D, and PLP-L-D at pH 7.4. B) CD spectra of PLP-L C) PLP-D, and D) PLP-L-D at three different pHs. Polymers were analysed at 0.1 mg/mL in phosphate buffer at the specified pH between 185 and 260 nm.

The two hypotheses could, however, be indirectly proven by analysing the structural data obtained by SANS in a later section. When the PLP polymer lacks secondary structure, it could be more flexible and take up a random coil conformation which should in theory have a larger volume in solution.

As previously mentioned, far UV region of CD spectra could provide useful structural and environmental data of the aromatic groups in different conditions (Kelly and Price, 2000; Kelly, Jess and Price, 2005; Greenfield, 2006). As shown in Figure 3-7A, the three PLP enantiomers had similar CD spectra at pH 7.4 between 285 to 320 nm. This indicated that the aromatic ring in the three polymers have similar orientation and neighbouring environment even when all three polymers had very different CD spectra in the far-UV region (Kelly and Price, 2000; Kelly, Jess and Price, 2005). Additionally, the three polymers all respond to pH change similarly in the near-UV region (Figure 3-7). All three polymers had inversed signals when the pH was changed to 6.0 and 4.0 while the spectra at the lower pH were very similar. This observation is interesting as the three

polymers all have transition pH at approximately 4, but the spectra were inversed at pH 6.0. Therefore, despite having different secondary structure, the aromatic component of three polymers were oriented in similar fashion and respond to pH changes in a similar fashion.

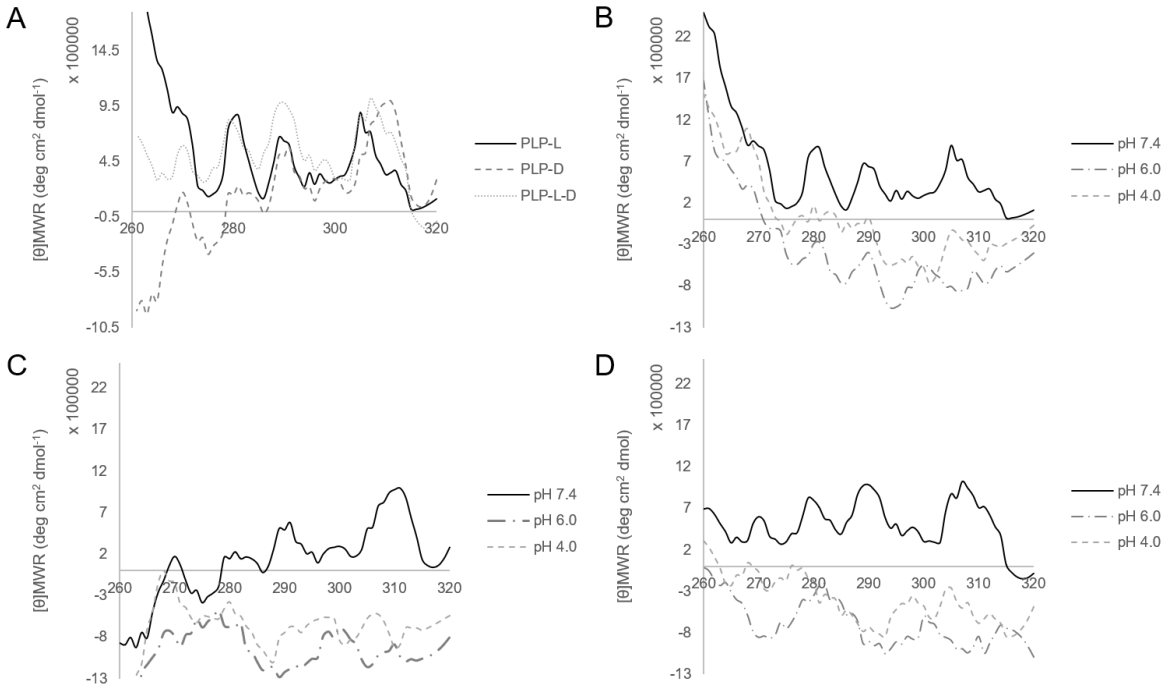

Figure 3-7: Near UV Circular Dichroism spectra of A) an overlay of PLP-L, PLP-D, and PLP-L-D at pH 7.4. B) CD spectra of PLP-L C) PLP-D, and D) PLP-L-D at various pHs. Polymers were analysed at 0.1 mg/mL in phosphate buffer at the specified pH between 260 and 320 nm.

3.3.1.2.6 SANS data analyses for PLP enantiomers

SANS data was obtained to determine the dimension of different PLP enantiomers and compare the structural differences at a high resolution. As shown in Figure 3-8, the three polymers have very similar spectrum at pH 7.4. The intermediate region indicated that all three polymers adopted a cylindrical shape at pH 7.4, which is similar to the helical structure of PLP discussed in CHAPTER 2. differences of the three spectra are mainly in the low-Q region (Q<0.01) where, in the case of PLPs, the ratio of length and radius was determined. As shown in Table 3-1, all three PLP enantiomers adopted a cylinder structure with approximately the same length (within 10%) compared to PLP-L at around

200 nm. However, there were some variabilities in the low Q region, indicating that the radius of PLP-D and PLP-L-D rods were slightly smaller than that of PLP-L. According to the models, PLP-D and PLP-L-D had diameter of 8.2 Å and 8.5 Å respectively. As there were a lot of variability in low Q region of PLP-D and PLP-L-D, it is difficult to conclude whether the measurement was accurate and whether the derived radius was a true representation of PLP-D and PLP-L-D at pH 7.4.

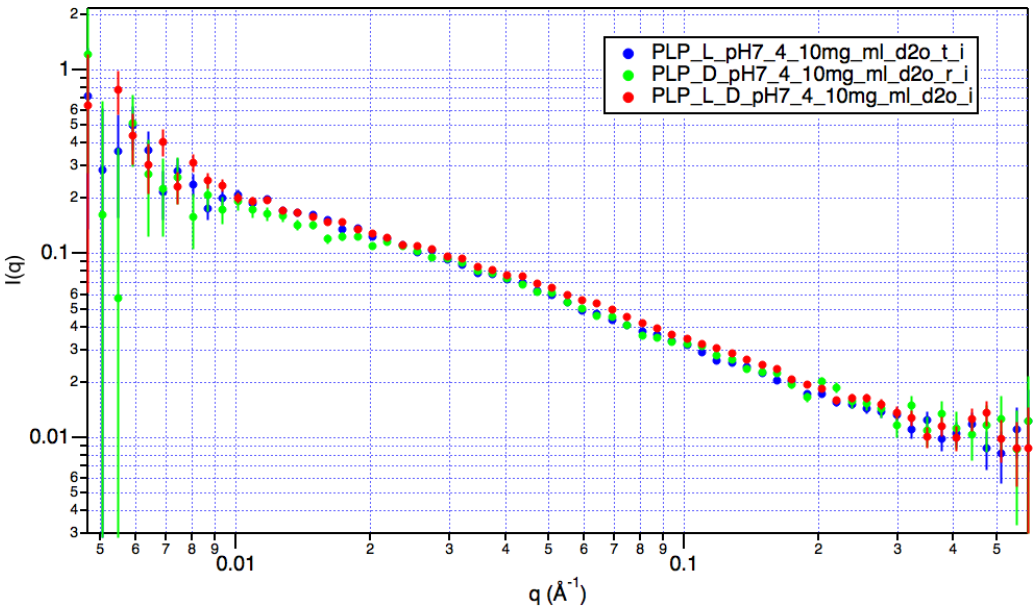

Figure 3-8: SANS spectra of PLP-L, PLP-D, and PLP-L-D at pH 7.4 in deuterated phosphate buffer solution. Deuterated phosphate buffer at selected pH was used as background. Spectra were fitted with the best matching models to determine the shape and dimensions of the polymer in solution. The simulated model and dimensions are presented in the Table 3-1.

pH	PLP-L	PLP-D	PLP-L-D
Form	Cylinder	Cylinder	Cylinder
Length (Å)	200	178	226
Diameter (Å)	14	8.2	8.5
Volume Fraction	0.002	0.0036	0.0014
SLD (10^{-6})	1	1	1

Table 3-1: The list of proposed dimensions of PLP enantiomers at pH 7.4 compared to SANS predicted dimensions. The dimensions were derived from models that were simulated to best fit the SANS spectra of PLP enantiomers shown in Figure 3-8.

The three PLP enantiomers were also studied at pH 6.1 and 4.1 to compare the pH-induced conformational changes. As shown in Figure 3-9, pH affected the low Q region and the high Q region of the SANS spectrum of PLP-L. The changes translated to an increase in the diameter as the pH decreases. As discussed in the previous chapter, it is hypothesised that the individual rods bundle to form a larger rod, and as pH decrease, more rods form an even larger bundle. The projected dimensions of PLP-L could be found in Table 3-2.

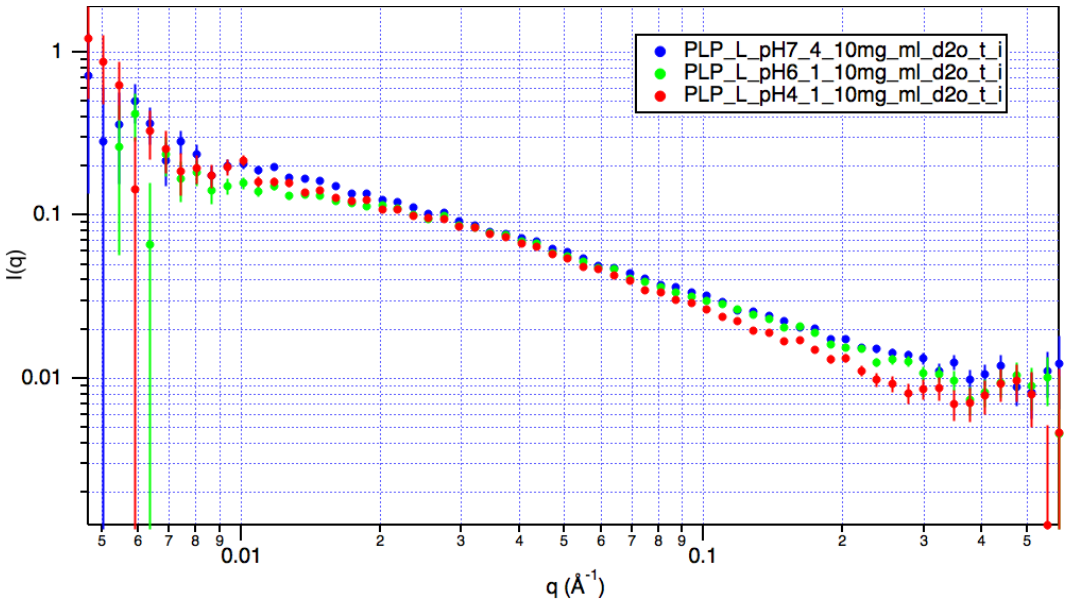

Figure 3-9: SANS spectra of PLP-L at pH 7.4, 6.1 and 4.1 in deuterated phosphate buffer solution. Deuterated phosphate buffer at selected pH was used as background. Spectra were fitted with the best matching models to determine the shape and dimensions of the polymer in solution. The simulated model and dimensions are presented in the Table 3-2.

pH	4.1	6.1	7.4
Form	Cylinder	Cylinder	Cylinder
Length (Å)	200	200	200
Diameter (Å)	21	16	14
Volume Fraction	0.0009	0.0015	0.002
SLD (10^{-6})	1	1	1

Table 3-2: The list of dimensions and projected structures of PLP-L at three pHs. The dimensions were derived from models that were simulated to best fit the SANS spectra shown in Figure 3-9.

As shown in Figure 3-9, similar to PLP-L, PLP-D forms a rod structure and the dimensions were affected by a change in pH. The observation of decrease of intensity in the high Q region on the right side of Figure 3-9 was similar to what was observed in the spectra of

PLP-L at the three pHs. The predicted dimensions of PLP-D's structure in deuterated phosphate buffer can be found in Table 3-3. As shown in the table, the length and diameter of the PLP-D rod slightly increase as pH decreases. Interestingly, the low Q region of PLP-D did not change to the extent as PLP-L did and along with an increase in rod length, the PLP-D diameter did not increase as significantly. As described earlier, the dimensions of the assigned shape were derived from a model that best fit the spectra and may, in some cases, deviate from the true form of the polymer in solution. For PLP-D, if the length were fixed at 200 nm, the diameters of PLP-D at the three pHs would be comparable to the diameters predicted for PLP-L and would fit the bundle-aggregation theory. The theory was proposed in CHAPTER2 where the smaller individual PLP rods does not change conformation as pH changes, but aggregates into a larger bundle resulting in the observed diameter increase.

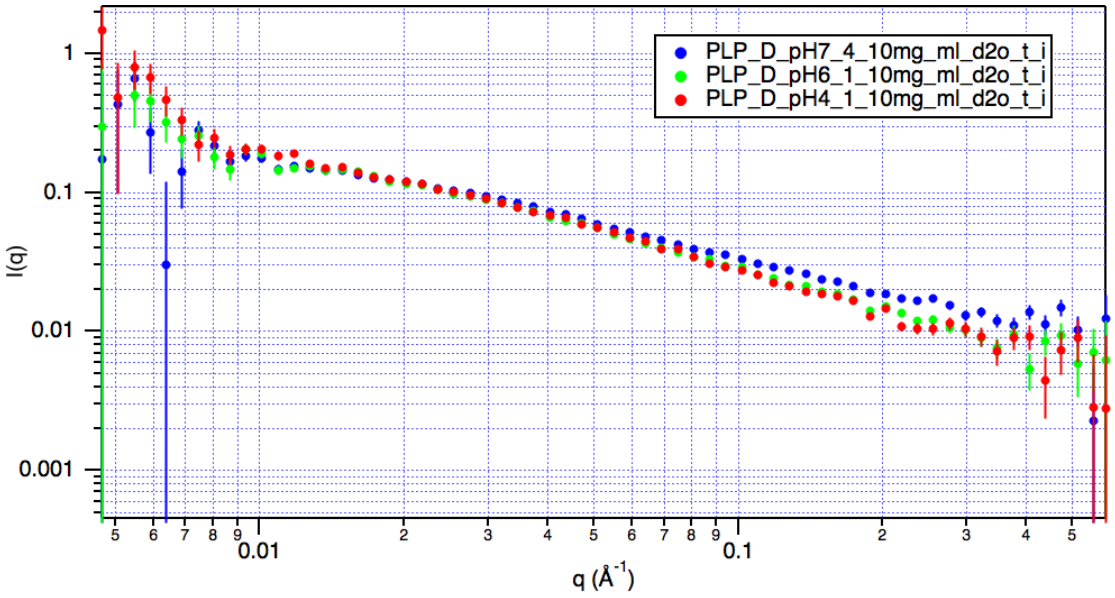

Figure 3-10: SANS spectra of PLP-D at pH 7.4, 6.1 and 4.1 in deuterated phosphate buffer solution. Deuterated phosphate buffer at selected pH was used as background. Spectra were fitted with the best matching models to determine the shape and dimensions of the polymer in solution. The simulated model and dimensions are presented in the Table 3-3.

pH	4.1	6.1	7.4
Form	Cylinder	Cylinder	Cylinder
Length (Å)	219	213	178
Diameter (Å)	10.1	9.2	8.2
Volume Fraction	0.00093	0.0011	0.0036
SLD (10^{-6})	1	1	1

Table 3-3: The list of dimensions and projected structures of PLP-D at three pHs. The dimensions were derived from models that were simulated to best fit the SANS spectra shown in Figure 3-10.

In the case of PLP-L-D, the polymer forms cylindrical polymers at all three tested pHs. At pH 7.4, the length was in the 200 Å range with diameter at 8.5 nm according to model that best fit the SANS spectrum (Table 3-4). Notable changes were observed in the high Q region similar to PLP-L and PLP-D as the pH decreases. Interestingly, the change in the low Q region was more significant than both PLP-L and PLP-D. Judging from the change in slope at the low Q region, notably larger structures that are potentially aggregates were observed (Figure 3-11). It is not surprising as PLPs were previously determined to precipitate at pH below the transition pH at around 4. Limited by the models chosen, the projected diameter may slightly deviate from the actual diameter of the objects. Even with a less precise diameter, a trend of increase in diameter of the cylinder as pH decreases could still be observed (Table 3-4). Like PLP-D, the observation in PLP- L-D also provide evidence to support the bundle-aggregation theory.

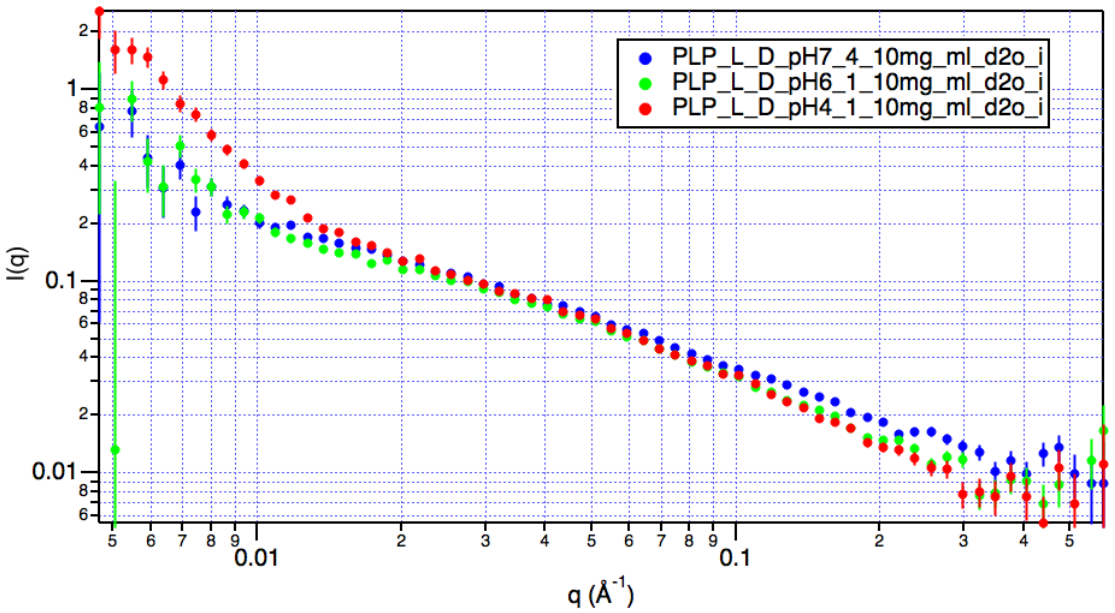

Figure 3-11: SANS spectra of PLP-L-D at pH 7.4, 6.1 and 4.1 in deuterated phosphate buffer solution. Deuterated phosphate buffer at selected pH was used as background. Spectra were fitted with the best matching models to determine the shape and dimensions of the polymer in solution. The simulated model and dimensions are presented in the Table 3-3.

pH	4.1	6.1	7.4
Form	Cylinder/ Aggregates	Cylinder	Cylinder
Length (Å)	200	220	226
Diameter (Å)	20	9.7	8.5
Volume Fraction	0.001	0.001	0.0014
SLD (10^{-6})	1	1	1

Table 3-4: The list of dimensions and projected structures of PLP-L-D at three pHs. The dimensions were derived from models that were simulated to best fit the SANS spectra shown in Figure 3-11.

3.3.1.3 Biological Activities of PLP enantiomers

The biological activities of PLP enantiomers were studied in the aspect of how efficient are PLPs in facilitating intracellular delivery of membrane impermeable fluorescent dye and how cytotoxic are the PLPs at different concentration and incubation time.

3.3.1.3.1 Intracellular Delivery Efficiency of PLPs

Membrane impermeable calcein was used to evaluate the intracellular delivery efficiency of PLPs in HeLa cells. 2 mM of calcein was co-incubated with PLP-L, PLP-D, PLP-L-D or equal amount of PLP-L and -D for 24 hours. As shown in Figure 3-12, all the PLPs were able to increase intracellular calcein concentration of HeLa cells by at least 10%. There was no significant difference in delivery efficiency observed between the four conditions. This suggested that the PLP intracellular delivery mechanism was not helical-sense sensitive. In other words, HeLa cells may not have discriminated between clockwise or counterclockwise helical PLP enantiomers that were implied through CD spectroscopy data. This observation could indicate two scenarios. Firstly, the interaction of the cell and polymer may not be receptor-mediated. The reason being cell surface receptors tend to have high specificity and can usually distinguish between enantiomers. The fact that all the PLPs had similar intracellular delivery efficiencies suggested that the role of discriminative receptors mediating the delivery may be minimal. Secondly, the difference in sense of the helix did not affect the overall interaction of the polymer and cell. It may be the case that when the polymers bundle into a larger cylindrical structure as proposed in this thesis, the helical sense would not distinctive enough to be recognised by the HeLa cell. This is to say that the scale of the sense may be too small for the HeLa cell to perceive as different. The fact that PLP-L-D and equal amount of PLP-L and PLP-D had comparable intracellular delivery with PLP-L and PLP-D strongly supports these two theories, but would require more in-depth studies to confirm each scenario.

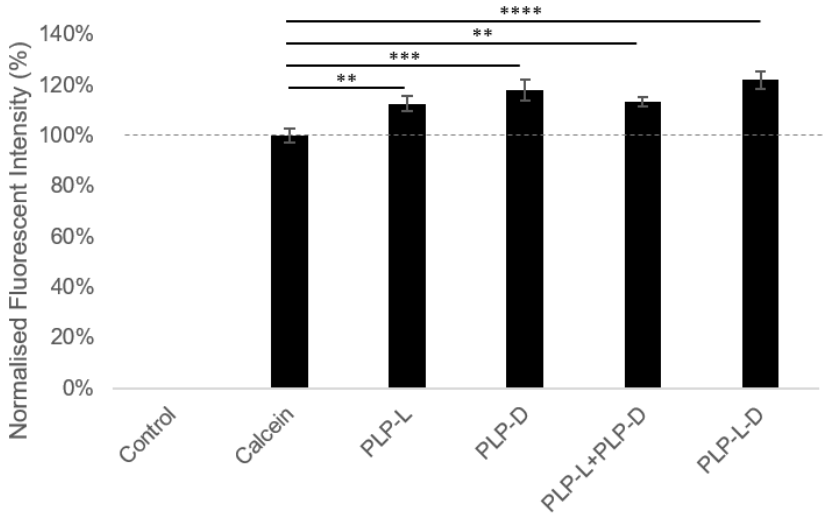

Figure 3-12: Intracelluar calcein concentration of HeLa cells with or without PLP polymers determined by flow cytometry. HeLa cells were incubated with 2mM of calcein in the presence or absence of 1 mg/mL of polymer for 24 hours. PLP-L+PLP-D represented condition using total polymer concentration of 1 mg/mL using equal amounts of PLP-L and PLP-D. Cells without calcein incubation were used as control. The fluorescent signal was normalised to calcein only without polymer. Data were derived from three replicates. Error bars represent standard error. ** ($p < 0.004$); *** ($p = 0.0002$); **** ($p < 0.0001$).

3.3.1.3.2 Biocompatibility of PLP

The biocompatibility of PLPs were determined by assessing metabolic activities of HeLa cell after 12 and 24 hours incubation with PLPs using a commercially available MTS assay (Chen, 2007; Mercado, 2016). As shown in Figure 3-13A, the three PLPs were all well tolerated by HeLa cells even at concentration as high as 10 mg/mL. Interestingly, all three PLPs raised the signal at 10 mg/mL which may not necessarily reflect an increase in the metabolic activity of HeLa cells. As MTS assay rely on the absorbance of formazan as 490 nm, where aromatic groups in PLP could potentially interfere. Concentration-related effect was not observed in PLP-L at 12-hour incubation, however, PLP-D and PLP-L-D had the most effect on cell metabolic activity at 2 mg/mL and 5 mg/mL respectively. A more significant impact on the cell metabolic activity could be observed after 24 hours of PLP incubation but all three polymers were still well tolerable at 2 mg/mL (Figure 3-13B). From the MTS assay result, PLP-L, PLP-D, and PLP-L-D had very similar toxicity profile in HeLa cells and seem to be well tolerated at 10 mg/mL and 2 mg/mL for 12- and 24-hour incubations respectively.

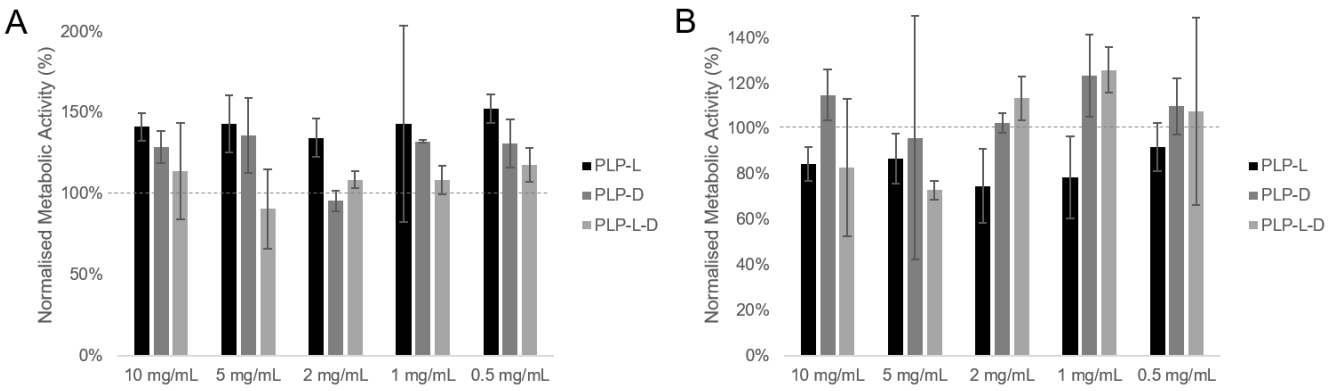

Figure 3-13: Metabolic activity of HeLa cells after incubation with PLP-L, PLP-D, or PLP-L-D at various concentrations for A) 12 hours and B) 24 hours. Data were normalised to cells incubated in the absence of polymer at the same incubation time. Data were derived from three replicates. Error bars represent standard error.

3.3.2 Syntheses and Characterisation of PP-50 Enantiomers

The parental polymer PLP was synthesised as aforementioned into three different enantiomers. Two forms of PLP, namely PLP-L and PLP-D, were used to synthesise PP-50. L-phenylalanine or D-phenylalanine were used to modify either PLP-L or PLP-D, yielding four total combinations or PP-50. The chirality of phenylalanine was listed first followed by the chirality of lysine in the nomenclature of the polymer.

L-phenylalanine grafted PLP-L (PP-50-L-L), which was referred to as PP-50 in previous chapters, was synthesised using protocols as previously described. PP-50-L-D, PP-50- D-L, and PP-50-D-D were synthesised using the same protocol but substituting L- phenylalanine for D-phenylalanine or PLP-L for PLP-D (Figure 3-14). The syntheses were also scaled down by one fifth due to limited starting material. Grafting was achieved by standard DCC reaction and subsequently purified to yield cream color solids. No observable differences during the reaction for the four PP-50s occurred. The polymers were characterised using ^{1}H-NMR and FTIR to confirm their chemical composition. The transition pH was determined by UV-vis spectrophotometry in PB at various pH and the poly-dispersity was obtained by SEC. CD and SANS were used to study the macro- and micro-structure of the four polymers in different pH conditions. Lastly, confocal microscopy, flow cytometry, and MTS assay were used to study the biological activities of the four PP-50 enantiomers.

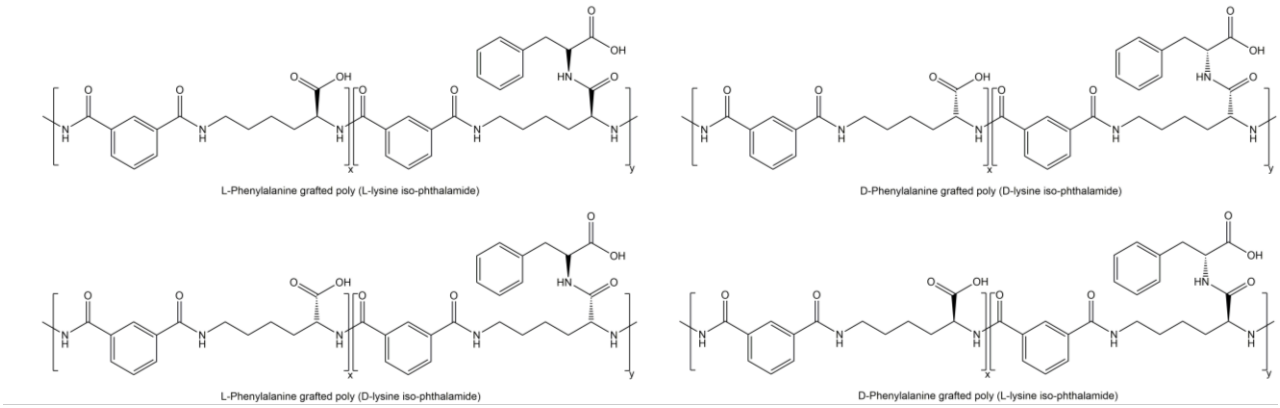

Figure 3-14: Chemical structure of PP-50-L-L, PP-50-L-D, PP-50-D-L, and PP-50-D-D. The Chiral centres on the α-carbon of lysine were specified and assigned either L or D while the chirality of the grafted phenylalanine was also specified by either L or D.

3.3.2.1 ^{1}H-NMR of PP-50 enantiomers

The four PP-50s were each characterised in DMSO-d_6 by ^{1}H-NMR and shown to have identical peaks representing the five hydrogens on the phenyl group at 7.3 ppm (Figure 3-15). The peaks agreed with what was previously reported by Chen *et al.* and in Chapter 2 of this thesis. Integrated ratios of the peaks suggested that the grafting percentage are listed in Table 3-5 below. PP-50-L-L had the highest grafting percentage of the four enantiomers at 41.4% while PP-50-L-D, PP-50-D-L, and PP-50-D-D had a grafting percentage of 30.2, 31.4, and 31.8%. As mentioned in the earlier section, the reactions other than PP-50-L-L were scaled down. The DCC grafting reaction is most efficient in anhydrous conditions and any residue of water would affect the reaction efficiency. In a scale down reaction, water in the environment, in lyophilised polymers, or dissolved in the solvent would have a greater impact due to its higher relative concentration. Judging from the grafting percentage, the relatively higher water content due to scaling down of the reaction was most likely the reason for PP-50-L-L to have the highest grafting percentage of all the four enantiomers.

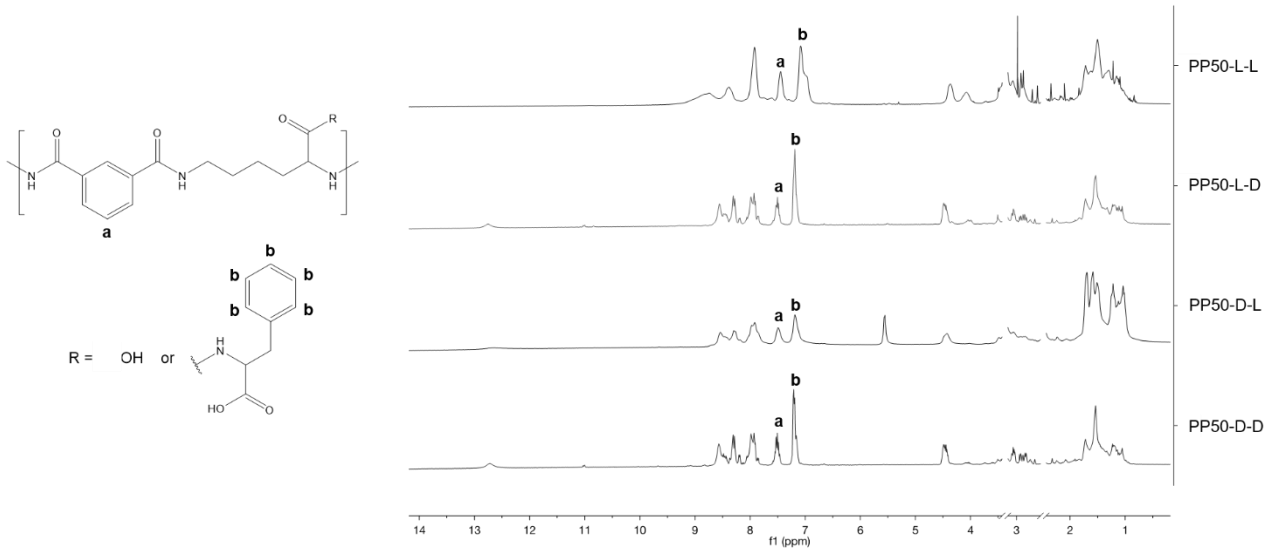

Figure 3-15: Chemical structure of PP-50 and ^{1}H-NMR Spectra of PP-50-L-L, PP-50-L-D, PP-50-D-L, and PP-50-D-D in DMSO-D_6. The protons on the chemical structure of PP-50s were each assigned to a legend and labelled on the ^{1}H-NMR spectrum. The DMSO peak at 2.5 and H_2O peak at 3.3 ppm were removed for better visualisation of the spectra.

	PP-50-L-L	PP-50-L-D	PP-50-D-L	PP-50-D-D
Integrated Ratio	1:2.07	1:1.51	1:1.57	1:1.59
Grafting Percentage	41.4%	30.2%	31.4%	31.8%

Table 3-5: Phenylalanine grafting percentage of four PP-50 enantiomers. Grafting percentages were derived from the ^{1}H-NMR spectra of PP-50 using the appropriate peaks and corresponding hydrogen molar ratios.

3.3.2.2 FTIR of PP-50 enantiomers

To further confirm the chemical structure of the four PP-50 enantiomers are consistent, they were characterised by FTIR (Figure 3-17). The spectra of the four PP-50 enantiomers exhibited similar characteristics at 3,300 cm^{-1} (N-H and O-H stretch), 2940 cm^{-1} (Methylene C-H stretch and aromatic C-H stretch), 1,630 cm^{-1} (amide band I), 1,530 cm^{-1} (amide band II), and 1,270 cm^{-1} (C-O stretch). The FTIR spectra from the four PP- 50 enantiomers agree with the ^{1}H-NMR result and strongly suggested that the four polymers had identical chemical structures.

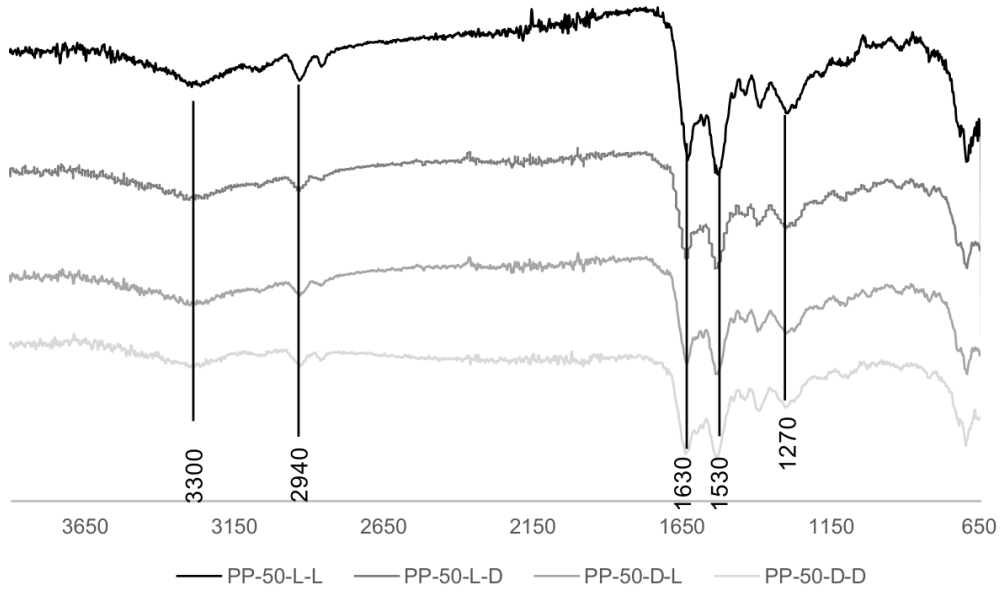

Figure 3-16: FTIR spectrum of PP-50-L-L, PP-50-L-D, PP-50-D-L, and PP-50-D-D. Peaks labelled were assigned to the appropriate functional groups of the four polymers. Key function groups were labeled on the spectra.

3.3.2.3 Size Exclusion Chromatography of PP-50s

As shown in Figure 3-17, all four PP-50s had very similar elution time at approximately 14 minutes and 22 minutes. As described in CHAPTER 2, the SEC system used for this study was not optimal for PLP-based polymer which resulted in a different molecular weight from the previously reported for PP-50 (Chen, 2007). The poly dispersity index observed indicated that PP-50-D-D had the highest variability at 2.65, PP-50-L-L was the second more poly dispersed at 2.21. PP-50-L-D and PP-50-D-L had the lowest poly dispersity of the four polymers at 2.06 and 2.09 respectively. The poly dispersity determined by SEC was higher than the PDI of PLP-L and PLP-D at approximately 1.87. This is expected as the grafting process was performed in a non-controlled fashion and longer polymer chains would receive more Phe grafting making the Mw of the chain even higher (Chen, 2007).

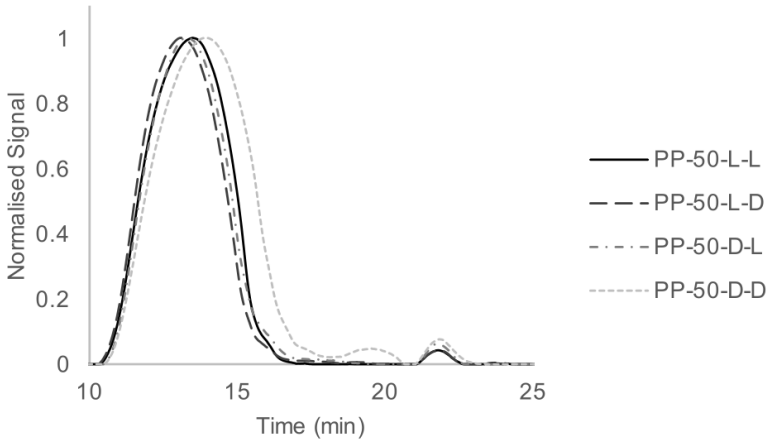

	Mn (kDa)	Mw (kDa)	PDI
PP-50-L-L	292.21	645.54	2.21
PP-50-L-D	336.02	693.63	2.06
PP-50-D-L	287.52	601.65	2.09
PP-50-D-D	212.13	562.30	2.65

Figure 3-17: Size exclusive chromatography spectrum of PP-50-L-L, PP-50-L-D, PP-50-D-L, and PP- 50-D-D. Molecular weight and polydispersity for each of the four PP-50s were determined by comparing to a standard curve constructed by PS and results are presented in the table below the spectra.

3.3.2.4 Transition pH of PP-50s

The transition pH of PP-50s were determined by UV-vis in 0.1 M PB in a wide range of pHs. Each polymer was tested three times at a given pH to determine the point where 1 mg/mL PP-50 precipitates. As shown in Figure 3-18, PP-50-D-L had the lowest transition pH at 4.8 followed by PP-50-L-L at 4.9, PP-50-D-D at 5.0 and PP-50-L-D at 5.3. This observation was surprising as PP-50-L-L should have the highest grafting percentage and in turn should have the highest transition pH. All three other PP-50s had similar grafting percentage but varied poly dispersity index. Therefore, from this experiment no pattern could be drawn for which characteristic impacted the transition pH of PP-50s. However, the experiment agreed with previous observation that by grafting hydrophobic amino acid to PLP, the transition pH of the resulting polymer could be raised (Chen, 2007).

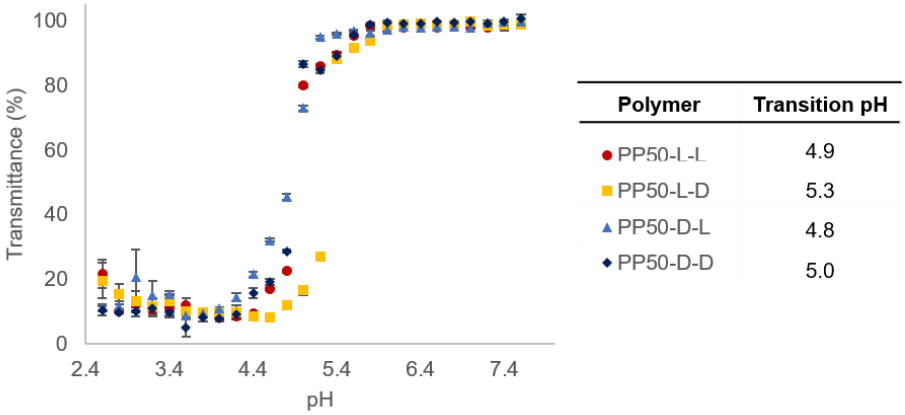

Figure 3-18: Variation of the turbidity of PP-50-L-L, PP-50-L-D, PP-50-D-L, and PP-50-D-D in different pH conditions. The turbidity of polymers in phosphate buffer at pH between 2.5 and 7.8 were measured at λ = 460 nm. Each data point was derived from three replicates. Error bars represent standard error.

3.3.2.5 CD Spectra of PP-50s

Previously in this chapter, CD was used as a tool to observe the secondary structure and determine the sense of PLP enantiomers. It was demonstrated that PLP-L and PLP-D adopted a similar rod-like structure while having the opposite sense. In this section, the far UV CD spectra of four PP-50s will be examined and discussed to understand the effect of polymer components' chirality had on the overall structure.

Shown in Figure 3-19A is the far UV spectrum of PP-50-L-L, a PLP-L grafted with L-Phe, compared to the inverse spectra of Protein A. Protein A is a well-defined triple-helix polypeptide commonly used in the purification of antibodies and the CD spectrum of the protein is well defined with 80% of the structure to be in the form of α-helix (Redmann and Rhodes, 1979; Graille *et al.*, 2000; Yashima *et al.*, 2009). Due Protein A's affinity towards immunoglobulins, it is commonly used in commercial settings to isolate and purify immunoglobulins. The spectrum of Protein A in this figure was inversed for the ease of comparison to PP-50-L-L. As seen in the figure, Protein A had two peaks at 222 and 209 nm and a strong inverse peak at 195 nm, which is typical for α-helix structure of proteins. In the same figure, PP-50-L-L had two peaks at 215 and 198 nm while having a strong inverse peak at 185 nm at pH 7.4. The spectrum pattern was somewhat similar to that of protein A but with the peaks shifted slightly further

down the far UV region and more intense. Note that the CD spectra were all corrected to a per unit basis and signal strengths were usually compared among polypeptides. Although PP-50- L-L cannot be directly compared to Protein A despite both being polyamines, it is a good referent to support that PP-50 adopts a consistent secondary structure to generate a strong CD spectrum. As shown in the Fig 3-19A, the CD signal at 215 and 198 nm of PP- 50-L-L did not change dramatically which was expected from results obtained in the previous chapter.

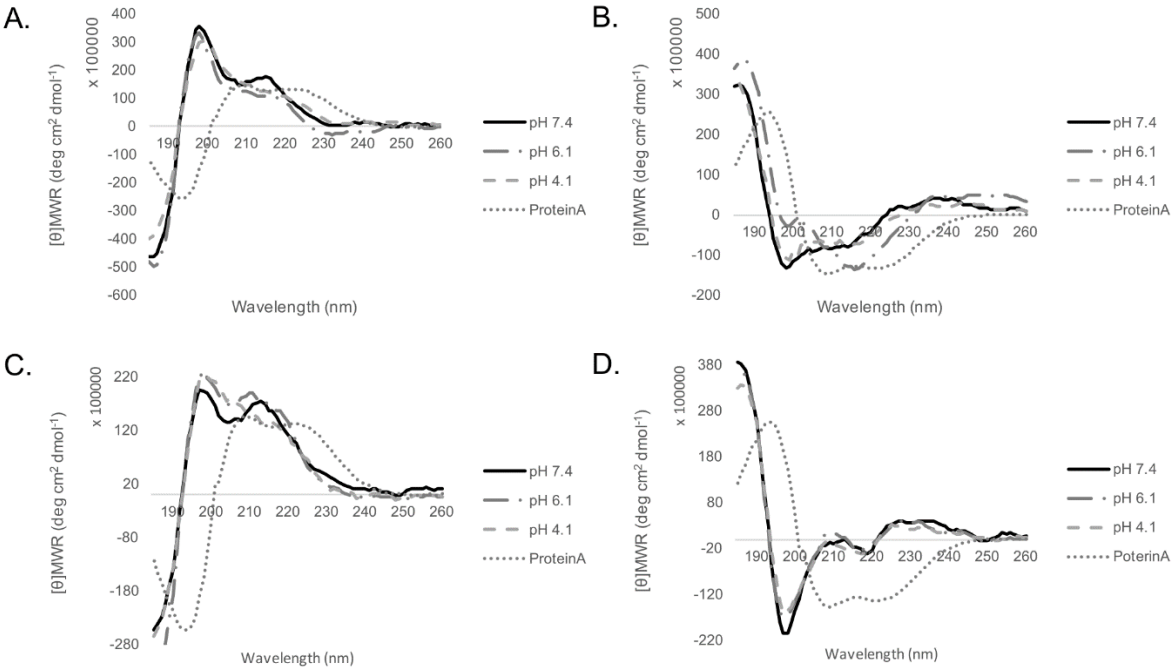

Figure 3-19: Far UV Circular Dichroism spectra of A) PP-50-L-L B) PP-50-L-D C) PP-50-D-L, and D) PP-50-D-D at three selected pHs. Protein A, a triple helix protein, was included as a reference either in its original spectrum or inversed at pH 7.4. Polymers were analysed at 0.1 mg/mL in phosphate buffer at the specified pH while protein A was analysed at 0.05 mg/mL at pH 7.4 in phosphate buffer between 185 and 260 nm.

PP-50-L-D, which is L-Phe grafted on PLP-D, similarly to PP-50-L-L had an inversed spectrum compared to its backbone. This phenomenon was observed in the previous chapter. Here with four variables of PP-50s, how the CD spectrum of PLP-based polymers are affected by grafting could be further studied. On Figure 3-19A and Figure 3-19C are PP-50s with PLP-L backbone while Figure 3-19B and Figure 3-19C are the ones with PLP-D backbone. Regardless of whether L- or D-Phe was grafted onto the backbone, the resulting PP-50 polymer had an inverse CD spectrum compare to its backbone. However, there were obvious differences in CD spectrum when comparing polymers having the same chirality for the lysine in the backbone and grafted phenylalanine. It could be observed from Figure 3-19 that PP-50-L-L and PP-50-D-D had CD spectra representing mirror images of each other while PP-50-L-D and PP-50-D-L are mirror images. The main difference of the two pairs could be seen from the peak at 198 nm where when the chirality of Phe align with Lys in the backbone had approximately two-fold increase in magnitude. This result implied that the two pair of polymers have slightly different packing patterns despite having similar chemical structure, transition pH, molecular weight, and poly dispersity. How this difference would affect the polymer microstructure and biological activity would be discussed in later sections.

3.3.2.6 SANS Spectra of PP-50s

The PP-50 enantiomers were characterised with SANS to understand how chirality of the grafted Phe and the Lys in the polymer backbone would affect the formation of secondary structure in solution. The four polymers were each studied in conditions described in CHAPTER 2 with 0.1 mM deuterated PB aqueous solutions at pH 4.1, 6.1 and 7.4.

As shown in Figure 3-20, the four PP-50 enantiomers each exhibited different spectrum at pH 7.4. As discussed in CHAPTER 2, PP-50-L-L adopted a barbell form in which two spheres cap a single long rod. PP-50-D-L at pH 7.4 had a SANS spectrum similar to PP-50-L-L, however, the best fit model suggested that the spectrum was consisted of long rods and lamellar structure. Interestingly, PP-50-L-D was determined to form a parallel

pipe structure in solution at pH 7.4 where rods were organised into a surface. This is very likely the precursor of a lamellar structure that PP-50 are capable of forming. In the case of PP-50-D-D, it was difficult to fit into a model and the closest shape determined was a cylindrical structure. The dimensions determined for the cylinder was, however, smaller compared to what was previously observed in PLPs and PP-50s. Each PP-50 enantiomers will be further discussed throughout this section.

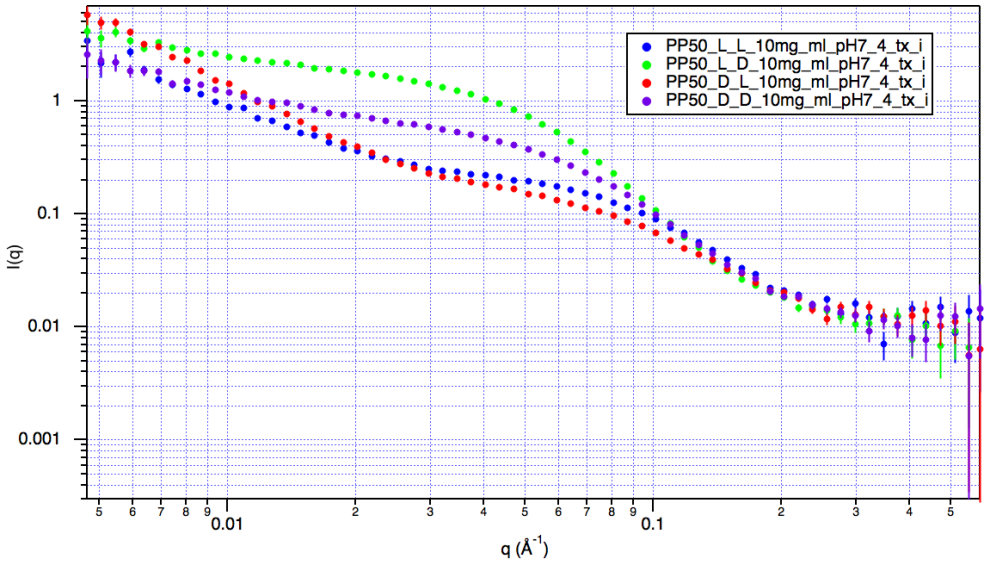

Figure 3-20: SANS spectra of four PP-50 enantiomers in deuterated phosphate buffer solution at pH 7.4. The four spectra were placed in the same graph to demonstrate the structural differences and similarities between the PP-50s.

As the SANS spectra of PP-50-L-L was discussed in CHAPTER 2, the spectra would not be repeated here in this chapter. The forms and dimension of PP-50-L-L could be found in the table below. As previously discussed, the polymer forms a barbell structure and transitioned into lamellar structure as pH decreased.

pH	4.1	6.1	7.4
Form	Lamellar	Fluid Lamellar/ Long Rods	Barbell
Length (Å)	-	240	282
Diameter (Å)	-	28	16.8
End Cap Diameter	-	-	38.9
Thickness (Å)	12	-	-

Table 3-6: The list of dimensions and projected structures of PP-50L-L at three pHs. The dimensions were derived from models that were simulated to best fit the SANS spectra shown in CHAPTER 2, Figure 2-16.

As shown in Figure 3-21, PP-50-L-D's SANS spectrum shifts in the low Q region as pH decreases which was unsurprising give PP-50-L-D was determined to be pH responsive in the previous section. However, PP-50-L-D, unlike PP-50-L-L, formed a parallel pipe structure at pH 7.4. The length of the structure was predicted to be 107 Å with width of 31 Å and height of 61.5 Å (Table 3-7). The length of the parallel pipes was shorter than what was determined for PLP-D and PP-50-L-L by a factor of 2 which was unexpected as PLP-D was the parental polymer and the total length of the modified polymer was unlikely to change.

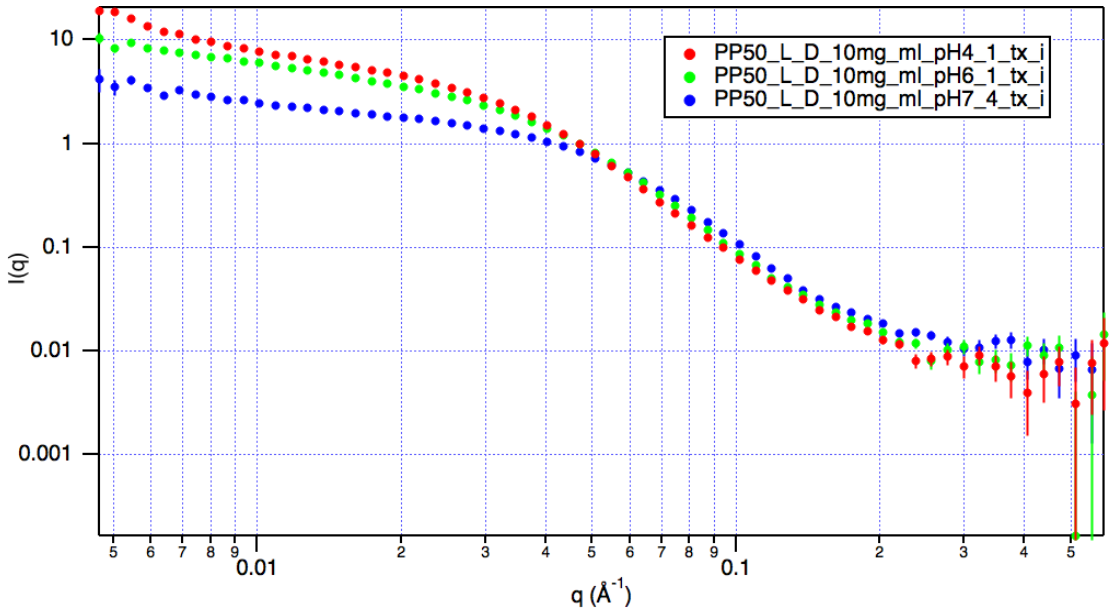

Figure 3-21: SANS spectra of PP-50-L-D at pH 7.4, 6.1 and 4.1 in deuterated phosphate buffer solution. Deuterated phosphate buffer at selected pH was used as background. Spectra were fitted with the best matching models to determine the shape and dimensions of the polymer in solution. The simulated model and dimensions are presented in the Table 3-7.

pH	4.1	6.1	7.4
Form	Lamellar/Ellipsoid	Ellipsoid	Parallel piped
Length (Å)	-	-	107
Width (Å)	-	-	31.8
Height (Å)	-	-	61.5
Thickness (Å)	10	-	-

Table 3-7: The list of dimensions and projected structures of PP-50-L-D at three pHs. The dimensions were derived from models that were simulated to best fit the SANS spectra shown in Figure 3-21.

As the pH decreases, PP-50-L-D transform into ellipsoid and ultimately a mixture of ellipsoid and lamellar structure with thickness of 10 Å at below the polymer's transition pH. The phenomenon is very similar to the transition of PP-50-L-L in different pH environments previously discussed.

For PP-50-D-L, the SANS spectra at the three pHs did not change as significantly as the two PP-50s discussed above (Figure 3-22). The structure of PP-50-D-L at pH 7.4 was projected to be a mixture of long rods and lamellar structure. Unfortunately, no reasonable result for the dimensions could be obtained from the model. As shown in Table 3-8, PP-50-D-L fully formed into lamellar structure as the pH decreased.

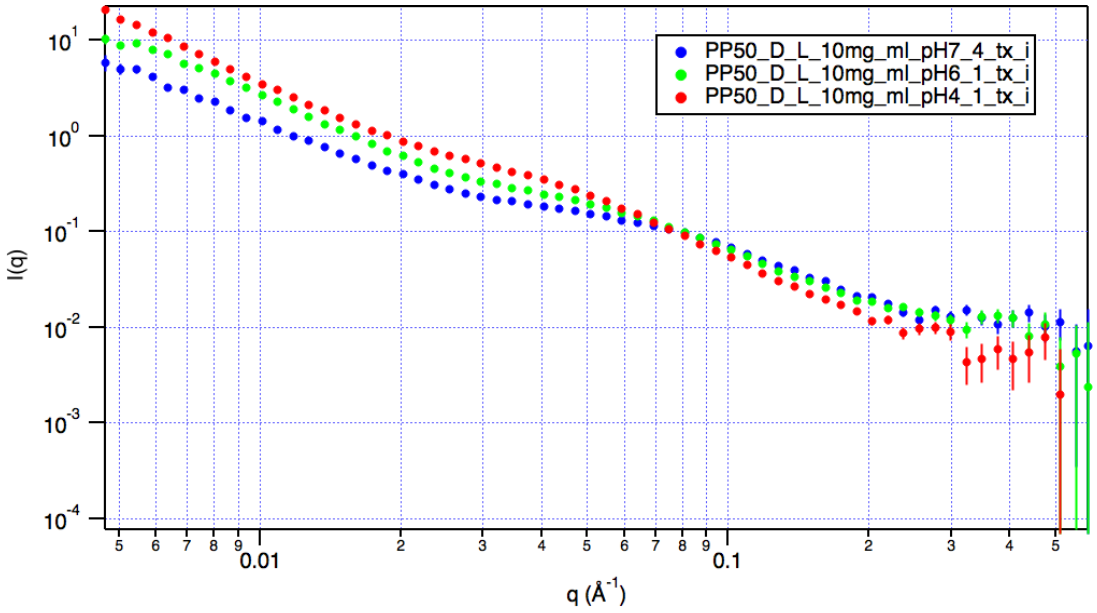

Figure 3-22: SANS spectra of PP-50-D-L at pH 7.4, 6.1 and 4.1 in deuterated phosphate buffer solution. Deuterated phosphate buffer at selected pH was used as background. Spectra were fitted with the best matching models to determine the shape and dimensions of the polymer in solution. The simulated models are presented in the Table 3-8. No reasonable dimension could be obtained from the model.

pH	4.1	6.1	7.4
Form	Lamellar	Lamellar	Lamellar/Long rods
Length (Å)	-	-	-
Diameter (Å)	-	-	-
Thickness (Å)	-	-	-

Table 3-8: The list of dimensions and projected structures of PP-50-D-L at three pHs. The forms were derived from models that were simulated to best fit the SANS spectra shown in Figure 3-22.

Lastly, PP-50-D-D was discussed in the beginning of this section to adopt a cylinder form at pH 7.4. The length assigned for the cylinder was 85 Å with a diameter of 8.6 Å which was shorter than what was observed for PLP-D and PP-50-L-L (Table 3-9). This discrepancy could be due to the fact that PP-50-D-D be a mixture of cylinder and other objects that is beyond what the single form factor model that is currently provided in the Igor software could fit to provide a accurate dimension measure (Figure 3-23). Therefore, other models may be more suitable for modelling PP-50-D-D. As shown in Figure 3-23, PP-50-D-D SANS spectra changed very significantly at pH lower than 7.4 compared to the other three PP-50s. Models suggested that PP-50-D-D formed lamellar structure as pH decreased like the three other PP-50 enantiomers.

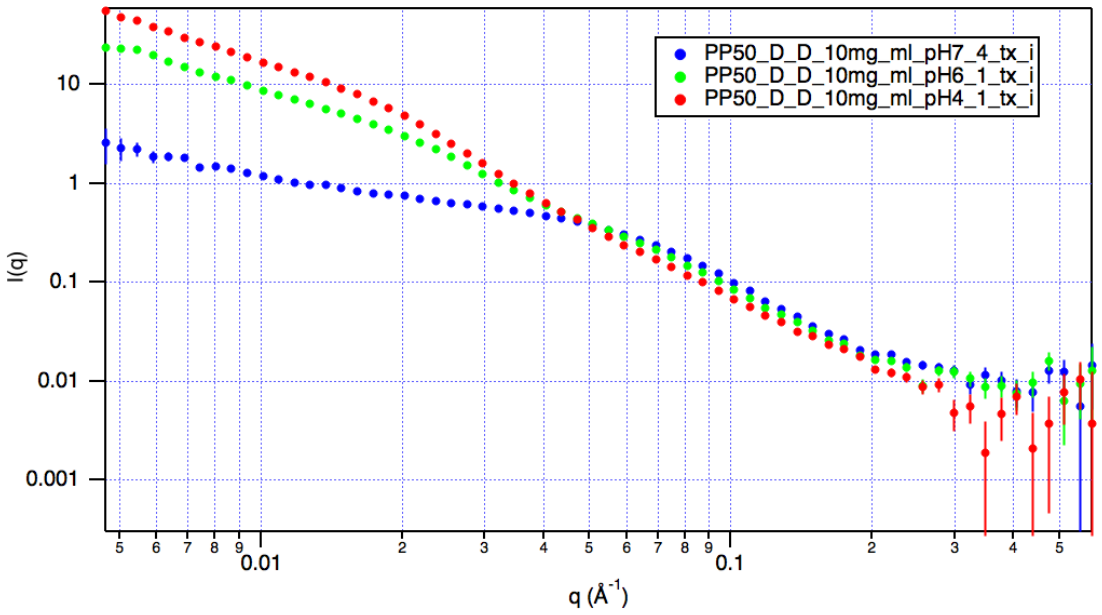

Figure 3-23: SANS spectra of PP-50-D-D at pH 7.4, 6.1 and 4.1 in deuterated phosphate buffer solution. Deuterated phosphate buffer at selected pH was used as background. Spectra were fitted with the best matching models to determine the shape and dimensions of the polymer in solution. The simulated model and dimensions are presented in the Table 3-9.

pH	4.1	6.1	7.4
Form	Lamellar	Lamellar	Rod
Length (Å)	-	-	85
Diameter (Å)	-	-	8.6
Thickness (Å)	-	-	-

Table 3-9: The list of dimensions and projected structures of PP-50-D-D at three pHs. The dimensions were derived from models that were simulated to best fit the SANS spectra shown in Figure 3-23.

Despite having somewhat different forms at pH 7.4, the four PP-50s all tend to form lamellar structure as the pH decreased. This result, along with the previously obtained turbidity result, strongly support that the four polymers are all pH responsive. It also indicated that the three other PP-50s may have similar intracellular delivery properties comparable to PP-50-L-L as forming lamellar structure was hypothesised as a key trait of efficient delivery. *In vitro* experimentation with the four polymers in HeLa cells in the following section will provide evidence to support the hypothesis.

3.3.2.7 Biological Activity of PP-50 enantiomers

3.3.2.7.1 Intracellular Calcein Delivery

The intracellular delivery efficiency of PP-50s were determined by co-incubating the polymer with a membrane impermeable fluorescent calcein. Confocal microscopy was used to determine the calcein dye distribution in HeLa cells and flow cytometry was used to quantify the amount of intracellular calein. As shown in Figure 3-24A, the blue fluorescent Hoechst 33342 dye was used to stain the nucleus of HeLa cells while calcein dye was green and encapsulated most likely in endosomes. When PP-50 polymer was co-incubated with membrane impermeable calcein, increased amount of intracellular calcein of HeLa cells could be seen. Additionally, calcein was distributed throughout HeLa cells while most intense signals were still concentrated in confined particles. This could agree with previous thought that PLP-based polymers facilitate the delivery of membrane impermeable particles through endocytosis (Eccleston *et al.*, 2000; Mercado *et al.*, 2016).

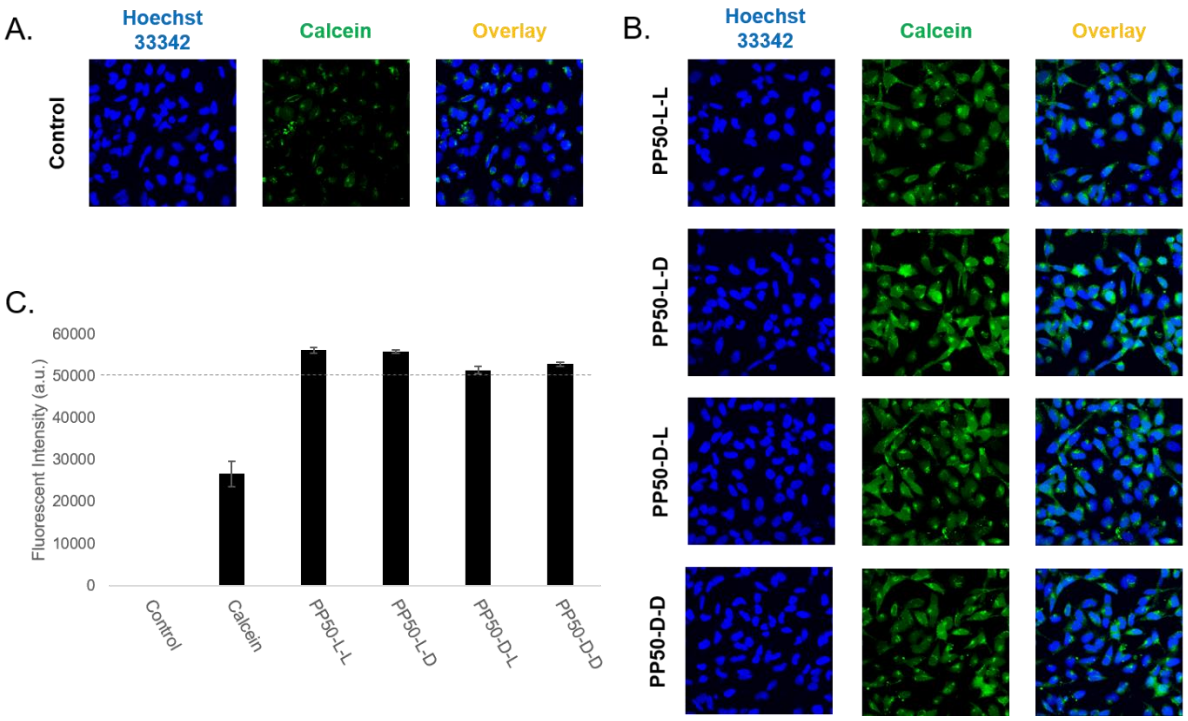

Figure 3-24: Confocal microscopy image and flow cytometry analyses of HeLa cells incubated in the presence and absence of PP-50 (1 mg/mL) for 24 hours. *A) Confocal microscopy image of cells incubated without polymer. B) Confocal microscopy image of cells incubated with PP-50 polymers. Cells were incubated with 2 mM calcein (green fluorescence) in the presence or absence of polymer and subsequently stained with 5 μg/ml Hoechst 33342 (blue fluorescence). C) Flow cytometry analyses of calcein uptake in HeLa cells in the presence or absence of PP-50 polymer after 24-hour incubation. Fluorescence was obtained using a FACScan flow cytometer. Data were derived from three replicates. Error bars represent standard error.*

Flow cytometry data in Figure 3-24C showed that the four PP-50s used to facilitate calcein intracellular delivery were effective. All four polymers were able to increase the intracellular calcein concentration by two-fold compare to calcein alone in HeLa cells after 24-hour co-incubation. As shown in the figure, PP-50-L-L and PP-50-L-D were able to increase the intracellular calcein level by the most. This is expected for PP-50-L-L as it had the highest grafting percentage compared to the three other PP-50s. The PP-50-L-D result on the other hand was surprising as it had approximately 30% grafting of D-Phe.. Despite the variation, the experiment provided evidence that all four PP-50 polymers were effective in facilitating intracellular delivery of calcein. Additionally, the data further support the possibility that forming lamellar structure is an important factor for the intracellular delivery by the PP-50 polymers.

3.3.2.7.2 Cytotoxicity of PP-50 enantiomers

Commercially available MTS assay which determines the metabolic activity of cells was used to test the cytotoxicity of PP-50 polymers at 24- or 48-hour incubation time with 2 or 5 mg/mL of polymer concentration in HeLa cells. 2 and 5 mg/mL were selected as the concentrations for the toxicity experiments as they are higher than the 1 mg/mL concentration previously used in PLP and PP-50 intracellular delivery experiments. As shown in Fig 3-25A, all four PP-50 except PP-50-L-D at 2 mg/mL was well tolerated after 24-hour of incubation in HeLa cells. PP-50-L-D was still tolerable as the cells maintained 79.89% metabolic activity compared to cells without polymers after 24 hours. However, at 5 mg/mL all four PP-50s showed dose-dependent toxicity after 24-hour incubation. Of the four PP-50s, PP-50-L-D still had the highest effect on HeLa cell metabolic activity when incubated for 24 hours.

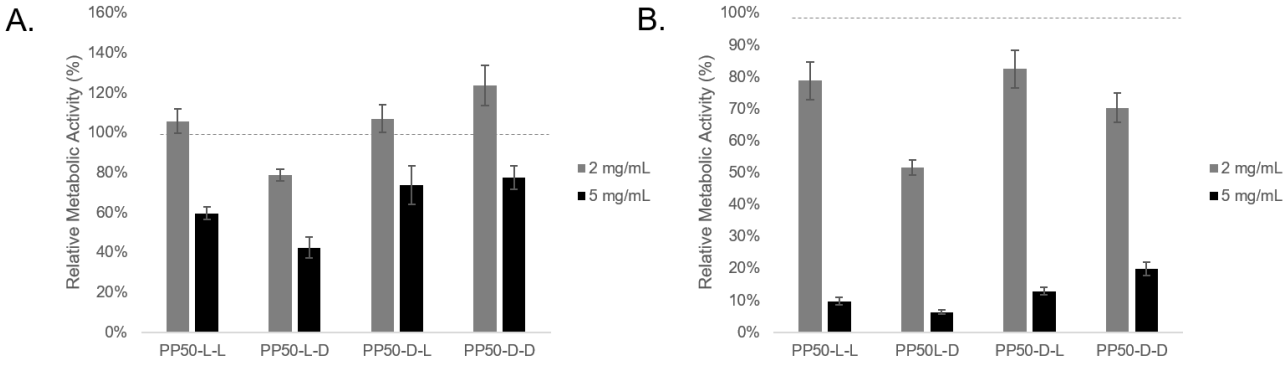

Figure 3-25: Metabolic activity of HeLa cells after incubation with PP-50-L-L, PP-50-L-D, PP-50-D-L, and PP-50-D-D at 2 mg/mL or 5 mg/mL for A) 24 hours and B) 48 hours. Data were normalised to cells incubated in the absence of polymer at the same incubation time. Data were derived from three replicates. Error bars represent standard error.

The polymers showed enhanced toxicity at 2 mg/mL when incubated with HeLa cells for 48 hours (Fig 3-25B). PP-50-L-L, PP-50-D-L, and PP-50-D-D were still tolerated by HeLa cells as the metabolic activity was still maintained above 70% compared to the control group. PP-50-L-D, interestingly, was still the most cytotixic polymer of the four PP-50s, reducing the metabolic activity of HeLa cells to 51.68% after 48-hour incubation at 2

mg/mL. When polymer concentration was increased to 5 mg/mL, all four PP-50s induced high toxicity (< 20% relative metabolic activity) in HeLa cells after 48-hour of incubation. To conclude, the four PP-50s had very similar effect on cells metabolic activity in experimented conditions and the chirality of the amino acid in the polymer backbone and grafted amino acid did not induce a significant difference. Additionally, all four PP-50s were well tolerated by HeLa cells after 24-hour of incubation. The tested concentrations were higher than the usual intracellular delivery experimental condition of below 1 mg/mL and within 24-hour incubation. Therefore, all four PP-50s could be safely applied to HeLa cells as intracellular delivery agents. To further study the impact of chirality of amino acids on the cytotoxicity of PP-50s additional commercially cytotoxicity tests such as Annexin V-FITC apoptosis assay or lactate dehydrogenase (LDH) membrane integrity assay could be applied.

3.4 Conclusion

In this chapter, three PLP and four PP-50 enantiomers were synthesised and characterised using lysine and phenylalanine isomers. The different enantiomers were used to explore the different characteristics to provide a better understanding of the polymer behavior, intracellular delivery mechanism, and cytotoxicity.

The chemical structure of PLP enantiomers were characterised by ^{1}H-NMR and FTIR and confirm to be chemically identical enantiomers. CD spectra showed that PLP-D adopted similar helical secondary structures to that of PLP-L described in the previous chapter but with the opposite sense. It was also confirmed by CD that PLP-L-D overall did not exhibit optical activity, but the optical inactivity was possibly caused by the destructive signal

addition of co-existing clockwise and counterclockwise helical domains. In addition to the CD data, SANS data confirmed that all three PLP enantiomers adopted a rod-like structure. The diameter of the three PLP enantiomers increased as pH decreased, which suggested that the three polymers respond to pH similarly to PLP and support the previously proposed theory that individual polymers bundle into larger rods at low pH. In terms of intracellular delivery efficiency and cytotoxicity, the three polymers have very similar profiles. These results indicated that the mammalian cell does not discriminate against the three PLP enantiomers and all three polymers were well tolerated.

In this study, PLP enantiomers was successfully modified by phenylalanine of different chirality, more specifically L- or D-, to yield four PP-50 enantiomers. The four PP-50 enantiomers were determined by ^{1}H-NMR and FTIR to be chemically similar but the enantiomer other than PP-50-L-L all had approximately 10% lower grafting percentages. The four polymers were subsequently determined to be pH responsive and had distinctive CD spectra in different pH environments. Although the four PP-50 enantiomers had slightly different SANS spectra, all the polymers were able to form lamellar structures below pH 6.1. Unsurprisingly, the four polymers had very similar intracellular delivery efficiency of membrane impermeable calcein in HeLa cells. The result provided additional evidence that the ability of polymers to form lamellar structures would determine the ability to deliver payload intracellularly.

In conclusion, using amino acids of different chirality to synthesise pH-responsive polymers did not affect the overall structure and characteristic. The chirality of the material also did not contribute to any observable impact to the polymer interaction with HeLa cells as the intracellular delivery profile and cytotoxicity profile of the enantiomers were comparable.

Chapter 4 THE SYNTHESIS AND CHARACTERISATION OF SECOND GENERATION PLP-LIKE POLYMERS

4.1 Introduction

4.1.1 Biomaterials

Biomaterials are defined by the Williams Dictionary of Biomaterials as the materials intended to interface with the biological systems, to evaluate, to treat, augment or replace any tissue organ or function of the body in 1999 (Williams, 1999). As the field of material science and healthcare advanced, the definition no longer could define and precisely describe all the material substances in contact with the biological system. In the materials front, as materials evolve and become ever more complex, the classical view of the three major forms, namely metallic, ceramic, and polymeric has become less applicable. On the healthcare front, materials were traditionally used as implants or grafts, but other applications such as nanoparticles for drug delivery or polymer scaffold for regenerative medicine had been redefining the field in the past two decades. Therefore, a more precise definition of biomaterials was revised by Williams as: "*A biomaterial is a substance that has been engineered to take a form which, alone or as part of a complex system, is used to direct, by control of interactions with components of living systems, the course of any therapeutic or diagnostic procedure, in human or veterinary medicine.*" (Williams, 2014). And as all materials engineered to be used to interact with the biological system, the compatibility, especially reducing adverse effect the material may generate, is crucial for the usefulness of the material.

4.1.2 Long-term cytotoxic effect of artificial polymers

The short-term toxicity effect of artificial polymers for intracellular delivery was well documented. For example, cationic gene delivery polymers were well known to be cytotoxic to mammalian cells (Lv *et al.*, 2006). Polyethylenimine (PEI), one of the most successful polymers of this class would reduce 293T cell viability by 40% with 4-hour incubation in transfection experiments(Yue *et al.*, 2011; Benjaminsen *et al.*, 2013). The toxicity may decreases the amount of potentially valuable cells but at the same time

adversely affect the remaining cells. Therefore, the importance of creating an effective delivery system that does not exhibit acute cytotoxicity or deemed biocompatible is warranted.

In the case of long-term toxicity, there is limited literature characterising the adverse effect *in vitro* which may well be due to the cost and technical difficulties associated with these studies. Other indirect effects of artificial polymers or nanoparticles that may be generated such as genetic mutation or cell receptor expression, were also not well understood. In some cases, biomaterials may induce undesirable adverse effects, for example hydroxyapatite (HAP) induces inflammatory reaction in the central nervous system that could trigger more serious downstream events that are still under investigation (Leite, Pereira and Granjeiro, 2015). Metabolites or breakdown products of polymers could also be a concern that may alter mammalian cell behaviour when materials are incubated for a prolonged period. In this study and previous publications, the short-term cytotoxicity of PLP and PLP-based polymers were well characterised and determined to be well tolerated by a number of immortalised cell lines. It is, however, concerning that the breakdown product of PLP contains water insoluble *iso*-phthalic acid. Therefore, before these potential effects could be determined, designing a polymer using soluble and known biocompatible components may provide a more desirable alternative.

4.1.3 Alternative polyamide polymers as intracellular delivery carrier

Eccleston *et la.* previously conducted a study examining the effect of different di-acids to select the optimal di-amide polymer for intracellular delivery. PLP was selected due to its high transition pH compared to other polymers. PLP also had the greatest membrane disruptive activity determined by lysis of sheep erythrocytes (Eccleston, Slater and Tighe, 1999; Eccleston *et al.*, 2005). This was, however, before the discovery that modification using hydrophobic amino acids could raise the transition pH and increase the intracellular delivery efficiency. As shown in CHAPTER 2, the L-phenylalanine (Phe) modification could increase the intracellular delivery efficiency of membrane impermeable calcein in HeLa cells by 100% compared to unmodified PLP (Figure 2-18).

Therefore, the topic of choosing the optimal di-acid for drug delivery polymer should be re-examined. In this study, the main focus would be on whether a naturally occurring di-acid, fumaric acid, could be used as the building block for an anionic pH responsive polymer like PLP. Additionally, the resulting polymer would be modified with Phe to examine whether comparable intracellular delivery efficiency to PP-50 could be achieved.

4.2 Materials and Methods

4.2.1 Materials

Chemicals were purchased from Sigma Aldrich and biological reagents for cell culture were purchased from Thermo Fisher/Invitrogen if not otherwise specified. Please refer to Chapter 2 section 2.2.1 for detail of the chemicals and reagents.

4.2.2 Synthesis of Poly (L-Lysine Fumaride)

The polymer poly (L-lysine fumaride) (PLF) was synthesised by a modified method by Eccleston *et al.* and Chen *et al.* (Chen and Natansohn, 1999; Eccleston, Slater and Tighe, 1999; Eccleston *et al.*, 2000). A schematic of the synthesis procedure and the chemical structure of PLF is provided in Figure 4-1. In a typical reaction, *L*-lysine methyl ester·2HCl (0.02 mol) and an acid acceptor, potassium carbonate (K_2CO_3 0.08 mol), were dissolved in deionised water (40 mL). The aqueous solution was placed in an ice bath and stirred with a Teflon-coated magnetic stir bar. A pre-cooled dry chloroform (3 mL) solution containing fumaryl chloride (0.02 mol) was added rapidly to the water solution. The reaction was allowed to proceed for 30 minutes, during which poly (L-lysine methyl ester fumaride) precipitated out of the solution. The polymer was transferred to a beaker containing deionised water (DI water) soaked for 3 hours. The raw material was dried overnight in a vacuum oven at 55 ºC. Dried poly (*L*-lysine methyl ester fumaride) was broken down and dissolved in DMSO. Same volume of 5 wt% NaOH solution in ethanol (2.5 molar equivalents to each poly (*L*-lysine methyl ester fumaride) subunit [MW = 226.2 Da], 1.25 M) was added slowly to the polymer solution.

The hydrolysed polymer precipitated out in 2-3 minutes and was collected by vacuum filtration and re-dissolved in DI water.

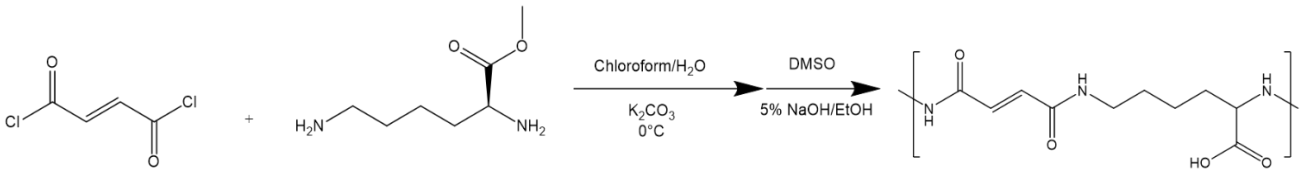

Figure 4-1: Reaction scheme for the synthesis poly (L-lysine fumaride). The synthesis is a polycondensation of L-lysine methyl ester and fumaryl chloride in Chloroform/Water solution. The resulting polymer was de-protected by NaOH solution in ethanol (EtOH).

The crude polymer solution was dialysed in Visking tubing membrane (MW cut-off 12-14 kDa) against deionised water for 1 week to remove inorganic salts, residual organic solvents, and low molecular weight oligomers. Solid impurities were removed by vacuum filtration. The pH of the solution was adjusted to 7.4 using 1M NaOH and lyophilised to yield the sodium form of poly (*L*-lysine fumaride).

4.2.3 Synthesis of Phenylalanine Modified Poly (L-Lysine Fumaride)

The grafting of L-phenylalanine onto PLF was achieved using the standard DCC promoted amide-coupling chemistry (Haslam, 1980). The experimental procedure followed the process described in CHAPTER 2, Section 2.2.3 Synthesis of Amino Acid-Modified Poly (L-Lysin Iso-Phthalamide) except for reducing all chemicals and solvents used by six-fold. The molar ratio of L-phenylalanine to available carboxylate group on PLF used in this study was 1:2 to create FP-50. Deprotection and purification steps were also carried out according to the section mentioned above.

4.2.4 PLF Polymer Characterization

4.2.4.1 ^{1}H-NMR

Polymers were dissolved in DMSO-D_6 and characterised by Bucker Advance 500 MHz NMR spectroscopy (Bruker Biospin GmbH, Germany). The ^{1}H-NMR spectrum was processed through peak picking and integration with MNova software (Mestrelab Research, Spain). The data was used to confirm polymer structure and calculate grafting percentage of modified PLP polymers.

4.2.4.2 FTIR

Absorption spectrum of PLF was collected using a Thermo Nicolet Nexus 870 spectrometer (Waltham, MA, USA) as the average of 32 scans with a wavenumber resolution of 4 cm^{-1} in the 600-4000 cm^{-1} range.

4.2.4.3 Measuring Polymer Transition pH by Turbidity

Polymers were each dissolved in DI water to make 10 mg/mL polymer stock solution. PB at different pHs were prepared by first making 0.1 M PB with corresponding amount of phosphoric acid, sodium phosphate monobasic and sodium phosphate dibasic. The pHs of the stock solutions were measured by a pH meter (n=3). The polymer solutions were added to PB buffer at various pH in a 1:10 dilution to make 1 mg/mL final concentration in clear Eppendorf semi-micro Vis cuvette (Eppendorf, UK). The UV spectra of the solutions were measured at 460 nm with a BMG Labtech SPECTROStar Nano (Allmendgruen, Germany).

4.2.4.4 Circular Dichroism

Stock solution of the polymers were prepared by dissolving lyophilised polymers in their sodium form in DI water at 1 mg/mL. Phosphate Buffer (PB) at different pHs were prepared by first making stock solution of 0.1 M PB with corresponding amount of phosphoric acid, sodium phosphate monobasic and sodium phosphate dibasic. The pHs of the stock solutions were measured by a pH meter (n=3) before diluted with DI water into 10 mM PB solution. Stock polymer solution were added to 10 mM PB at the corresponding pH for CD measurements with a final polymer concentration of 0.05 mg/mL for PLF and 0.1mg/mL for PLP. Spectra were recorded at 25ºC on an Aviv model 410 circular dichroism spectrophotometer (Aviv Instruments, Lakewood, NJ). Far UV-spectra were scanned from 185 nm to 260 nm while near UV-spectra were scanned from 260 nm to 320 nm. Data was collected for every 1-nm interval and averaged for 5 seconds. Each of the final spectra was the result of averaging three scans. All spectra were baseline corrected and smoothed with Aviv 540 software (Aviv Instruments, Lakewood, NJ). 10 mM PB of the tested pH were measured and used as blank for baseline correction. Mean Residual Ellipticities (MRS) were calculated with the following formula.

$$[\theta]_{MRW,\lambda} = N \times MRW \times \theta_\lambda / 10 \times c \times d \qquad \textbf{Function 4-1}$$

The θ_λ is the ellipticity measured in millidegrees at a given wavelength, *d* is the length of the cell in centimeters, *c* is the polymer concentration in grams per liter. The Mean Residue Weight (MRW) is the polymer subunit molecular weight. N is the number of peptide bonds in the PLP or PLF per subunit.

4.2.4.5 Small Angle Neutron Scattering (SANS)

SANS experiments were conducted in the same condition as described in CHAPTER 2, section 2.2.4.6 Small Angle Neutron Scattering (SANS).

4.2.5 Biological Activities

4.2.5.1 Cell Culture

Cells were handled and maintained as described in CHAPTER 2, section 2.2.5.1 Cell Culture using the same reagents if not otherwise specified.

4.2.5.2 Determining Intracellular Delivery of Calcein by Confocal Microscopy

HeLa cells were incubated in supplemented DMEM for 48 hours before the experiment in a 4-well 1.8 cm^2 chambered cover glass system (Nunc, UK) at $5x10^4$ cells/well and 500 μL/well. Cells were first washed twice with PBS and incubated with phenol red-free DMEM in the presence or absence of 2 mM calcein for 24 hours with or without polymers. Cells were then washed twice with PBS and incubated with 5 μg/mL Hoecht 33342 and 5 μg/mL propidium iodide (PI) in phenol red- and FBS-free DMEM for 20 minutes. Cells were washed again twice with PBS before phenol red- and FBS-free DMEM was added to each well and imaged under confocal microscopy.

4.2.5.3 Determining Intracellular Delivery of Calcein by Flow Cytometry

Calcein (a membrane impermeable fluorophore) was used as a tracer molecule to monitor the effect of polymer intracellular delivery efficiency. Disodium calcein salt was dissolved in PBS to make 200 mM stock solution. HeLa cells were seeded in 24-well plates at $5x10^4$ cells/mL in 0.5 mL supplemented DMEM to full confluence in 24 hours followed by incubation with 0.22 μm filter-sterilised supplemented media and 2 mM calcein in the presence or absence of polymers. Cells were washed twice with PBS, trypsinised and resuspended in phenol red-free DMEM supplemented with FBS spun down at 0.2 g for 5 minutes. The supernatant was removed and the cell pallets were resuspended in phenol red- and FBS-free DMEM and transferred into a Titertube 1 mL micro test tube (Bio-Rad, UK). Cells were analysed by Cytek DxP8 cell sorter (Cytek Bioscience, USA) with 10,000 event count measuring side scattering and fluorescent intensity at various emission

wavelengths. The results were processed by FlowJo software (Cytek Bioscience, USA) by quantifying fluorescent intensity of the gated cells. All experiments were conducted in triplicates.

4.2.5.4 Measuring Cytotoxicity of polymers

4.2.5.4.1 Cell metabolic activity determined by MTS assay

The MTS tetrazolium compound is reduced by metabolically active cells to a colored formazan product that could be quantified at an absorbance of 490 nm by a spectrophotometer. The absorbance of the formazan product and viable cells within the range of the cell concentrations was a linear relationship. Therefore, the reduction of cellular metabolic activity of HeLa cells, followed by polymer or chemical exposures, was determined by MTS assay. The assay was performed according to the manufacturer's protocol. Experiments were performed in six repeats. The spectra were recorded using a BMG Labtech SPECTROStar Nano (Allmendgruen, Germany).

4.2.5.5 Cell apoptosis study determined by AnnexinV/PI staining

HeLa cells were seeded in 24-well plates at $5x10^4$ cells/well in 500 μL supplemented media for 48 hours. Cells were then incubated with supplemented media with or without polymers for 24 and 48 hours. Cells were then washed with PBS twice, trypsinised, and then re-suspended in phenol red-free DMEM containing FITC-AnnxinV and PI. Untreated cells were used as a negative control. HeLa cells incubated with 1% saponin in DMEM for 10 minutes were used as a positive control for apoptosis. The apoptosis assay was then performed with Cytek DxP8 cell sorter (Cytek Bioscience, USA). The results were processed by FlowJo software (Cytek Bioscience, USA) to determine the cytotoxicity of the polymers.

4.3 Results and Discussion

4.3.1 Synthesis and Characterisation of PLF

After synthesis and purification, a yellow polymer was obtained. Synthesis of PLF was performed in a smaller scale and the yield of the initial methylated polymer poly (L-lysine methyl ester fumaride) PLMF was 33.2 % over two batches. In comparison, typical PLMP yield was 66.2%. The main reason that contributed to the difference could be the solvent for the chloride di-acid in the synthesis process of PLF. Instead of using water soluble acetone, chloroform was used to dissolve fumaryl chloride as it is not soluble in more polar solvents. Additionally, the scale of the reaction for PLF was 10-fold smaller than the PLP reaction conducted in this study. As chloroform is less soluble in water where L-lysine methyl ester was dissolved in, there would be less contact between the chloroform and water interface making the reaction less efficient. Despite the yield of PLMF being two-fold lower than PLP the synthesis yielded enough polymer for further analysis. PLF was characterised via ^{1}H-NMR and FTIR to confirm its chemical structure.

4.3.1.1 PLF Characterisation by ^{1}H-NMR

The NMR spectrum of PLF in DMSO-d_6 is shown in Figure 4-2 with the appropriate assigned proton depicted in a chemical drawing. Peak assignment: 6.78-6.92 ppm (a, -HC=CH-), 8.36-8.39 ppm (b, f, -NH-), 3.10-3.12 ppm (c, -CH_2-) 1.29-1.73 ppm (d, -$(CH_2)_3$-). The spectrum confirmed the PLF contains the di-amide, ethylene and long amine chain structures. The result confirmed that even with the new chemical synthesis process, the polymerisation reaction was still able to produce a polymer with a similar structure as PLP.

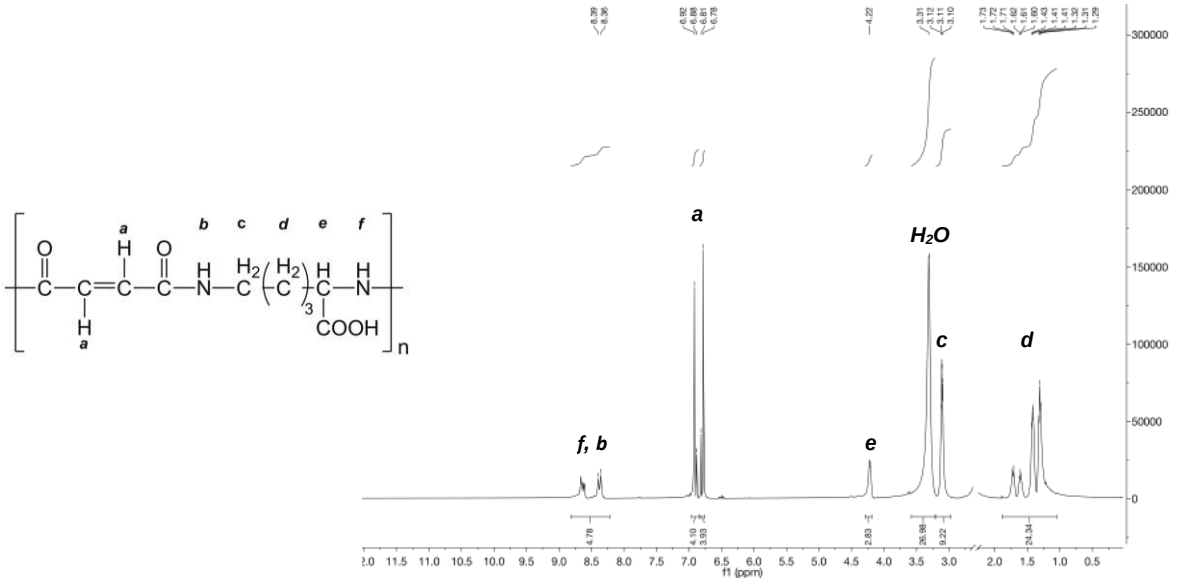

Figure 4-2: Chemical structure and ^{1}H-NMR Spectrum of poly (L-lysine fumaride) in DMSO-D_6. The protons on the chemical structure of PLP were each assigned to a legend and labelled on the ^{1}H-NMR spectrum. DMSO peaks at 2.5 ppm were removed for better visualisation of the spectra.

4.3.1.2 PLF Characterisation by FTIR

The FTIR spectra of PLF was compared to PLP in Figure 4-3 to compare the difference and similarity in functional groups and chemical structure. The spectra of PLF showed a number of similar characteristics as PLP including the carboxylate C=O stretch (1710 cm^{-1}), amide C=O stretch (1630 cm^{-1}), amide N-H bend (1530 cm^{-1}) and the hydroxy group O-H stretch (3300 cm^{-1}). The difference in structure could be observed in unique peaks of PLF spectra at the C-H out-of-plane bend (1450 cm^{-1}) and *trans*-C-H out-of-plane bend for alkene groups (970 cm^{-1}). Additionally, the slightly lower intensity at 1530 cm^{-1} for PLF spectra compared to that of the PLP demonstrated the lack for C=C-C aromatic ring stretch.

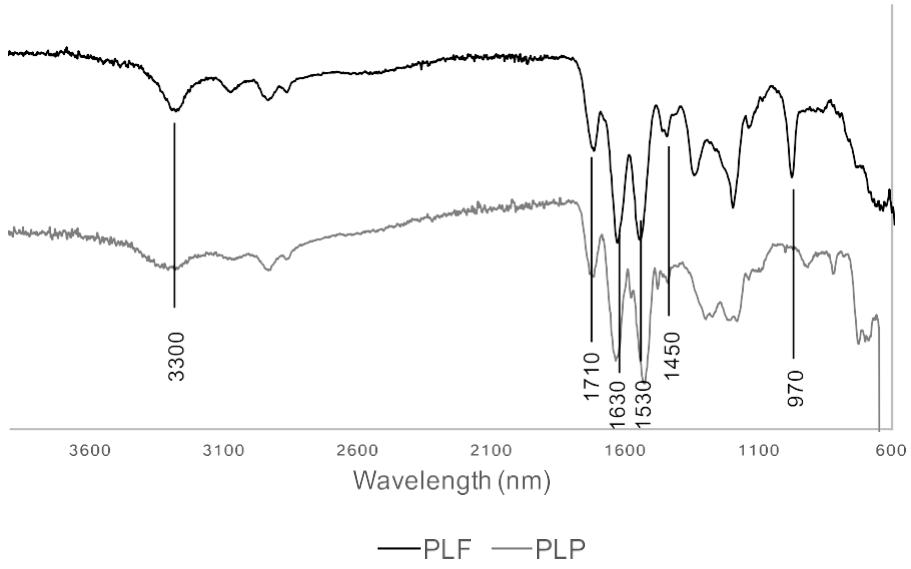

Figure 4-3: FTIR spectrum of poly (L-lysine fumaride). The spectrum of PLP was included below the PLF spectrum for comparison. Peaks labelled were assigned to the appropriate functional groups of the polymers.

The FTIR data complimented the ^{1}H-NMR result discussed in the earlier section as evidence that PLF had similar functional groups including amide and carboxylic acid compared to PLP. The two techniques could confirm that PLF, like PLP, is a poly-amides with pendant carboxylic acid groups. The major difference in the primary structure in PLF is that the fumaride group replaced the iso-phthalamide. This opens up the question on how the change would affect the secondary structure and function of the polymer which would be discussed in later sections.

4.3.1.3 Measuring Transition pH of PLF by Turbidity

It was previously determined that PLP undergoes conformational change as the environmental pH decreases and that was what contributed to the membrane disruptive activity of the polymer (Eccleston *et al.*, 2000, 2005). Since PLF was determined to have similar poly-amide and carboxylate structure, it may also adopt the pH responsive and membrane disruptive characteristic. In order to determine whether PLF respond to

change in environmental pH shift, the turbidities of PLF in various phosphate buffer (0.1 M) was measured by recording the transmittance at 460 nm. This technique has been previously reported for the determination of pH dependence of PLP and PLP-based polymers (Eccleston *et al.*, 2005; Yue, Eccleston and Slater, 2005; Chen, 2007). Precipitation of the polymers caused drastic decrease in transmittance at a specific pH.

Consistent with the result reported in previous chapters and work done previously, PLP had transition pH at 4.3 (Chen, 2007). As shown in Figure 4-4, the transition pH of PLF was determined to be at pH 3.5. This value is significantly lower than that of the PLP. This could be explained by the lack of aromatic group in PLF compared to PLP. It was previously reported that the precipitation of PLP as the pH decreases was caused by the protonation of carboxylate group and consequently weakening of the ionic repulsion between polymer subunits (Chen, 2007). This event caused the π-π interaction of aromatic ring and the hydrophobic interaction to become the dominant force over ionic repulsion. As suggested in the previous chapters, PLP polymer rods bundle into a larger cylindrical structure. Since PLF lacks aromatic rings compare to PLP, the hydrophobic interaction is the sole force that drives the polymer to aggregate once protonated, a lower transition pH for PLF is, therefore, expected. The turbidity experiment confirmed that PLF, which precipitates at low pH, indeed has pH responsive characteristic like PLP. The structural and functional differences of the two polymers were determined through other techniques and discussed in the following sections.

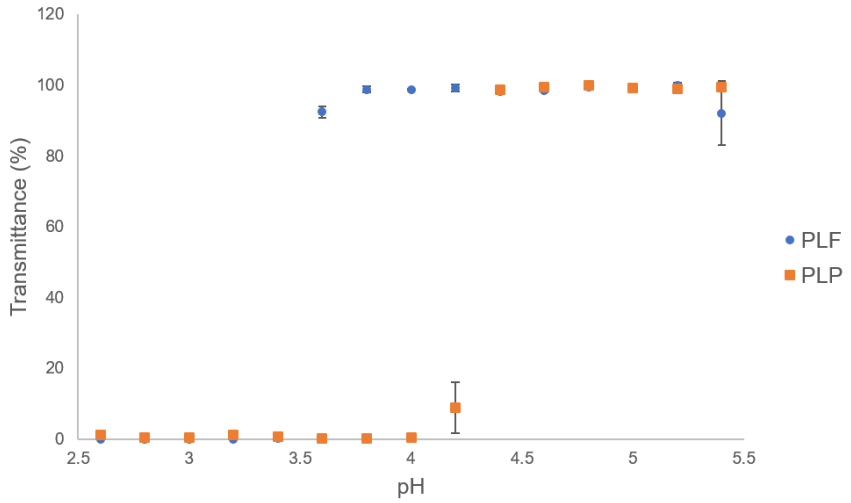

Figure 4-4: Variation of the turbidity of PLF and PLP in different pH conditions. The turbidity of polymers at 1 mg/mL in 0.1M phosphate buffer at pH between 2.5 and 7.8 were measured at λ = 460 nm. Estimated transition pH determined for PLF was 3.5 and for PLP was 4.3.

4.3.1.4 Circular Dichroism of PLF

Far-UV CD spectra from PLF showed that it, like PP-50, it had a CD spectrum with an inverse sign compared to that of PLP's. CD spectrum of PLF had a positive peak at 215 nm rather than the negative observed on the spectrum of PLP. Additionally, the absolute signal strength of PLF at 215 nm was twice as strong as that was observed in PLP and the change in cotton effect at different pH was more prominent with PLF (Figure 4-5). Interestingly, the strongest signal for PLF was observed at pH 6.1, which is far from the transition pH of 3.6 determined for PLF. The CD spectrum at pH 6.1 for PLF was twice in strength compared to PLF at physiological pH. Although the change was not as intense as the three-fold increase observed in PLP at pH 4.0 and pH 7.4, the overall strength of the PLF CD spectra was significantly more intense than that of PLP. PLP, on the other hand, had the strongest CD signal at pH 4.0 which is relatively close to its transition pH. Whether this observation was of significance would later be determined and discussed by the intracellular delivery efficiency experiment determined by using a membrane impermeable fluorophore, calcein.

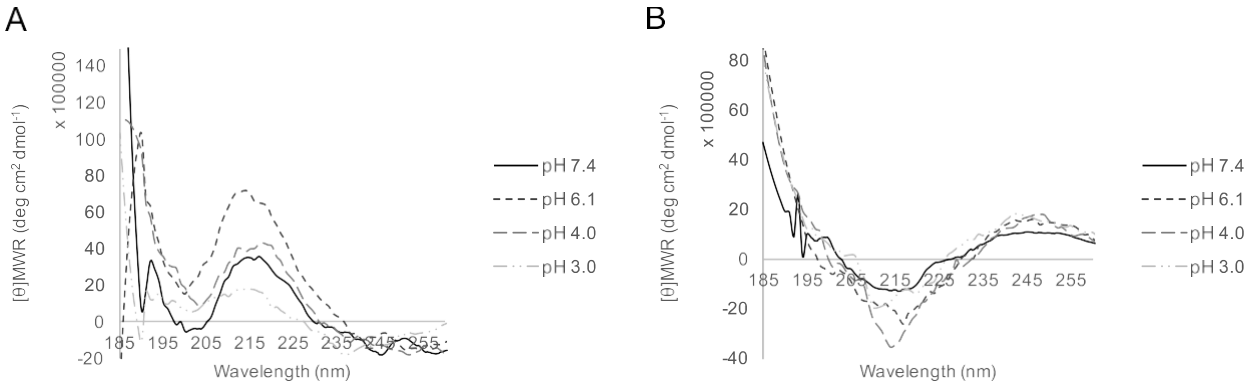

Figure 4-5: Circular Dichroism spectra of A) PLF and B) PLP at various pHs. Polymers were analysed at 0.1 mg/mL in phosphate buffer at the specified pH between 185 and 260 nm.

4.3.1.5 SANS Data Analyses for PLF

SANS is a non-destructive and high-resolution technique to study the structure of macromolecules in solution. The technique could provide the shape of dimension of the macromolecule of interest in great detail and, as shown in previous chapters, ideal for the study of pH responsive polymers. To understand the structure difference between PLF and PLP, PLF was characterised by SANS in three different pHs, specifically 7.4, 6.1, and 4.1.

As shown in Figure 4-6, the SANS spectra of PLF did not change significantly as pH decreases. This phenomenon is interesting since PLF was determined by the turbidity experiment to be pH responsive and precipitate from phosphate buffer at pH 3.6. It could be argued that PLF has not reached its transition pH, therefore, did not express a observable difference in its SANS spectra at the three studied pHs. By the slope of the intermediate region of the spectra, PLF was projected to be a cylindrical structure with length of 1000 Å and diameter of 14 Å. The length of the rod is significantly longer than that of PLP at approximately 200 Å. The diameter for PLF at pH 7.4 is very similar to the diameter of PLP at the same pH. In comparison to PLP, the diameter recorded by SANS of PLF does not increase as pH decreases. Whether these differences between the two polymers would contribute to difference in biological activities would be explored in later sections of this chapter.

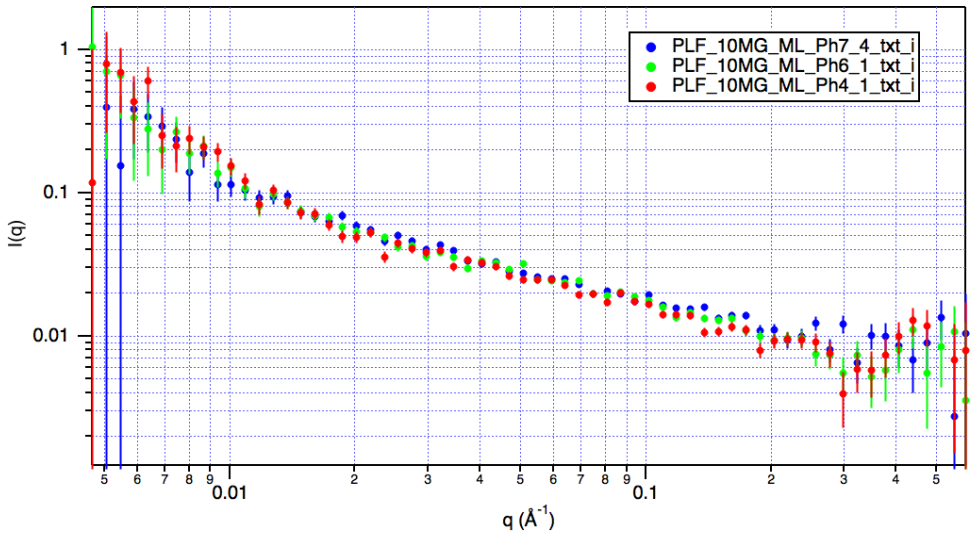

Figure 4-6: SANS spectra of PLF at pH 7.4, 6.1 and 4.1 in deuterated phosphate buffer solution. Deuterated phosphate buffer at selected pH was used as background. Spectra were fitted with the best matching models to determine the shape and dimensions of the polymer in solution.

4.3.2 Intracellular Delivery Efficiency of PLF compared to PLP

The intracellular delivery of PLF, like PLP, was assessed both in terms of increased calcein fluorescent signal and endosomal escape by flow cytometry and confocal microscopy. As shown in Figure 4-7A, PLF was able to increase intracellular calcein concentration in HeLa cells at polymer concentration as low as 0.5 mg/mL when incubated for 24 hours with similar level compared to PLP. Dose-dependence of the increase in intracellular calein concentration could be observed in both PLF and PLP. At 5 mg/mL PLF was able to increase the calcein concentration by 48% compared to calcein only. This result clearly demonstrated that PLF was able to increase the intracellular calcein concentration at an efficiency comparable to PLP despite lacking the aromatic ring. Interestingly, the transition of PLF was considerably lower than that of PLP but did not play a significant role on the intracellular delivery of calcein in HeLa cells. This observation may be related to the CD data obtained for PLF where the strongest signal

was observed at pH 6.1 rather than the transition pH 3.6 which indicate that the PLF polymer formed the most organised secondary structure at pH 6.1. This result could well affect how transition pH was defined for pH-responsive polymers. On the one hand, the transition pH of a polymer could be set at the pH where it aggregated. On the other hand, the transition pH of a polymer could be set at a pH where it had the most organised secondary structure and membrane disruptive activity. Setting a consistent definition could provide a more informative guidance when characterising these polymers.

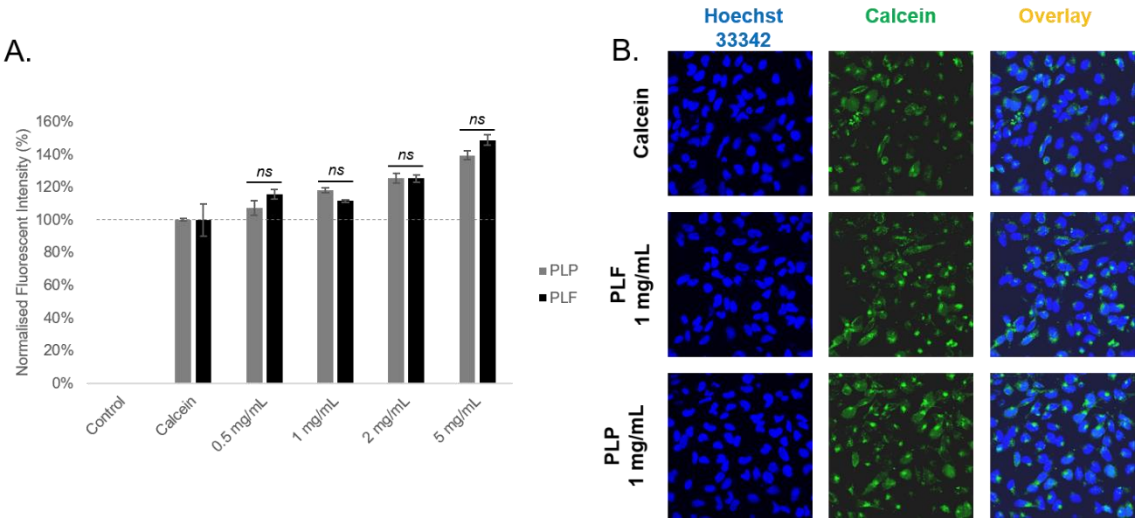

Figure 4-7: Flow cytometry analyses and confocal microscopy image of HeLa cells incubated in the presence and absence of PLF and PLP for 24 hours. A) Flow cytometry analyses of calcein uptake in HeLa cells in the presence or absence of PLF and PLP polymers after 24-hour incubation at various concentrations. Fluorescence was obtained using a FACScan flow cytometer. Data were derived from three replicates. Error bars represent standard error. B) Confocal microscopy image of cells incubated with or without polymer. Cells were incubated with 2 mM calcein (green fluorescence) in the presence or absence of polymer and subsequently stained with 5 µg/ml Hoechst H33342 (blue fluorescence).

The ability for PLF to facilitate endosomal escape was determined by confocal microscopy and compared to PLP. As shown in Figure 4-7B, HeLa cells incubated in the presence of 1 mg/mL PLF had slightly increased calcein fluorescence intensity compared to calcein alone. There are also more HeLa cells that had caclein distributed evenly in cells compared to calcein alone. The calcein distribution in HeLa cells observed in the presence of PLF is similar to that of the PLP. The two analyses provided evidence that

PLF could facilitate intracellular delivery of membrane impermeable calcein at a similar level to PLP and the delivery occurs at a dose-dependent manner.

4.3.3 Cytotoxicity of PLF Compared to PLP

Although it was previously demonstrated that PLP was well tolerated by immortalised cell lines such as HeLa and SAOS-2 osteosarcoma cells (Eccleston *et al.*, 2000; Mercado and Slater, 2016). The main concern with PLP was that the breakdown product, *iso*-phthalic acid, is water insoluble and not present in natural systems. It may pose long-term cytotoxic or undesirable effects when introduced to more sensitive cell lines such as stem cells or at the tissue level. Thus, the rationale of creating an intracellular delivery polymer with soluble natural occurring components. To compare the biocompatibility of PLF and PLP, MTS and AnnexinV/PI assays were performed on HeLa cells at different polymer concentration and incubation time to assess the short-term cytotoxicity effects.

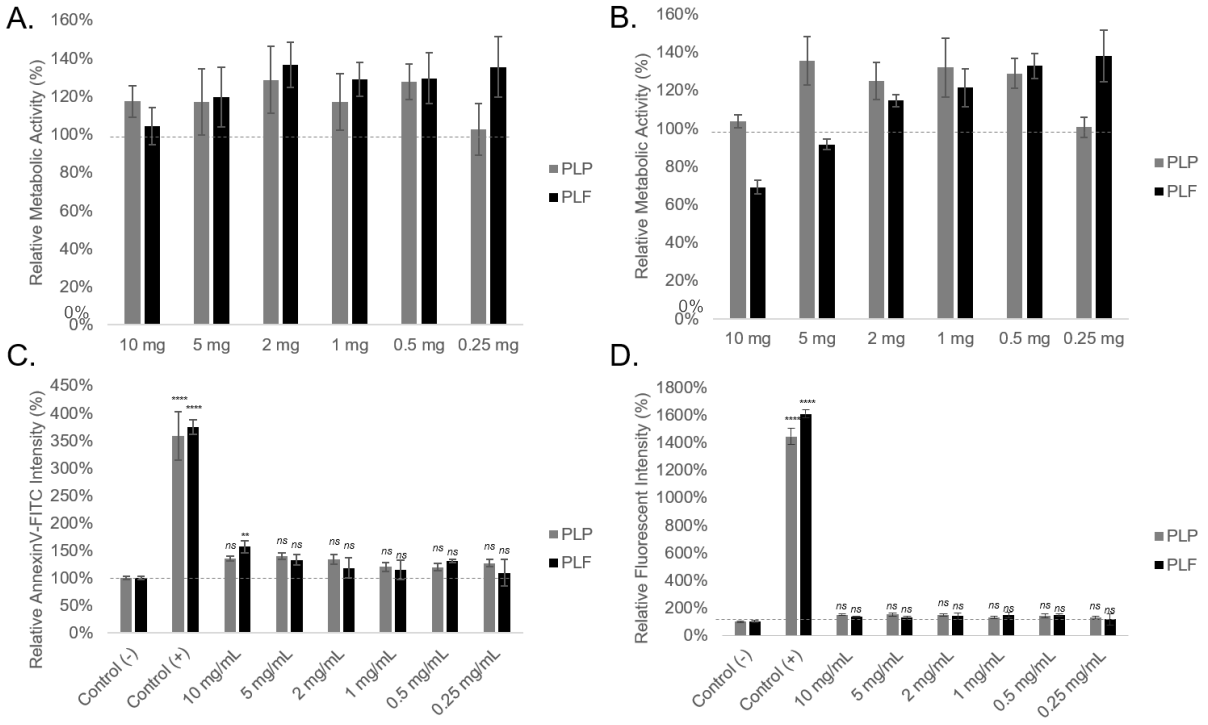

Figure 4-8: Evaluating the cytotoxicity of PLF and PLP by measuring metabolic and apoptotic activity of HeLa cells after incubation with PLF or PLP at various concentrations by flow cytometry. A) Metabolic activity of HeLa cells after 24-hour incubation with or without polymers at different concentrations. B) Metabolic activity of HeLa cells after 48-hour incubation with or without polymers at different concentrations. C) Apoptotic activity of HeLa cells after incubation with or without polymers for 24 hours measured by AnnexinV-FITC assay. D) Apoptotic activity of HeLa cells after incubation with or without polymers for 24 hours measured by PI staining. Data were normalised to cells incubated in the absence of polymer at the same incubation time. Data were derived from three replicates. Error bars represent standard error.

As shown in Figure 4-8A, metabolic activities determined by commercially available MTS assay of HeLa cells after 24-hour incubation with PLF and PLP were compared. The decrease in metabolic activity was in a dose dependent manner for PLF and PLP (above 2 mg/mL). Overall, PLF increased the metabolic activity of HeLa cells by on average 25% after 24-hour incubation at concentration below 5 mg/mL. HeLa cells incubated with 10 mg/mL of PLF had the same metabolic activity as the control without polymers. PLP, on the other hand, had more variable effects on the metabolic activity of HeLa cells, but was overall well tolerated at concentration as high as 10 mg/mL.

When HeLa cells were incubated with PLF for 48 hours, however, the polymer started to induce adverse effect on HeLa cells at concentrations above 5 mg/mL (Figure 4-8B). The

metabolic activity of HeLa cells decreased in a dose-dependent manner to PLF concentration. The metabolic activity was 9.5% below the control at 5 mg/mL of PLF and 31% at below at 10 mg/mL while PLP did not negatively impact the metabolic activity even at 10 mg/mL. The cytotoxicity of polymers, however, could not solely be determined through MTS assays. Past publications indicated that the MTS assay heavily relies on the enzymatic activity of components in the mitochondria and endoplasmic reticulum (ER) that are prone to a number of interferences (Vistica *et al.*, 1991; Van Tonder, Joubert and Cromarty, 2015). Additionally, exogenous fumarate was previously reported to induce redox-dependent senescence that reduces the proliferation of mammalian cells *in vitro* (Zheng *et al.*, 2015).

To more accurately depict the cytotoxic effects of PLF compared to PLP, AnnxinV-FITC and PI were used to determine the number of cells undergoing apoptosis and the membrane integrity of cells after 24-hour incubation with polymers at different concentrations. As shown in Figure 4-8C, PLF increased AnnexinV-FITC staining in HeLa cells in a dose dependent manner. At 10 mg/mL, PLF increased the fluorescent intensity by 56% compared to the 36% increase by PLP. However, PLP did induce on average 30% of the fluorescent intensity across different polymer concentrations. The two polymers induced significantly less fluorescent intensity compared to the positive control induced by saponin, which increased AnnexinV-FITC staining by more than 260%. The membrane integrity of HeLa cells incubated with the polymers was examined using PI, a membrane impermeable DNA-binding fluorescent dye. As shown in Figure 4-8D, PLF did not significantly affect the membrane integrity of HeLa cells after 24-hour incubation. It increased the PI staining by 17% at 10 mg/mL compared to the 68% PLP induced. PLP significantly affected the membrane at concentrations above 5 mg/mL. At 10 mg/mL PLP induced same membrane permeability at approximately 65% as the saponin control. The result indicated that PLP negatively impacted the membrane integrity of HeLa cells at concentrations above 5 mg/mL after 24-hr incubation while PLF had a more moderate impact at a concentration of 10 mg/mL.

The cytotoxicity results obtained through MTS and AnnexinV/PI assays concluded that PLF exhibited a dose-dependent toxicity profile and is well tolerated by HeLa cells at

concentrations below 5 mg/mL. Despite more negatively affecting HeLa cell metabolism at concentrations above 5 mg/mL after 48-hr incubation, PLF induced less apoptosis and membrane integrity compared to PLP. These results confirmed that PLF is well tolerated by HeLa cells and overall exhibited a similar, if not better, safety profile compared to PLP.

4.3.4 Effect of Amino Acid Modification on PLF

4.3.4.1 Synthesis and Characterisation of PF-50

As shown previously in this chapter, PLF has the pH responsiveness and intracellular delivery characteristics similar to PLP. FTIR and NMR results also confirmed that PLF is a poly-amide with pendant carboxylate groups that could easily be modified. Following similar logic to modifying PLP with hydrophobic amino acids to increase intracellular delivery efficiency, PLF could also be modified using the same strategy to potentially increase intracellular delivery significantly (Figure 4-9). In this study, L-phenylalanine was chosen as the hydrophobic amino acid to be grafted onto free carboxylate groups on PLF at a molar ratio of 1:2 to create PF-50. Phe was chosen as the modifier is due to the fact that it was the most established and effective entity for modifying PLP. After synthesis and purification following same protocol as PP-50 synthesis, a yellow solid was acquired. The FP-50 polymer was characterised by NMR and SANS.

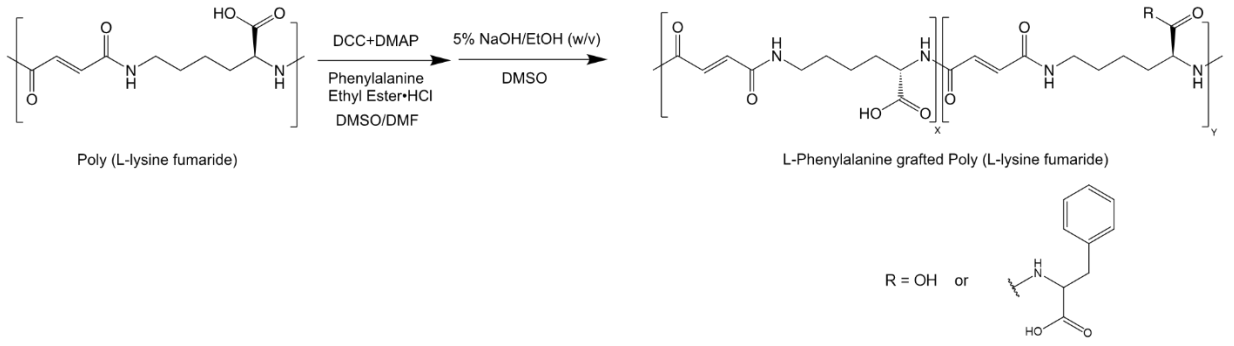

Figure 4-9: Reaction scheme for the synthesis of L-phenylalanine grafted poly (L-lysine fumaride). The reaction was achieved through standard DCC/DMAP coupling. The L-phenylalanine group is denoted as R and y varies by grafting percentage.

4.3.4.2 Characterisation of PF-50

After synthesis and purification, PF-50 was characterised by ^{1}H-NMR and FTIR to determine the chemical composition and functional structure. As shown in Figure 4-10, the ^{1}H-NMR spectrum revealed that the successful grafting of phenylalanine onto the PLF backbone confirmed by the unique peak at 7.13 ppm. The peak represents five protons on the phenyl group which was not seen on the ^{1}H-NMR spectrum of PLF (Figure 4-2). The grafting percentage of Phe was calculated to be 41.6% by comparing the integrated area of peaks at 6.56 ppm (two protons on the alkene group on the PLF backbone) and 7.13 ppm (five protons on the phenyl group). However, PF-50 has limited solubility in DMSO as shown by the high content of DMSO and H_2O impurities.

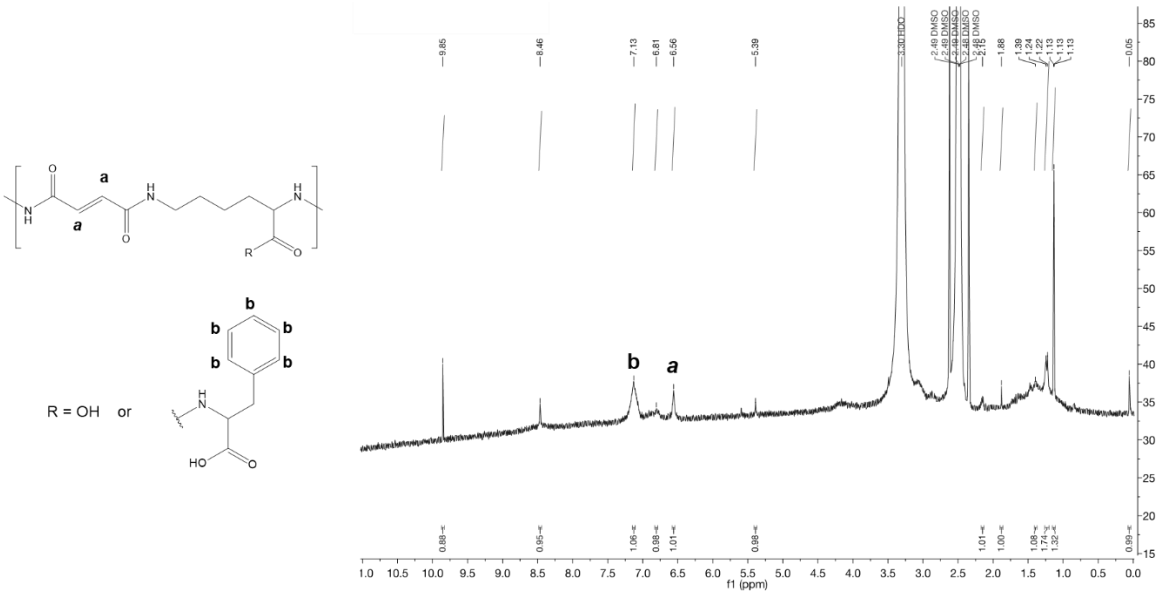

Figure 4-10: Chemical structure of PF-50 and ^{1}H-NMR Spectra of PF-50 in DMSO-D$_6$. The protons on the chemical structure of PF-50 were each assigned to a legend and labelled on the ^{1}H-NMR spectrum. The two protons on the trans alkene were assigned **a** while the five protons on the phenyl group of the grafted Phe were assigned **b**. The PLF ^{1}H-NMR could be found in Figure 4-2 in the section "PLF characterization by ^{1}H-NMR."

As shown in Figure 4-11, the FTIR spectrum of PF-50 revealed that the polymer contains key functional groups including *trans*-C-H out-of-plane bend for alkene groups (970 cm^{-1}), C-H out-of-plane bend (1450 cm^{-1}), amide C=O stretch (1630 cm^{-1}), amide N-H bend (1530 cm^{-1}) and hydroxy group O-H stretch (3300 cm^{-1}). Most functional

groups of PF-50 on the FTIR spectrum were similar to PLF shown in Figure 4-3 except the peak at 1550 cm^{-1} (between 1530 and 1630 cm^{-1} on the figure) for PF-50, as the higher intensity at the absorption represents the C=C-C aromatic ring stretch of the grafted Phe.

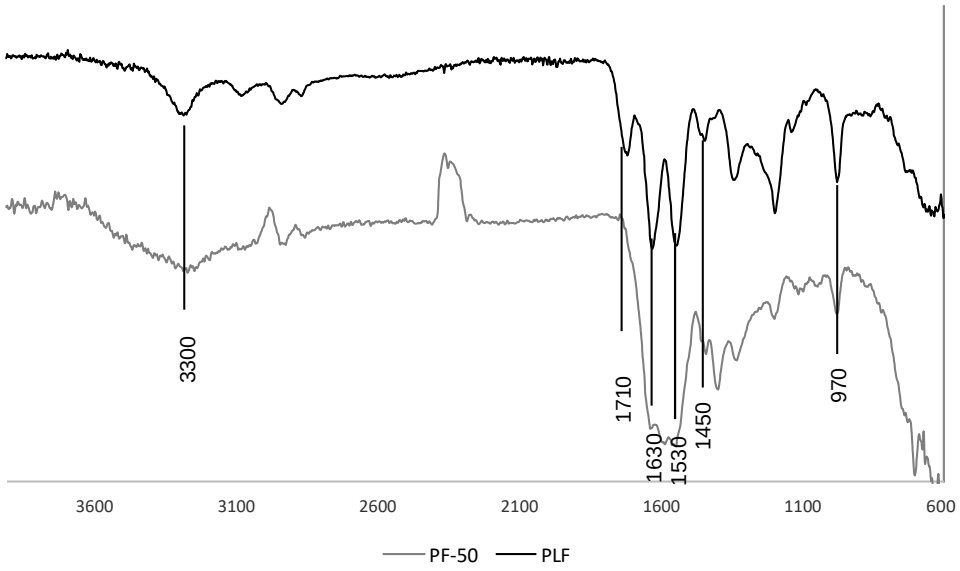

Figure 4-11: FTIR spectrum of PLF and PF-50. The spectrum of PLF was included above the PF-50 spectrum for comparison. Peaks labelled were assigned to the appropriate functional groups of the polymers.

4.3.4.3 SANS Analyses of PF-50

SANS was applied to characterise PF-50 to study the structure and determine the underlying pH-responsiveness. As shown in Figure 4-12, PF-50 adopted a rod like structure due to the slope of the intermediate region (0.01 $Å^{-1}$ < q < 0.1 $Å^{-1}$) of the PF-50 SANS spectra at pH 7.4, 6.1 and 4.1. According to the analysis of the spectrum at pH 7.4, PF-50 is a cylinder with approximately length of 1500 Å and diameter of 35 Å. The increase in diameter compare to PLF's diameter of 14 Å was expected as the modification added pendant groups to the PLF backbone. The increase in length, however, was unexpected as the modification shouldn't have modified the length of individual PLF rods. It is very likely that the modification caused the uneven stacking of smaller cylinder into a larger bundle in a misaligned fashion causing the overall length to increase. The spectra

of PF-50 at pH 6.1 and 4.1 indicated that PF-50 adopted a cylindrical structure but with more stacking and aggregation compared to PF-50 at pH 7.4.

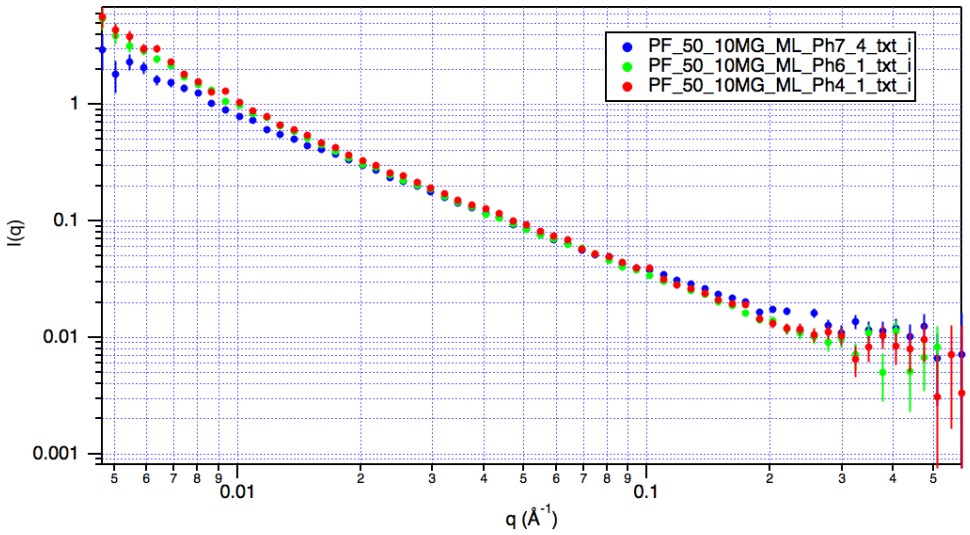

Figure 4-12: SANS spectra of PF-50 at pH 7.4, 6.1 and 4.1 in deuterated phosphate buffer solution. Deuterated phosphate buffer at selected pH was used as background. Spectra were fitted with the best matching models to determine the shape and dimensions of the polymer in solution.

PF-50 adopting a cylindrical form across the three pH was somewhat unexpected. As in previous chapters, modification of PLP with Phe resulted in a polymer that could form a lamellar structure usually at the lower pH. The studies in the previous two chapters suggested that the adoption of a lamellar structure was important to the intracellular delivery characteristic of PLP-based pH-responsive polymers. The fact that PF-50 did not form a lamellar structure at lower pH tested in this study could affect its ability to facilitate the intracellular delivery of membrane impermeable molecules in mammalian cells. In the following section, the intracellular delivery efficiency of PF-50 in HeLa cells will be further discussed.

4.3.4.4 Intracellular Delivery Activity of FP-50

As a proof of concept, intracellular delivery capacity of the phenylalanine modified PLF, PF-50, was evaluated using a membrane impermeable calcein by flow cytometry. Calcein

was incubated with HeLa cells in the presence or absence of FP-50 for 2 or 24 hours. As shown in Figure 4-13, at 2 hours incubation, PF-50 was not able to increase the intracellular calcein concentration of HeLa cells at 0.5 or 1 mg/mL. After 24-hour co-incubation with calcein and 0.5 mg/mL or 1 mg/mL of PF-50, the intracellular calcein concentration of HeLa cells increased by 10.9 and 13.5% respectively. The increase in intracellular calcein concentration for PF-50 was very similar to that of PLF and PLP but significantly lower than PP-50. This result suggested that although the Phe modification of PLF was successful, the effect of the modification on intracellular delivery efficiency was not as significant as the one observed between PLP and PP-50. It was determined in the previous section that PF-50 respond to pH changes and aggregates at lower pH, but it could not form lamellar structures at pH as low as 4.1. This may be problematic for endocytosis-dependent transmembrane transport as if the pH of the endosome falls below pH 4.0 it may merge with other vesicles to for lysosomes. The lysosome contains various enzymes that could digest any potential molecules that PF-50 could transport into the cell. The result suggested that the Phe modification of PLF could not increase the intracellular delivery efficiency and the resulting polymer PF-50 does not have the same characteristic as Phe modified PLP.

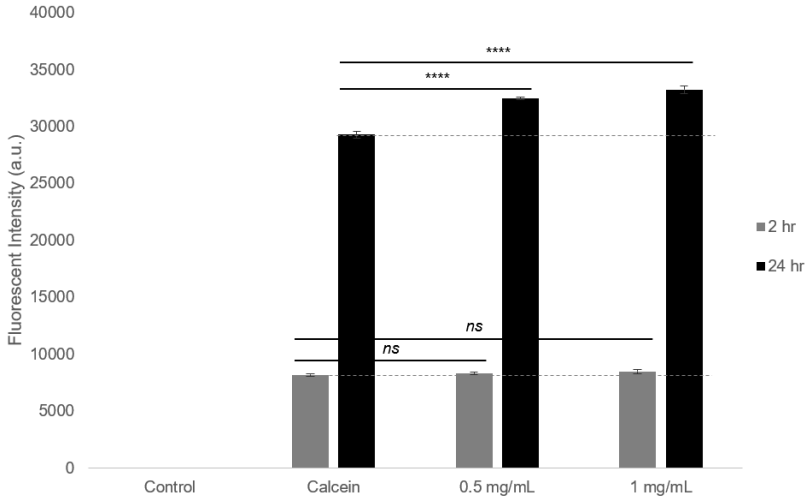

Figure 4-13: Intracelluar calcein concentration of HeLa cells with or without PF-50 polymers determined by flow cytometry. HeLa cells were incubated with 2mM of calcein in the presence or absence of 0.5 or 1 mg/mL of polymer for 2 or 24 hours. Cells without calcein incubation were used as control. The fluorescent signal was normalised to calcein only without polymer. Data were derived from three replicates. Error bars represent standard error.

4.4 Conclusion

In this chapter, the reason for finding a more biocompatible polymer than PLP but with similar characteristic was discussed. As one of the building components of PLP, iso-phthalic acid, is water insoluble and may cause long-term adverse effect to the biological system, a natural occurring di-acid was chosen for the synthesis of a new PLF polymer. PLF was proven to be pH-responsive but has a transition pH3.5 which is lower to PLP's 4.3 (Figure 4-4, Ch 4 Measuring Transition pH of PLF by Turbidity). Additionally, CD and SANS determined that PLF adopts an organised cylindrical secondary structure similar to PLP but approximately five times longer (Ch 4 SANS Data Analyses for PLF). Despite these differences, PLF was able to facilitate intracellular delivery of membrane impermeable calcein in HeLa cells with the same efficiency as PLP (Figure 4-7, Ch 4 Intracellular Delivery Efficiency of PLF Compared to PLP). Cytotoxicity data of PLF and PLP in HeLa cells suggested that PLF was well tolerated at a comparable level to PLP up to concentration as high as 10 mg/mL for 24-hour incubation but had less effect on the membrane integrity (Figure 4-8, Ch 4 Cytotoxicity of PLF Compared to PLP). The results indicated that PLF was a strong candidate that warrants further development as a biocompatible intracellular delivery agent.

Modification of PLP with Phe resulted in a polymer, PP-50, that had much higher intracellular delivery efficiency and the same modification was explored in PLF. The Phe-modified PLF polymer, PF-50, had a moderate grafting efficiency of 83.2% and contains all the key functional groups. PF-50 adopted a cylinder secondary structure but, unlike PP-50, it does not form any lamellar structure at pH as low as 4.1 (Ch 4 SANS Analyses of PF-50). *In vitro* experiment with membrane impermeable calcein in HeLa cells suggested that PF-50 had only comparable intracellular delivery efficiency as PLF (Figure 4-13, Ch 4 Intracellular Delivery Activity of PF-50). The Phe modification did not result in an enhance delivery efficiency of the polymer. The failure to enhance efficiency with the modification could be due to the fact that PF-50 could not form a lamellar structure. The modification strategy did not work on PLF but as it was a preliminary experiment, perhaps other amino acids such as tyrosine (Tyr) or tryptophan (Trp) could

be used as modifier. As PLF was proven to be well tolerated and was as efficient as PLP in delivering calcein in HeLa cells, modification of PLF could still be an option worth further exploration.

Chapter 5 SYNTHESIS AND CRYOPRESERVATION APPLICATION OF AN ANTIOXIDANT GRAFTED PLP

5.1 Introduction

Cell therapy has made drastic advancements and is estimated to become a $5 billion industry in the US alone (Ram-Liebig *et al.*, 2015). With the recent approval from the US Food and Drug Administration (FDA) and European Medicines Agency (EMA) of CAR T-cell therapies namely Kymriah and Yescarta from Novartis and Gilead respectively, cell therapies would inevitably take a more important role in future medical treatments. Despite having several well-established cryopreservation protocols, cells remain subjective to cryo-damage with altered cell physiology. These damages include lipid and protein oxidation, which could adversely affect cell proliferation and function (Best, 2015). In more severe cases, oxidative stress could lead to apoptosis or necrosis in a number of cell types decreasing the overall cryosurvival rate (Bilodeau *et al.*, 2001; Wolkers *et al.*, 2001; Zhang *et al.*, 2015). Thus, it is critical to reduce the oxidative stress throughout the cryopreservation process for successful long-term cell storage.

For cells to survive the prolonged period of storage at critically low temperatures, the presence of cryoprotective agents (CRAs) such as dimethyl sulfoxide (DMSO) or glycerol are required (Anchordoguy *et al.*, 1987; Chen *et al.*, 2001; Liseth *et al.*, 2005; Luo, Li and Wang, 2008). DMSO is one of the most commonly used and effective CRAs to date, however, the cytotoxicity on cells and systemic adverse effects have prevented it from further advancement in the field of medicine (Galmes *et al.*, 2007; Jahnukainen *et al.*, 2007; Li *et al.*, 2010). Non-toxic components such as sugars are becoming the more promising reagent for cryopreservation protocols while the success have been hampered by the limited transmembrane transportation mechanisms (De Antoni *et al.*, 1989; Lynch, Chen and Slater, 2011). For example, disaccharides such as trehalose was proven to be an effective CRA during the freezing-thaw process. The molecule was shown to be able to maintain membrane structure and prevent undesirable membrane fusion which could occur during dehydration caused by freezing of water (Rudolph and Crowe, 1985). Trehalose is required to be present on both sides of the cell membrane while it could not diffuse across the membrane barrier (Lynch *et al.*, 2010; Lynch, Chen

and Slater, 2011; Mercado and Slater, 2016). Several methods have been studied to increase intracellular disaccharide concentration including introduction of ATP receptor channels or engineering membrane pores but deemed incompatible due to their irreversible damaging effect to the cell membrane (Chen *et al.*, 2001; Fyles *et al.*, 2001; Richard *et al.*, 2003; Alvarez-Lorenzo and Concheiro, 2013).

One recently developed method that successfully increases intracellular disaccharide transport in mammalian cells involves the application of amphiphilic polymers that increase the membrane permeability. Some of these polymers contains amphiphilic and charged domains designed to mimic the permeablising effect of viral and bacterial peptides (Brogden, 2005). A pH-responsive poly-amide, namely poly (L-lysine iso-phthalamide) or PLP, was previously developed by Eccleston *et al.* as a drug delivery system. The polymer was shown to increase the intracellular concentration of a membrane-impermeable fluorophore, calcein, while being biocompatible *in vitro* (Eccleston *et al.*, 2000, 2005). The delivery efficiency of PLP was further improved by Chen *et al.* after applying hydrophobic amino acid as a modifier of the pendant carboxylate group (Chen *et al.*, 2009). One of the most effective of such polymers, PP-50, was synthesised by reacting 50% molar ratio of L-phenylalanine with free carboxylate groups on PLP. Despite the successful loading of trehalose into mammalian cells including erythrocytes and SAOS-2 osteosarcoma cells by PP-50, limited success in cryopreservation was observed potentially due to the inability to alleviate effects of oxidative stress (Mercado and Slater, 2016).

This study was motivated by the attempt to create a dual functional polymer with effective intracellular delivery and anti-oxidative characteristics. As previously mentioned, intracellular transport efficiency of PLP could be further improved by hydrophobic amino acids. It is logical to assume that the modification with other hydrophobic molecules not limited to amino acids could achieve similar effects. There is a variety of naturally occurring hydrophobic molecules that could be explored and an application-specific design approach should be taken to maximise the effectiveness of the selection process. In this study, cryopreservation with disaccharide as cryoprotectant was selected as the target application with clear objectives. Firstly, using a drug delivery system to resolve the membrane impermeability issue of trehalose so that it could

effectively protect cells during cryostorage. Secondly, utilising anti-oxidative agents to alleviate oxidative stress throughout the cryopreservation process to improve cell survival and post cryostorage recovery. (±)-α-Tocopherol (vitamin E), a natural occurring hydrophobic molecule with antioxidative properties was selected to modify PLP. Vitamin E is a lipophilic molecule that can commonly be found in biomembranes with extreme potency for scavenging free radicals and is more effective in preventing lipid oxidation than vitamin C (Tappel, 1962; Packer, Slater and Willson, 1979; Burton and Traber, 1990). Chemically, vitamin E contains long alkyl chains with an aromatic ring structure that makes it ideal to interact with lipid membranes. The anti-oxidative and membrane interactive characteristics make vitamin E the ideal modifier for PLP. Furthermore, vitamin E cannot be delivered independently because it is insoluble in water.

Whether vitamin E could act as an effective modifier of PLP and whether the resulting polymer could act as a potent antioxidant will be explored in this chapter. Similar to previous chapters, the polymer will be fully characterised by various techniques to confirm the chemical structure. Subsequently, the vitamin E-modified PLP will be examined *in vitro* on its intracellular delivery efficiency and anti-oxidative effectiveness. Finally, the polymer will be used to test a trehalose-based cryopreservation protocol.

5.2 Materials and Methods

5.2.1 Materials

Chemicals were purchased from Sigma Aldrich and biological reagents for cell culture were purchased from Thermo Fisher/Invitrogen if not otherwise specified.

5.2.2 Synthesis and Characterisation of PVitE-25

5.2.2.1 Synthesis of PVitE-25

Poly (L-lysine iso-phthalamide) (PLP) was synthesised as previously reported by Eccleston *et al.* (Eccleston *et al.*, 2000, 2005). Vitamin-E was grafted onto PLP backbone at 25% molar ratio of available carboxylate group through esterification with standard DCC coupling reaction (Neises and Steglich, 1978). The reaction scheme of PVitE-25 synthesis is depicted in Figure 5-1.

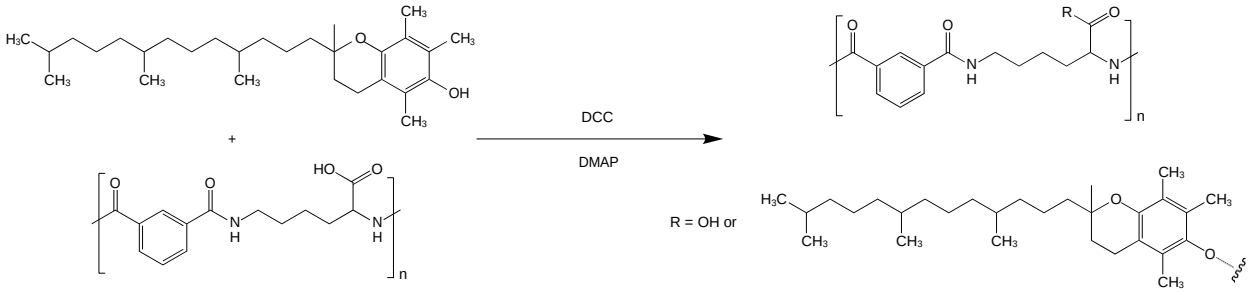

Figure 5-1: Reaction scheme of PVitE-25 synthesis. Standard DCC esterification using DMAP as catalyst to graft (±)-α-Tocopherol onto the PLP polymer backbone.

5.2.2.2 ^{1}H-NMR

Polymers were dissolved in DMSO-D_6 and characterised by Bucker Advance 500 MHz NMR spectroscopy (Bruker Biospin GmbH, Germany). The ^{1}H-NMR spectrum was processed through peak picking and integration with MNova software (Mestrelab Research, Spain).

5.2.2.3 FTIR

Absorption spectrum of polymers were collected using a Thermo Nicolet Nexus 870 spectrometer (Waltham, MA, USA) as the average of 32 scans with a wavenumber resolution of 4 cm^{-1} in the 600-4000 cm^{-1} range.

5.2.3 Biological Activities of PVitE-25

5.2.3.1 Cell Culture

HeLa cells were cultured and maintained as mentioned in the Materials and Methods Section of Chapter 2. The cells were maintained and cultured using the same protocol.

5.2.3.2 Cytotoxicity of polymers characterised by MTS assay

HeLa cells were seeded in 96-well plates at $5x10^3$ cells/well in 100 μL of supplemented media for 48 hours. Cells were then incubated with phenol red free DMEM supplemented FBS with or without PVitE-25 for 24 or 48 hours at different concentrations. The MTS assay was performed according to the manufacturer's recommendation. Data was collected at 480 nm with a SPECTROstar Nano plate reader (BMG Labtech Ltd., UK).

5.2.3.3 Cytotoxicity of polymers characterised by AnnexinV/PI staining

HeLa cells were seeded in 24-well plates at $5x10^4$ cells/well in 500 μL supplemented media for 48 hours. Cells were then incubated with supplemented media with or without PVitE-25 for 24 and 48 hours. Cells were then washed with PBS twice, trypsinised, and then re-suspended in phenol red-free DMEM containing FITC-AnnxinV and PI. Untreated cells were used as a negative control. HeLa cells incubated with 1% saponin in DMEM for 10 minutes were used as a positive control for apoptosis. The apoptosis assay was then performed with flow cytometry to determine the cytotoxicity of the polymers.

5.2.3.4 Characterisation of Polymer-mediated Intracellular Delivery of Calcein

Calcein (a membrane impermeable fluorophore) was used as a tracer molecule to monitor the effect of polymer intracellular delivery efficiency. HeLa cells were seeded in 24-well plates at $5x10^4$ cells/mL in 0.5 mL supplemented DMEM to full confluence in 24 hours followed by incubation with 0.22 μm filter-sterilised supplemented media and 2 mM calcein in the presence or absence of 1 mg/mL PVitE-25 polymer.

5.2.3.5 Anti-Oxidative Activity of PVitE-25 Determined by DCFH-DA

HeLa cells were incubated in supplemented DMEM for 48 hours before the experiment in 4-well 1.8 cm^2 chambered cover glass system (Nunc, UK) at $5x10^4$ cells/well and 500 μL/well. Cells were washed twice with PBS and incubated with phenol red- and FBS-free DMEM in the presence or absence of 1 mM H_2O_2 for 2 hours with or without polymer. Cells were then washed twice with PBS and incubated with 10 μM DCFH-DA, 5 μg/mL Hoechst 33342, 5 μg/mL PI in phenol red- and FBS-free DMEM for 20 minutes. Cells were washed again twice with PBS and DMEM was added to each well and imaged by confocal microscopy.

Image were processed using Image J. Fluorescent intensity per cell was calculated by the dividing total image fluorescent intensity by the total cell number. Cell numbers were determined by counting cells that had Hoechst 33342 stained nuclei.

5.2.4 Cryopreservation Utilising PVitE-25 and Trehalose Protocol

HeLa cells were seeded in 6-well plates at $5x10^5$ cells/mL in 1 mL of supplemented media for 24 hours. Cells were then incubated with phenol red-free DMEM media supplemented with 10% FBS with or without 200 mM of trehalose in the presence or absence of 1 mg/mL PVitE-25 for 4 hours. After the incubation, cells were washed three times with PBS, trypsinised and spun down. Cells were then resuspended in 10% (v/v) DMSO in FBS or 100 mM trehalose in 10% (v/v) phenol red free DMEM media in FBS at 10^6 cells/well. The solution containing cells was transferred into cryovials and cooled at 1 ˚C/min in a Mr. Frosty container in a -80 ˚C freezer overnight. The vials were then transferred into a liquid nitrogen cell bank and stored for at least 3 days before thawing. Experiments were performed in triplicate.

During the thawing process, each vial of 1 mL HeLa cells were diluted with 9 mL of supplemented DMEM and seeded in 96-well plates. Metabolic activities were assessed by MTS assay 24 and 48 hours after thawing. For the 48-hour timing, media was changed with supplemented DMEM 24 hours after thawing. MTS assay was performed as manufacturer's recommendation. Experiments were performed in six repeats.

5.3 Results and Discussion

PVitE-25 was synthesised by modification of PLP with vitamin E and characterised. The resulting polymer was tested for its effectiveness in intracellular delivery efficiency compared to PLP using membrane impermeable calcein. The anti-oxidative characteristic was determined by using the free-radical responsive fluorescence of 2',7'-dichlorofluorescin diacetate (DCFH-DA) in hydrogen peroxide challenged HeLa cells. After confirmation of the intracellular delivery efficiency and antioxidative characteristic of PVitE-25, the polymer was used to develop a trehalose-based cryopreservation protocol and compared to the industrial DMSO standard. The metabolic activity of cells post cryostorage was determined by MTS to evaluate the effectiveness of the protocols.

5.3.1 Synthesis and Characterisation of PVitE-25

PVitE-25 polymer was synthesised by grafting vitamin E onto PLP through the standard DCC esterification reaction. After purification and lyophilisation, a white porous solid was obtained. The polymer was characterised by ^{1}H-NMR and FTIR to determine the grafting percentage and the chemical structure.

As shown in Figure 5-2, the NMR spectrum of PVitE-25 had additional peaks before 4 ppm compared to the PLP spectrum, the most notable being the triplet peak at 2 ppm which corresponded to the three $-CH_3$ groups on the benzene ring of vitamin E (**b**). Since vitamin E, like PLP, contains aromatic ring structures, the high chemical shift regions used for calculating the molar number of monomers would no longer be accurate. Therefore, the single hydrogen on the beta carbon of L-lysine in the PLP backbone (δ = 4.33) was used as a reference instead. The grafting percentage of PVitE-25 was calculated by comparing the integrated area of the two peaks at δ = 2.01 and δ = 4.33 respectively with a 9:1 ratio which was 18.93%. This grafting percent of vitamin E translates to 75.72% reaction efficiency and there were no observed stability issues with the polymer during the purification and experiments.

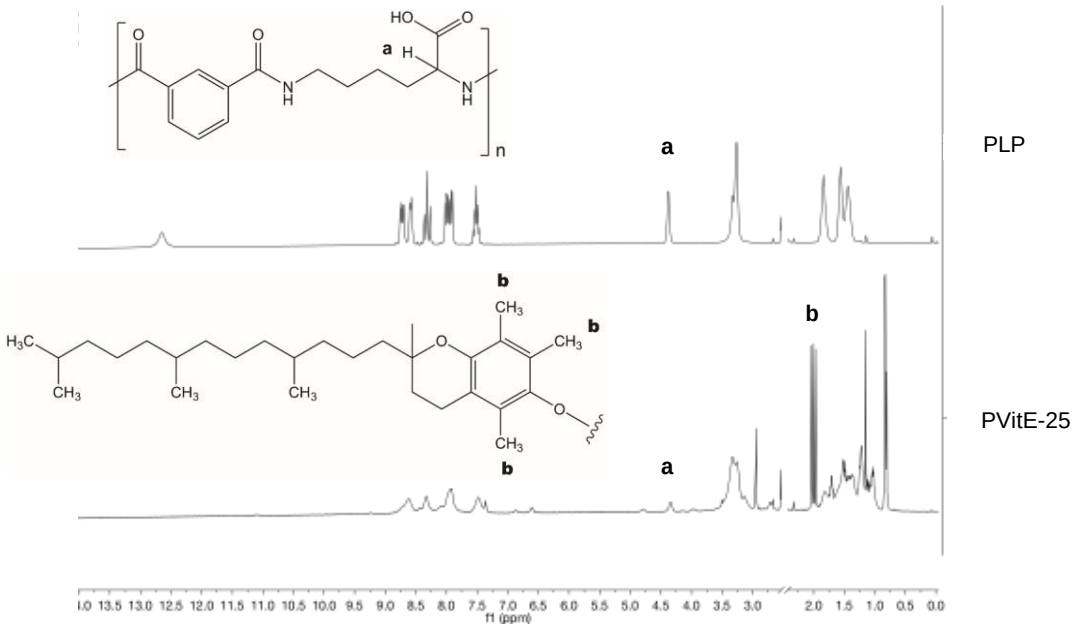

Figure 5-2: Chemical structure and ^{1}H-NMR Spectrum of PLP and PVitE-25 in DMSO-D_6. The proton (a) on the chemical structure of PLP and the three methyl groups (b) on vitamin E were each assigned to a legend and labelled on the ^{1}H-NMR spectrum. DMSO peaks at 2.5 ppm were removed for better visualisation of the spectra.

The molar ratio of vitamin E to pendant PLP carboxylate group for the reaction was selected at 25% because vitamin E is more hydrophobic than phenylalanine and it contains no carboxylate group which reduces the overall solubility of the resulting polymer.

Additionally, PVitE-25 was characterised by FTIR to confirm the polymer structure by identifying the key functional groups. The spectrum of PPVitE-25 showed a number of similar characteristics to PLP including the amide C=O stretch (1680 cm^{-1}), amide N-H bend (1550 cm^{-1}), aromatic C-H stretch (2940 cm^{-1}) and the hydroxy group O-H stretch (3300 cm^{-1}) (Figure 5-3). The lack of carboxylate C=O stretch (1710 cm^{-1}) in the PVitE-25 spectrum demonstrated the reduced carboxylate as it is partly replaced by ester C=O stretch while the intensified C-H stretch (2940 cm^{-1}) reflects the additional C-H groups on vitamin E.

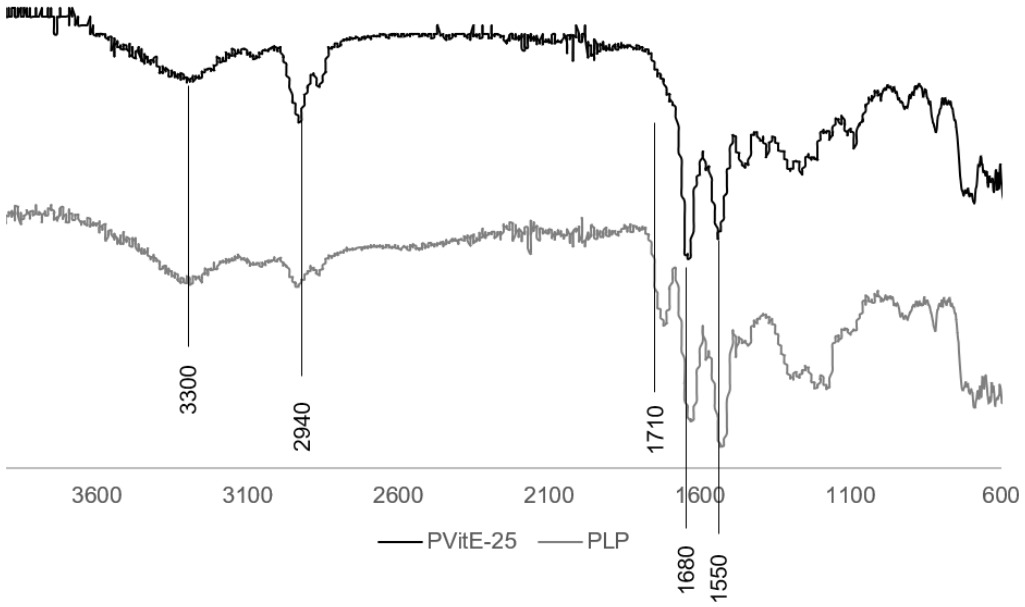

Figure 5-3: FTIR spectrum of PVitE-25. The spectrum of PLP was included below for comparison. Peaks labelled were assigned to the appropriate functional groups of the polymers.

Both NMR and FTIR confirmed the successful modification of PLP by vitamin E and the resulting polymer contains the key functional groups. Further characterisation of the interaction of PVitE-25 in vivo will be discussed in the following sections.

5.3.2 *Cytotoxicity of PVitE-25*

To determine the biocompatibility of PVitE-25, HeLa cells incubated with the polymer for various duration at different concentrations were characterised with commercially available MTS assay and AnnexinV-PI apoptosis assay. As shown in Figure 5-4A, PVitE-25 did not exhibit any cytotoxic effect to HeLa cells below 1 mg/mL up to 48 hours according to MTS assay. In fact, there was a slight increase in cell metabolic activity when PVitE-25 was incubated with cells below 1 mg/mL for 24 hours. The only time where cytotoxic effect was observed was when PVitE-25 was incubated with HeLa cells at 2 mg/mL for 48 hours. However, cells incubated in the condition still retained approximately 78.94% $\pm$ 4.33% of metabolic activity that of untreated cells.

AnnexinV apoptosis assay showed that up to 2 mg/mL, PVitE-25 did not induce apoptosis in HeLa cells after 24-hour incubation (Figure 5-4B). The increased signal was on average 27% across different concentrations of PVitE-25 compared to the negative control of untreated cells, whereas the positive control with saponin increased by 15-folds. These results suggest that PVitE-25 was well tolerated by HeLa cells with a 24-hour incubation period at 2 mg/mL. 48-hour incubation with PVitE-25 induced measurable apoptosis activity compared to the negative control group. However, the induced apoptosis activity of HeLa cells was significantly lower than the positive control suggesting that PVitE-25 was tolerable to HeLa cells.

As shown in Figure 5-4C, HeLa cells incubated with PVitE-25 at 2 mg/mL for 24 hours was relatively intact compared to saponin, a strong cell permeabilising agent, treated cells (Seeman, Cheng and Iles, 1973). PVitE-25 slightly increased the membrane impermeable PI staining of cellular DNA regardless of the concentration after 24-hour incubation, suggesting the polymer only minimally affected the membrane integrity. At 48-hour incubation, PVitE-25 increase the PI staining slightly higher which was expected as AnnexinV staining indicated PVitE-25 induced high apoptosis activity with longer polymer incubation time.

The three assays all suggested that PVitE-25 was well tolerated by HeLa cells at 2 mg/mL with 24-hour incubation. PVitE-25 was slightly toxic with 48-hour incubation but still tolerable by HeLa cells. The application with PVitE-25 would not require an incubation time longer than 24 hours, therefore, the toxicity beyond that would not be a concern.

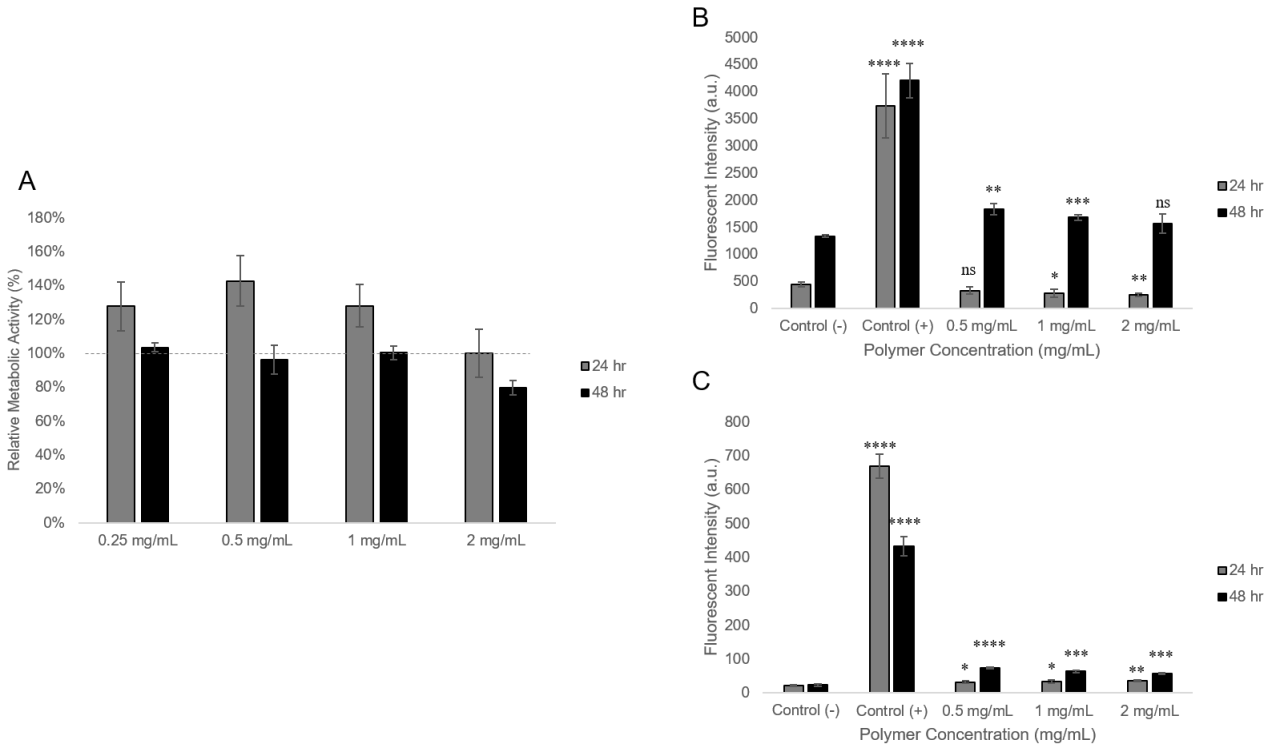

Figure 5-4: The cytotoxicity of PVitE-25 at different incubation period and concentration. A) Metabolic activity of HeLa cells after 24- and 48-hour incubation with PVitE-25 determined by MTS assay. Untreated cells were used as control and the measurements were set to be 100% relative metabolic activity. B) Annexin V staining of HeLa cells after 24- and 48- hour incubation with PVitE-25 polymer at different concentrations. Control (-) and control (+) were untreated cells and cells incubated with 1% saponin for 10 minutes. C) PI staining of HeLa cells after 24- and 48- hour incubation with PVitE-25 polymer at different concentrations. Control (-) and control (+) were untreated cells and cells incubated with 1% saponin for 10 minutes.

5.3.3 *Intracellular delivery activity of PVitE-25*

To evaluate the intracellular delivery activity of PVitE-25, the polymer was co-incubated with membrane impermeable calcein with HeLa cells. The delivery efficiency of PVitE-25 was shown in Figure 5-5A where it induced a significantly higher intracellular delivery efficiency of calcein compared to PLP. The PVitE-25-induced increase in intracellular calcein concentration behaved in a dose-dependent manner. The result suggested that the modification with vitamin E was successful and the resulting polymer could be an efficient intracellular delivery agent. The delivery kinetic of the calcein with the polymer was also characterised to provide information for the estimation of polymer incubation time for future delivery applications. Incubation of 4 hours with calcein and PVitE-25 was

able to generate a difference in intracellular calcein concentration in HeLa cells while longer incubation time induced further increase.

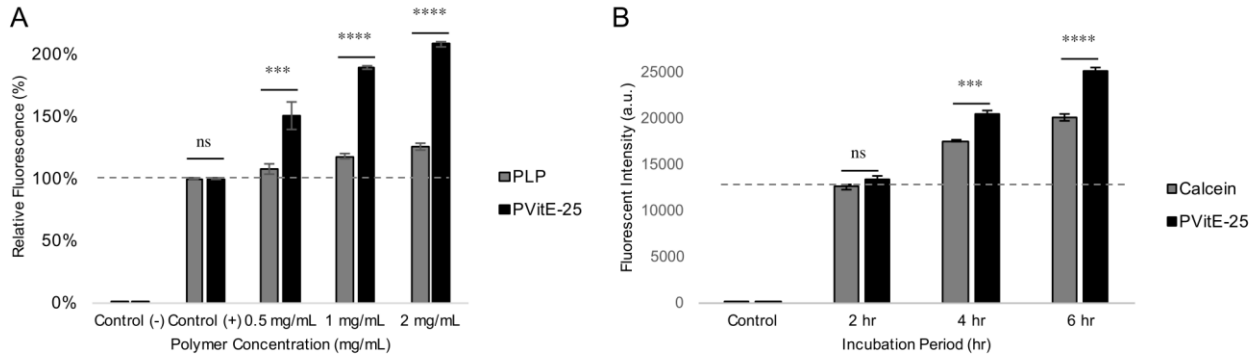

Figure 5-5: Intracellular calcein concentration of HeLa cells with or without PVitE-25 polymers determined by flow cytometry. A) Intracellular delivery of calcein by co-incubation with PVitE-25 or PLP for 24 hours at different polymer concentration. B) Intracellular delivery of calcein at different incubation length with 1 mg/mL of PVitE-25.

The increase in intracellular calcein concentration is a good indicator for the intracellular delivery activity, but the distribution of intracellular calcein should also be determined. Previous publication suggested that modified PLP polymers facilitate intracellular delivery through endocytosis pathways (Mercado *et al.*, 2016). The distribution of intracellular calcein delivered by PVitE-25 was characterised by confocal microscopy (Figure 5-6). A slight increase in calcein concentration was observed after 2-hour incubation and calcein was distributed throughout the cytosol. With 6-hour incubation, similar to 2-hour incubation, calcein could be observed throughout the cytosol but with a larger increase in intracellular calcein. These results are evidence that PVitE-25 was able to efficiently deliver membrane impermeable fluorescent dye into the cell cytosol and could be used as an intracellular delivery vehicle.

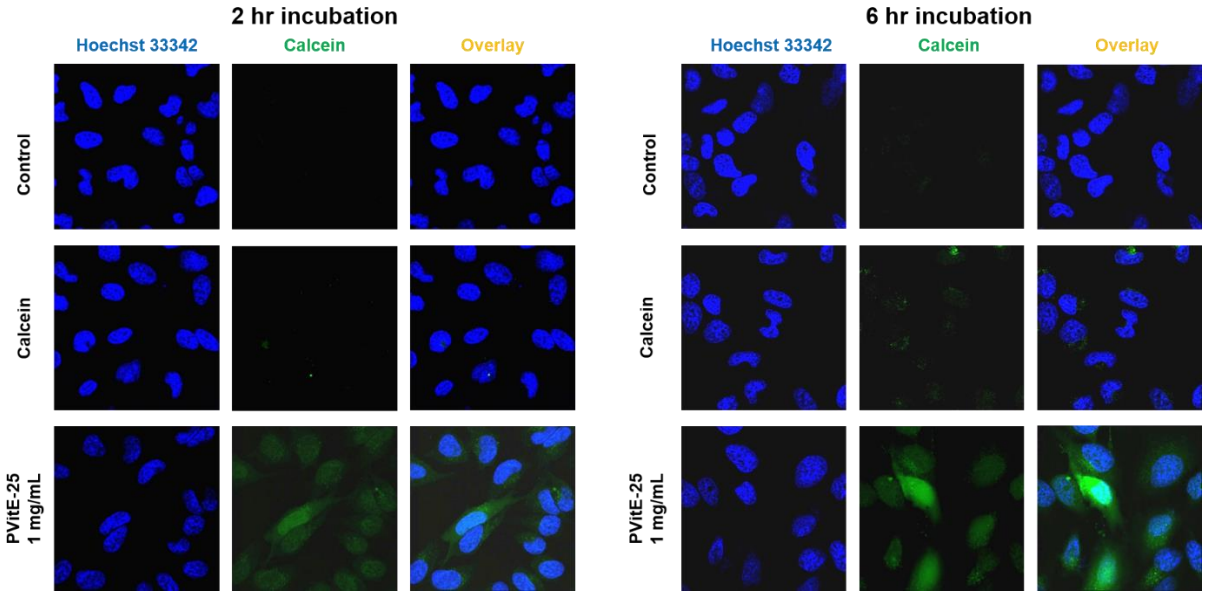

Figure 5-6: Confocal image of HeLa cells after co-incubation with calcein and PVitE-25. Calcein distribution was used to assess endosomal escape efficiency of PVitE-25. Cell nuclei were stained with Hoechst 33342 (blue). A) 2-hour incubation. B) 6-hour incubation.

5.3.4 *Anti-oxidative activity of PVitE-25*

To assess the anti-oxidative characteristic of PVitE-25, dichloro-dihydro-fluorescein diacetate (DCFH-DA), a fluorometric probe to measure oxidative species was used (Aranda *et al.*, 2013). As shown in Figure 5-7A, DCFH-DA emits blue fluorescence and as it is oxidised into DCF, the fluorescent becomes green. The probe has been used as a reliable assay to quantify reactive oxygen species. In order to determine the optimal probe to reactive oxygen species concentrations, a preliminary experiment was carried out incubating DCFH-DA with HeLa cells at different concentration with subsequent incubation with hydrogen peroxide. Results proved that DCFH-DA was able to generate measurable difference in fluorescent signal with 10 μM of DCFH-DA and 0.5 mM of H_2O_2 (Figure 5-7B). To ensure the reliability of the assay, 10 μM of DCFH-DA and 1 mM of H_2O_2 were selected for assessing the anti-oxidative characteristic of PVitE-25 in HeLa cells.

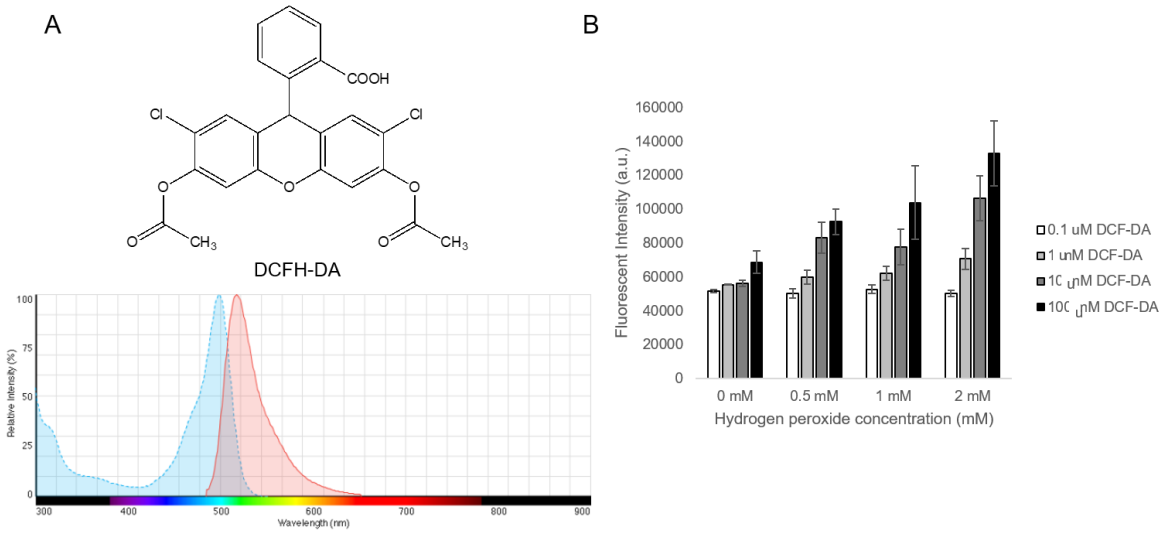

Figure 5-7: Chemical structure and emission spectrum of oxidation-reactive fluorophore, DCFH-DA. A) Chemical structure of DCFH-DA and the emission spectrum before (depicted in blue) and after (depicted in red) oxidisation. B) DCF, a fluorophore after DCFH oxidization, fluorescent signal at different DCFH-DA and hydrogen peroxide, an oxidising agent, concentration.

After the appropriate setting for the DCFH-DA assay was selected to measure reactive oxygen species in HeLa cells, polymers were introduced for the study of anti-oxidative effects. As shown in Figure 5-8A, hydrogen peroxide (1 mM) was able to induce a significant fluorescent signal in HeLa cells and could be observed under confocal microscopy. When the cells were pre-incubated with PLP before the reactive oxygen species (ROS) induction, the DCFH-DA fluorescence was decreased by 14.0 $\pm$ 9.2 % ($p > 0.05$, ns). However, when HeLa cells were incubated with hydrogen peroxide in the presence of PVitE-25 (1 mg/mL) for 2 hours, the amount DCFH-DA fluorescent signal was significantly reduced by 85.4 $\pm$ 7.3 % (Figure 5-8B, $p < 0.05$). The result suggested that the vitamin E moiety retains its antioxidative activity when incorporated into PVitE-25 and is able to mitigate oxidative stress within the cell cytoplasm.

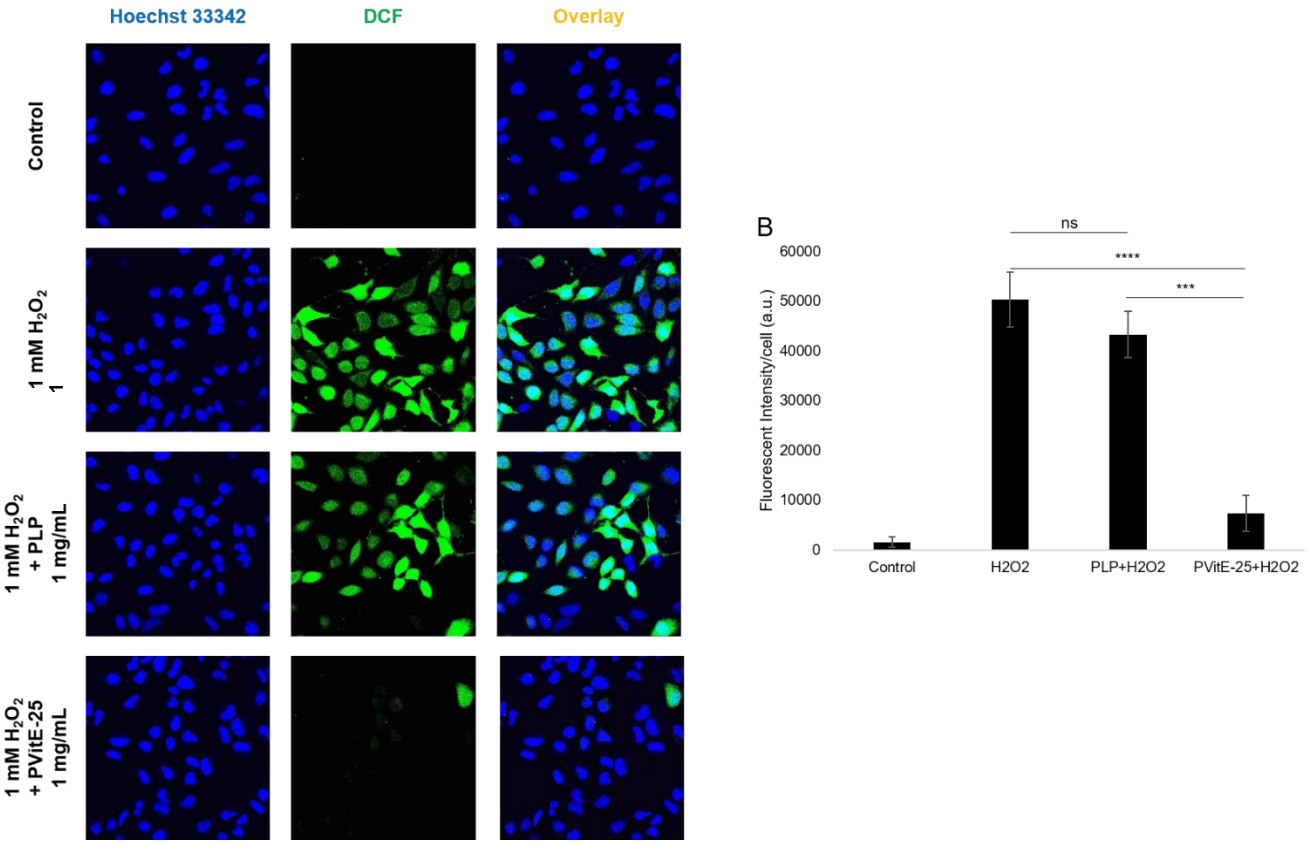

Figure 5-8: Assessment of anti-oxidative activity of PVitE-25 in HeLa cells by DCFH-DA assay. A) Confocal images of HeLa cells incubated with ROS-reactive dye DCFH-DA to assess the level of ROS. The green fluorescent represents DCF which was oxidised from DCFH. Higher fluorescent level corresponds to higher ROS levels. ROS production was induced by incubation with 1 mM H_2O_2 for 2 hours in the presence of PVitE-25 or PLP. B) Quantification of cellular ROS level using DCF fluorescent intensity by image processing with Image J (n=3).

5.3.5 Cryopreservation of Mammalian Cells Utilsing Trehalose/PVitE-25 Protocol

The effectiveness of PVitE-25 was further tested in the cryopreservation of HeLa cells. In this study, PVitE-25 was used in conjunction with trehalose as a cryostorage protocol to compare with the standard DMSO protocol. The viability of HeLa cells after different cryopreservation protocols was determined by MTS assay 24 and 48 hours after reconstitution with supplemented DMEM. As shown in Figure 5-9, cells preserved using PVitE-25 combined with the trehalose treatment protocol reached 82.7 $\pm$ 5.5% viability 24 hours after thawing compared to the standard DMSO preservation method. Additionally, cells preserved with the PVitE-25-based protocol were able to reach comparable metabolic activity 48 hours after thawing as of the standard DMSO protocol while polymer

alone (10.9 ± 2.0%) and unmodified polymer backbone (2.5 ± 1.5%) failed to protect cells post-thawing.

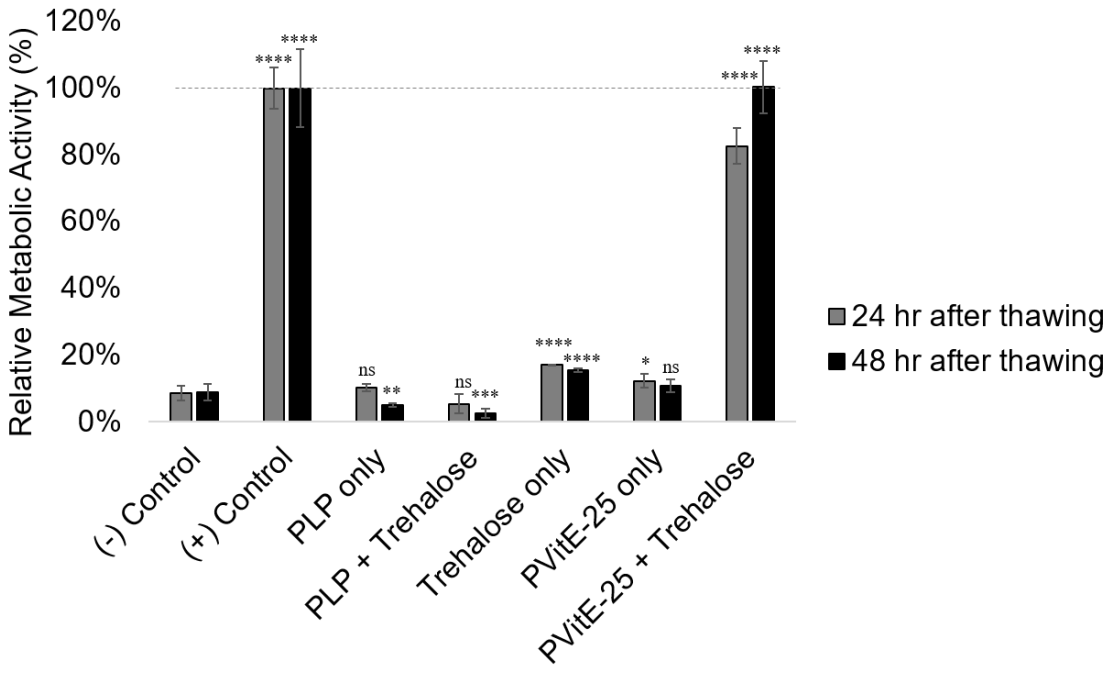

Figure 5-9: Metabolic activity of HeLa cells 24 and 48 hours after reconstitution from cryostorage determined by MTS assay. HeLa cells were treated with different cryopreservation protocols. Untreated HeLa cells were used as a reference while positive control was DMSO-based protocol and negative control was frozen cells without cryoprotectant. Cryopreservation was done in triplicates and MTS was done in six repeats.

It is believed that the successful cryostorage in this study was achieved for the following two reasons: Firstly, PVitE-25 delivered the membrane impermeable trehalose into the cell cytosol and enabled trehalose to be an effective cryoprotectant (Rudolph and Crowe, 1985; Chen *et al.*, 2001; Lynch *et al.*, 2010). Secondly, the anti-oxidative property of PVitE- 25 alleviated the detrimental effects induced by ROS to cells during the freeze thaw cycle and improve the survival of cells undergoing cryopreservation (Tampo *et al.*, 2003; Mishra *et al.*, 2009; Li *et al.*, 2010). The cryopreservation result highlighted the successful development of the first synthetic cell permeating polymer system with an anti-oxidative property and the potential for it be an effective system for other biomedical applications.

5.4 Conclusion

In this chapter, a novel design and development of a biocompatible intracellular delivery polymer with antioxidative property was discussed. The modification of PLP with an anti-oxidative agent, vitamin E, produced a functionally active aqueous soluble form of the antioxidant that retained the ability to enhance the transport of hydrophilic molecules such as trehalose into cells while retaining biocompatibility.

With vitamin E modification, the resulting PVitE-25 polymer had enhanced intracellular delivery efficiency compared to unmodified PLP. The intracellular concentration of membrane impermeable calcein was increased by over 100% when co-incubated with PVitE-25 at 2mg/mL while PLP co-incubation at the same concentration only resulted in a 10% increase. Confocal microscopy showed that the PVitE-25 delivered payload was equally distributed in the cytosol, verifying that the polymer was capable of causing membrane permeabilisation or endosomal escape. This result supported that modification with hydrophobic molecules containing aromatic groups could increase PLP delivery effectiveness. Additionally, PVitE-25 was able to achieve high intracellular calcein delivery with a lower grafting percentage compared to Phe modification. This indicated that there may be other natural occurring hydrophobic molecules, especially the ones known to be present in the cell membrane, that could further enhance PLP delivery efficiency.

The vitamin E modified PLP retained its biocompatibility profile and was well tolerated by HeLa cells at 24 and 48-hour incubations. PVitE-25 did not induce measurable apoptosis or compromise membrane integrity in HeLa cells after 24-hour incubation even at 2 mg/mL. Even with 48-hour incubation, PVitE-25 was tolerated by HeLa cells. As biocompatibility is the important differentiating factor of PLP-based polymer compared to other methods such as lipofectamine, it is essential to retain this characteristic while modifying PLP polymers for enhanced activities.

Another key characteristic that PVitE-25 polymer exhibited in the study was the anti-oxidative functionality that neutralised ROS generated from 1 mM H_2O_2 challenge in HeLa cells. ROS-responsive, membrane permeable DCFH-DA, would be oxidised into fluorescent DCF and used to measure the amount of ROS present. In this study, H_2O_2 was able to induce high DCF intensity when incubated with or without PLP, but in the presence of PVitE-25 fluorescent intensity was reduced by 85.4 ± 7.3 %. The result supported that, PVitE-25 obtained the functionality, similar to vitamin E, to neutralise ROS and protected cells from H_2O_2 challenge. This is the first instance that a modifying agent could enhance intracellular delivery and enable additional functionality of PLP.

It was suggested that cells face ROS during the freezing and thawing process during cryopreservation and would cause detrimental results (Mishra *et al.*, 2009; Li *et al.*, 2010; Tatone *et al.*, 2010). Although trehalose, was a proven cryoprotectant that exhibited potential anti-oxidative benefit, it was clearly not enough when combined with PLP-based polymer to sustain high cell survival rate after cryopreservation (Luo, Li and Wang, 2008; Mercado and Slater, 2016). In this study, PVitE-25 with enhanced intracellular delivery efficiency and anti-oxidative functionality was further assessed for the cryopreservation of HeLa cells. When the polymer was used in conjunction with trehalose as a protocol to cryopreserve HeLa cells, it was as effective as the DMSO standard protocol judging by the metabolic activity of the reconstituted cells. This result highlighted the effectiveness of PVitE-25 as a dual functional delivery system and the importance of intelligent design when developing drug delivery system for the prospective biomedical application.

Chapter 6 CONCLUSIONS AND FUTURE WORK

6.1 Conclusions

This thesis presented experimental studies to understand the structure of biocompatible pH responsive polymers and their interaction with the biological system in order to design more effective entities for biomedical applications. More specifically, using synthetic methods to create variations of the PLP polymers and determine which polymers were more effective drug delivery system. The main outcome of this study was the development of a PLP-derivative that act as a both an intracellular delivery system and an anti-oxidative agent that successfully applied for the cryopreservation of mammalian cells.

A proper design of any system would require in depth understanding of the components. There was limited information available on the structure and intracellular delivery mechanism of PLP and its derivatives. Firstly, CD and SANS were applied for the first time to characterise the structure of PLP. It was revealed that PLP forms an optically active helical secondary structure that is 200 Å by length. As pH decreases from physiological norm, the length of PLP remains the same while the macrostructure of the polymer changes. SANS results supported the theory that PLP forms a larger bundle with multiple rods as pH decreases. This contradicts the previous hypothesis that PLP is a flexible polymer chain at pH 7.4 and condense into a globular structure at lower pH.

Modification of PLP with hydrophobic amino acids was previously reported as an effective strategy to enhance polymer intracellular delivery efficiency. PP-50, a Phe, grafted PLP was determined by CD to have a significant different secondary structure compared to PLP. Moreover, PP-50 was determined by SANS to forms a lamellar macrostructure at lower pH rather than a rod structure compared to PLP. Therefore, the ability to form a larger macrostructure may be an important factor for PP polymers to be more effective agent for membrane permeabilisation and intracellular drug delivery.

To further understand the difference between PLP and PP polymers, three PLP and four PP-50 enantiomers were synthesised and characterised using lysine and phenylalanine isomers. The different enantiomers were used to explore the different characteristics to provide a better understanding of the polymer behavior, intracellular delivery mechanism, and cytotoxicity.

CD spectroscopy showed that PLP-L and PLP-D adopted similar helical secondary structures but with the opposite sense. It was also confirmed by CD that PLP-L-D overall did not exhibit optical activity, but the optical inactivity was possibly caused by the destructive signal addition of co-existing clockwise and counterclockwise helical domains. SANS data further supported that all three PLP enantiomers adopted rod-like structures which form larger stacked rods as pH decreases. In terms of intracellular delivery efficiency and cytotoxicity, the three PLP polymers have very similar profiles. These results indicated that the mammalian cell does not discriminate against the three PLP enantiomers and all three polymers were well tolerated.

After PLP enantiomers were characterised, PLP-L and PLP-D were modified by phenylalanine of different chirality, more specifically L- or D-, to yield four PP-50 enantiomers. The four PP-50 enantiomers were determined to be chemically similar, pH responsive, and had distinctive CD spectra in different pH environments. Although the four PP-50 enantiomers had slightly different SANS spectra, all the polymers were able to form lamellar structures at pH below 6.1. Unsurprisingly, the four polymers had very similar intracellular delivery efficiency of membrane impermeable calcein in HeLa cells. The result provided additional evidence that the ability of polymers to form lamellar structures would determine the ability to deliver payload intracellularly.

Experimental results supported that using amino acids of different chirality to synthesise pH-responsive polymers did not affect the overall structure and characteristics. The chirality of the material also did not contribute to any observable impact to the polymer interaction with HeLa cells as the intracellular delivery profile and cytotoxicity profile of the enantiomers were comparable.

After systematically studying the effect that chiral molecule and pendant modification have on PLP characteristics, an attempt was made to further explore the possibility to replicate PLP with all naturally occurring components. Fumarate, a di-acid important for the Krebs cycle, was selected for the synthesis of a biocompatible polyer. The resulting PLF polymer was proven to be pH-responsive but has a transition pH of 3.5 which is lower than PLP's 4.3. Additionally, CD and SANS determined that PLF adopts an organised cylindrical secondary structure similar to PLP but approximately five times longer. Despite these differences, PLF was able to facilitate intracellular delivery of membrane impermeable calcein in HeLa cells with the same efficiency as PLP. However, Phe modified PLF did not result in enhanced membrane activity. SANS determined that PF-50 adopted a cylinderical secondary structure but, unlike PP-50, does not form any lamellar structure at pH as low as 4.1. *In vitro* experiment with membrane impermeable calcein in HeLa cells suggested that PF-50 had only comparable intracellular delivery efficiency as PLF. The modification strategy did not work on PLF but as it was a preliminary experiment, perhaps other amino acids such as tyrosine (Tyr) or tryptophan (Trp) could be used as modifier. As PLF was proven to be well tolerated and was as efficient as PLP in delivering calcein in HeLa cells, modification of PLF could still be an option worth further exploration.

With a better understanding of PLP and pH responsive polymers as drug delivery systems, an application specific new design approach was adopted. Cryopreservation with the delivery of membrane impermeable cryoprotectant was selected as a pilot application to test the effectiveness of this approach. Previously, PP-50 was used as a delivery system to transport trehalose as cryoprotectant into osteosarcoma cells but only achieved 64% cryosurvival rate compared to the standard DMSO protocol (Mercado and Slater, 2016). The shortfall may not be due to the delivery efficiency of PP-50 but potentially other aspects, such as the oxidative stress that cells encounter during the freeze-thaw cycle of cryopreservation. Based on these understandings, a lipophilic anti-

oxidative agent, vitamin E, was selected as a modifier to produce a functionally active PLP polymer with enhanced ability to transport membrane impermeable molecules. With vitamin E modification, the resulting PVitE-25 polymer had enhanced intracellular delivery efficiency compared to unmodified PLP with the ability to distribute payload in the cytosol. Additionally, PVitE-25 was able to achieve comparable intracellular calcein delivery with 25 grafting percentage compared to the 50% of Phe modification. While PVitE-25 had enhanced intracellular delivery efficiency, the polymer retained its biocompatibility profile and was well tolerated by HeLa cells at 24 and 48-hour incubations. Finally, PVitE-25 polymer exhibited anti-oxidative functionality that neutralised ROS generated from 1 mM H_2O_2 challenge in HeLa cells.

In this study, PVitE-25 with enhanced intracellular delivery efficiency and anti-oxidative functionality was further assessed for the cryopreservation of HeLa cells. When the PVitE-25 was used in conjunction with trehalose as a protocol to cryopreserve HeLa cells, it was able to achieve cyrosurival rate comparable to the DMSO standard protocol. This result highlighted the effectiveness of PVitE-25 as a dual functional delivery system and the importance of intelligent design when developing drug delivery system for the prospective biomedical application. With enhanced understanding of PLP structure and how different modification would affect the polymer functionality and characteristic, PLP could be further expand as a promising drug delivery platform for additional biomedical applications.

6.2 Future Work

6.2.1 Further Characterisation of PLP

In this thesis, circular dichroism spectroscopy and small angle neutron scattering were applied for the first time to provide important structural information of PLP and modified-PLP polymers. The data supported that PLP adopted a helical secondary structure at pH 7.4. The sense of the helix, however, was not able to be determined. In other words, whether PLP forms a clockwise or counter-clockwise helix was not confirmed.

Characterisation methods including single-crystal X-ray crystallographic analysis and atomic force microscopy (AFM) could provide a more comprehensive picture of PLP structure. Single-crystal X-ray crystallographic analysis was described as a reliable and versatile method to determine the helical structure at an atomic level including the sense of the helix (Yashima, 2010). The method would require uniformed oligomers to be isolated and crystallised which could be challenging for PLP with higher polydispersity. AFM, a common technique for probing the structure of macromolecules, could potentially be a more suitable method for it is not limited by the polydispersity of the sample. The method utilises a very fine needle that comes into contact with the samples to map out the structure at atomic resolution (Butt, Cappella and Kappl, 2005). Kumaki *et al.* were able to use AFM to determine the helical sense and dimension of selected polymers (Kumaki, Sakurai and Yashima, 2009). The technique could potentially provide a more accurate measure for the dimension of PLP polymers and the sense of the polymer helical structure.

6.2.2 Circular Dichroism spectroscopy of PLP polymers with GUV

CD spectroscopy is a versatile technique to provide macromolecule secondary structure in solution. In this dissertation, PLP and PP-75 were characterised with CD in the presence of GUV and yielded interesting preliminary results. PLP and PP-75 CD spectra did not change at pH 7.4 in the presence of GUV. However, the CD spectrum of PP-75 was observed to be less prevalent in the presence of GUV at pH 5.1 and lead to the hypothesis that PP-75 interacts with the lipid lamellar at lower pH. However, the CD spectrum of PLP in the presence of GUV at pH 5.1 remained unchanged. This could potentially be due to the fact that pH 5.1 was above the transition pH of PLP and it had weak interaction with the GUV membrane. Therefore, to confirm whether PLP and other PLP-derived polymers interact with the lipid membrane more preferably at lower pH or their transition pHs, polymers could be experimented with GUV at different pHs including the polymer's transition pHs. The study could also provide information on how PLP polymers interact with lipid membranes and the structural information could help with understanding of the polymer membrane permeablisation mechanism.

6.2.3 Long-term and in vivo toxicity studies of PLP and PLP-derived polymers

Biocompatibility of PLP and its derivatives was only studied *in vitro* and by studying cell metabolism, membrane integrity, and apoptosis activity. Studies characterising the long-term effect of PLP *in vivo* have yet to be conducted. To fully assess the biocompatibility of PLP and its derivatives, more comprehensive studies on cell morphology or protein expression after exposure to PLP polymers should be determined.

PP-75 was previously applied as a drug delivery system for siRNA to treat cancer by Khormaee *et al.* in immunocompromised mice (Khormaee *et al.*, 2013). It was the first instance that a PLP derivative was experimented *in vivo*. The more complex system in multicellular organism such as metabolism, renal clearance, and the immune system could all affect the polymers. For PLP derivatives to be used as a drug delivery system in clinical applications, how polymers interact with different tissue would have to be fully characterised. This includes short- and long-term cytotoxicity, tissue retention, and immunogenicity.

6.2.4 Modification of PLF with other amino acids containing aromatic rings

As discussed in Chapter 4, PLF was determined to be as potent as PLP in delivering membrane impermeable calcein and was well tolerated by HeLa cells. Modification of PLF with Phe did not result in a polymer with enhanced intracellular delivery. Additional amino acids such as Typ or Trp could potentially be more suitable modifiers for PLF to enhance membrane activity. Characterisation of the resulting polymer with SANS could provide additional data points to support whether lamellar structure formation is correlated to the enhanced intracellular delivery of Phe modified PLP.

6.2.5 Modification of PLP with other membrane interactive molecules

Vitamin E was not the only lipophilic molecule that has affinity towards the plasma membrane. Cholesterol is one of the most important components in the lipid membrane that determines the membrane fluidity of mammalian cells. Modification with cholesterol could potentially increase PLP interaction with the cell membrane and increase the intracellular delivery efficiency. Additionally, due to the importance of cholesterol for alternating membrane fluidity, the cholesterol modified PLP could potentially exhibit membrane modification properties and affect membrane signalling. For example, T lymphocytes from the human immune systems are stimulated through the recruitment of membrane T-cell receptors into a concentrated region (Montixi *et al.*, 1998). The recruitment of T-cell receptor that are normally evenly distributed on the cell membrane to a concentrated area would depend on the regional membrane fluidity. Any major disruption of membrane fluidity could modify the T-cell receptor recruitment could alter the activation of T lymphocytes. Therefore, cholesterol may become a functional modifier for PLP that is beyond enhancement of intracellular delivery efficiency similar to Vitamin E. Further studies on how cholesterol modification could be accomplished and how the resulting polymer would interact with biological membranes could be an interesting topic for future investigation.

References

Allen, J. A., Halverson-Tamboli, R. A. and Rasenick, M. M. (2007) 'Lipid raft microdomains and neurotransmitter signalling', *Nature Reviews Neuroscience*, 8(2), pp. 128–140. doi: 10.1038/nrn2059.

Alvarez-Lorenzo, C. and Concheiro, A. (2013) 'Bioinspired drug delivery systems', *Current Opinion in Biotechnology*. Elsevier Current Trends, 24(6), pp. 1167–1173. doi: 10.1016/J.COPBIO.2013.02.013.

Anchordoguy, T. J. *et al.* (1987) 'Modes of Interaction of Cryoprotectants with Membrane Phospholipids during Freezing', *Cryobiology*, 24, pp. 324–331.

Anderson, R. G. W. (1998) 'THE CAVEOLAE MEMBRANE SYSTEM', *Annual Review of Biochemistry*, 67(1), pp. 199–225. doi: 10.1146/annurev.biochem.67.1.199.

Andrae, R., Schulze-Hartung, T. and Melchior, P. (2010) 'Dos and don'ts of reduced chi-squared'. Available at: http://arxiv.org/abs/1012.3754 (Accessed: 1 October 2019).

De Antoni, G. L. *et al.* (1989) 'Trehalose, a Cryoprotectant for Lactobacillus bulgaricus', *CRYOBIOLOGY*, 26, pp. 149–153.

Aranda, A. *et al.* (2013) 'Dichloro-dihydro-fluorescein diacetate (DCFH-DA) assay: A quantitative method for oxidative stress assessment of nanoparticle-treated cells', *Toxicology in Vitro*, 27(2), pp. 954–963. doi: 10.1016/j.tiv.2013.01.016.

Behr, J.-P. (1997) 'The Proton Sponge: a Trick to Enter Cells the Viruses Did Not Exploit', *Chimia*, 51, pp. 34–36. Available at: http://docserver.ingentaconnect.com/deliver/connect/scs/00094293/v51n1/s26.pdf?expires=1545624548&id=0000&titleid=10984&checksum=6ACD652AC363D296C77B2B561F77568B (Accessed: 24 December 2018).

Benjaminsen, R. V *et al.* (2013) 'The Possible "Proton Sponge" Effect of Polyethylenimine (PEI) Does Not Include Change in Lysosomal pH', *Molecular Therapy*, 21(1), pp. 149–157. doi: 10.1038/mt.2012.185.

Bernacca, G. M. and Wheatley, D. J. (1998) 'Surface modification of polyurethane heart valves: effects on fatigue life and calcification.', *The International journal of artificial organs*, 21(12), pp. 814–9. Available at: http://www.ncbi.nlm.nih.gov/pubmed/9988359 (Accessed: 18 November 2018).

Best, B. P. (2015) 'Cryoprotectant Toxicity: Facts, Issues, and Questions.', *Rejuvenation research*. Mary Ann Liebert, Inc., 18(5), pp. 422–36. doi: 10.1089/rej.2014.1656.

Bilodeau, J.-F. *et al.* (2001) 'Thiols prevent H2O2-mediated loss of sperm motility in cryopreserved bull semen', *Theriogenology*, 56(2), pp. 275–286. doi: 10.1016/S0093-691X(01)00562-3.

Bischofberger, M., Iacovache, I. and van der Goot, F. G. (2012) 'Pathogenic pore-forming proteins: function and host response.', *Cell host & microbe*. Elsevier, 12(3), pp. 266–75. doi: 10.1016/j.chom.2012.08.005.

Boussif, O. *et al.* (1995) 'A versatile vector for gene and oligonucleotide transfer into cells in culture and in vivo: polyethylenimine.', *Proceedings of the National Academy of*

Sciences of the United States of America, 92(16), pp. 7297–301. Available at: http://www.ncbi.nlm.nih.gov/pubmed/7638184 (Accessed: 24 December 2018).

Brogden, K. A. (2005) 'Antimicrobial peptides: pore formers or metabolic inhibitors in bacteria?', *Nature Reviews Microbiology*, 3(3), pp. 238–250. doi: 10.1038/nrmicro1098.

Brown, D. A. and London, E. (1998) 'FUNCTIONS OF LIPID RAFTS IN BIOLOGICAL MEMBRANES', *Annual Review of Cell and Developmental Biology*, 14(1), pp. 111–136. doi: 10.1146/annurev.cellbio.14.1.111.

Burton, G. W. and Traber, M. G. (1990) 'Vitamin E: Antioxidant Activity, Biokinetics, and Bioavailability', *Annual Review of Nutrition*. Annual Reviews 4139 El Camino Way, P.O. Box 10139, Palo Alto, CA 94303-0139, USA , 10(1), pp. 357–382. doi: 10.1146/annurev.nu.10.070190.002041.

Butt, H.-J., Cappella, B. and Kappl, M. (2005) 'Force measurements with the atomic force microscope: Technique, interpretation and applications', *Surface Science Reports*. North-Holland, 59(1–6), pp. 1–152. doi: 10.1016/J.SURFREP.2005.08.003.

Chen, C. and Zhuang, X. (2008) 'Epsin 1 is a cargo-specific adaptor for the clathrin-mediated endocytosis of the influenza virus', *Proceedings of the National Academy of Sciences*, 105(33), pp. 11790–11795. doi: 10.1073/pnas.0803711105.

Chen, J. P. and Natansohn, A. (1999) 'Synthesis and Characterization of Novel Carbazole-Containing Soluble Polyimides', *Macromolecules*, 32(10), pp. 3171–3177. doi: 10.1021/ma981609b.

Chen, R. (2007) *Design and In-vitro Testing of pH-responsive Biopolymers for Drug Delivery*. University of Cambridge.

Chen, R. *et al.* (2009) 'The role of hydrophobic amino acid grafts in the enhancement of membrane-disruptive activity of pH-responsive pseudo-peptides', *Biomaterials*. doi: 10.1016/j.biomaterials.2008.12.036.

Chen, T. *et al.* (2001) 'Beneficial Effect of Intracellular Trehalose on the Membrane Integrity of Dried Mammalian Cells', *Cryobiology*. Academic Press, 43(2), pp. 168–181. doi: 10.1006/cryo.2001.2360.

Christensen, K. *et al.* (2009) 'Ageing populations: the challenges ahead', *The Lancet*. Elsevier, 374(9696), pp. 1196–1208. doi: 10.1016/S0140-6736(09)61460-4.

Christie, R. J. and Grainger, D. W. (2003) 'Design strategies to improve soluble macromolecular delivery constructs.', *Advanced drug delivery reviews*, 55(3), pp. 421–37. Available at: http://www.ncbi.nlm.nih.gov/pubmed/12628325 (Accessed: 24 December 2018).

Chu, T.-W., Yang, J. and Kopeček, J. (2012) 'Anti-CD20 multivalent HPMA copolymer-Fab′ conjugates for the direct induction of apoptosis', *Biomaterials*, 33(29), pp. 7174–7181. doi: 10.1016/j.biomaterials.2012.06.024.

Cousin, F. (2015) 'Small angle neutron scattering', *EPJ Web of Conferences*. Edited by M. Ceretti et al. EDP Sciences, 104, p. 01004. doi: 10.1051/epjconf/201510401004.

Dabai, F. *et al.* (2014) 'Tar Formation and Destruction in a Fixed Bed Reactor Simulating Downdraft Gasification: Effect of Reaction Conditions on Tar Cracking Products', *Energy & Fuels*. American Chemical Society, 28(3), pp. 1970–1982. doi: 10.1021/ef402293m.

Damm, E.-M. *et al.* (2005) 'Clathrin- and caveolin-1–independent endocytosis', *The Journal of Cell Biology*, 168(3), pp. 477–488. doi: 10.1083/jcb.200407113.

Delgado, C., Francis, G. E. and Fisher, D. (1992) ‘The uses and properties of PEG-linked proteins.’, *Critical reviews in therapeutic drug carrier systems*, 9(3–4), pp. 249–304. Available at: http://www.ncbi.nlm.nih.gov/pubmed/1458545 (Accessed: 24 December 2018).

Dou, D. *et al.* (2018) ‘Influenza A Virus Cell Entry, Replication, Virion Assembly and Movement.’, *Frontiers in immunology*. Frontiers Media SA, 9, p. 1581. doi: 10.3389/fimmu.2018.01581.

Duncan, R. (2003) ‘The dawning era of polymer therapeutics’, *Nature Reviews Drug Discovery*, 2(5), pp. 347–360. doi: 10.1038/nrd1088.

de Duve, C. (1974) ‘The participation of lysosomes in the transformation of smooth muscle cells to foamy cells in the aorta of cholesterol-fed rabbits.’, *Acta cardiologica*, Suppl 20, pp. 9–25. Available at: http://www.ncbi.nlm.nih.gov/pubmed/4548625 (Accessed: 24 December 2018).

Eccleston, M. . *et al.* (2000) ‘pH-responsive pseudo-peptides for cell membrane disruption’, *Journal of Controlled Release*, 69(2), pp. 297–307. doi: 10.1016/S0168-3659(00)00316-3.

Eccleston, M. E. *et al.* (2005) ‘Design and In-vitro Testing of Effective Poly(l-Lysine Iso-Phthalamide) Based Drug Targeting Systems for Solid Tumours’, *Food and Bioproducts Processing*. Elsevier, 83(2), pp. 141–146. doi: 10.1205/fbp.04401.

Eccleston, M. E., Slater, N. K. H. and Tighe, B. J. (1999) ‘Synthetic routes to responsive polymers; Co-polycondensation of tri-functional amino acids with diacylchlorides’, *Reactive and Functional Polymers*. doi: 10.1016/S1381-5148(98)00073-X.

Forrest, M. L. and Pack, D. W. (2002) ‘On the kinetics of polyplex endocytic trafficking: implications for gene delivery vector design.’, *Molecular therapy : the journal of the American Society of Gene Therapy*, 6(1), pp. 57–66. Available at: http://www.ncbi.nlm.nih.gov/pubmed/12095304 (Accessed: 24 December 2018).

Freskgaard, P.-O. *et al.* (1994) ‘Assignment of the Contribution of the Tryptophan Residues to the Circular Dichroism Spectrum of Human Carbonic Anhydrase II’, *Biochemistry*. American Chemical Society, 33(47), pp. 14281–14288. doi: 10.1021/bi00251a041.

Fyles, T. M. *et al.* (2001) ‘Membrane Activity of Isophthalic Acid Derivatives: Ion Channel Formation by a Low Molecular Weight Compound’. American Chemical Society. doi: 10.1021/LA0105937.

Galmes, A. *et al.* (2007) ‘Long-term hematological reconstitution and clinical evaluation of autologous peripheral blood stem cell transplantation after cryopreservation of cells with 5% and 10% dimethylsulfoxide at -80 degrees C in a mechanical freezer.’, *Haematologica*. Haematologica, 92(7), pp. 986–9. doi: 10.3324/haematol.11060.

Graille, M. *et al.* (2000) ‘Crystal structure of a Staphylococcus aureus protein A domain complexed with the Fab fragment of a human IgM antibody: structural basis for recognition of B-cell receptors and superantigen activity.’, *Proceedings of the National Academy of Sciences of the United States of America*, 97(10), pp. 5399–404. Available at: http://www.ncbi.nlm.nih.gov/pubmed/10805799 (Accessed: 24 December 2018).

Greenfield, N. J. (2006) ‘Using circular dichroism collected as a function of temperature to determine the thermodynamics of protein unfolding and binding interactions’. doi:

10.1038/nprot.2006.204.

Hammouda, B. (1995) ‘A TUTORIAL ON SMALL-ANGLE NEUTRON SCATTERING FROM POLYMERS’. Available at: https://www.ncnr.nist.gov/programs/sans/pdf/polymer_tut.pdf (Accessed: 24 March 2017).

Han, S. *et al.* (2007) ‘Novel cationic cholesterol derivative-based liposomes for serum-enhanced delivery of siRNA’, *International Journal of Pharmaceutics*, 353(1–2), pp. 260–9. doi: 10.1016/j.ijpharm.2007.11.026.

Hapala, I. (1997) ‘Breaking the Barrier: Methods for Reversible Permeabilization of Cellular Membranes’, *Critical Reviews in Biotechnology*, 17(2), pp. 105–122. doi: 10.3109/07388559709146609.

Haslam, E. (1980) ‘Recent developments in methods for the esterification and protection of the carboxyl group’, *Tetrahedron*. Pergamon, 36(17), pp. 2409–2433. doi: 10.1016/0040-4020(80)80219-5.

Hein, J. E. and Blackmond, D. G. (2012) ‘On the Origin of Single Chirality of Amino Acids and Sugars in Biogenesis’, *Accounts of chemical research*, 45(12), pp. 2045–2054. doi: 10.1021/ar200316n.

Helmreich, E. J. M. (2002) ‘Environmental influences on signal transduction through membranes: a retrospective mini-review’, *Biophysical Chemistry*, 100(1), pp. 519–534. doi: 10.1016/S0301-4622(02)00303-4.

Herod, A. A. *et al.* (2000) ‘Size Exclusion Chromatography of Soots and Coal-Derived Materials with 1-Methyl-2-pyrrolidinone as Eluent: Observations on High Molecular Mass Material’. American Chemical Society. doi: 10.1021/EF000023Z.

Holthuis, J. C. M. and Menon, A. K. (2014) ‘Lipid landscapes and pipelines in membrane homeostasis’, *Nature*, 510(7503), pp. 48–57. doi: 10.1038/nature13474.

Hooper, N. M. (1999) ‘Detergent-insoluble glycosphingolipid/cholesterol-rich membrane domains, lipid rafts and caveolae (review).’, *Molecular membrane biology*, 16(2), pp. 145–56. Available at: http://www.ncbi.nlm.nih.gov/pubmed/10417979 (Accessed: 24 December 2018).

Jahnukainen, K. *et al.* (2007) ‘Effect of cold storage and cryopreservation of immature non-human primate testicular tissue on spermatogonial stem cell potential in xenografts.’, *Human reproduction (Oxford, England)*. Oxford University Press, 22(4), pp. 1060–7. doi: 10.1093/humrep/del471.

Johnson, R. N., Kopečková, P. and Kopeček, J. (2009) ‘Synthesis and Evaluation of Multivalent Branched HPMA Copolymer−Fab′ Conjugates Targeted to the B-Cell Antigen CD20’, *Bioconjugate Chemistry*, 20(1), pp. 129–137. doi: 10.1021/bc800351m.

Johnson, R. N., Kopečková, P. and Kopeček, J. (2012) ‘Biological activity of anti-CD20 multivalent HPMA copolymer-Fab’ conjugates.’, *Biomacromolecules*. NIH Public Access, 13(3), pp. 727–35. doi: 10.1021/bm201656k.

Jones, A. T., Gumbleton, M. and Duncan, R. (2003) ‘Understanding endocytic pathways and intracellular trafficking: a prerequisite for effective design of advanced drug delivery systems’, *Advanced Drug Delivery Reviews*, 55(11), pp. 1353–1357. doi: 10.1016/j.addr.2003.07.002.

Jones, K. S. (2008) ‘Effects of biomaterial-induced inflammation on fibrosis and rejection’, *Seminars in Immunology*. Academic Press, 20(2), pp. 130–136. doi:

10.1016/J.SMIM.2007.11.005.

Karande, P. *et al.* (2005) 'Design principles of chemical penetration enhancers for transdermal drug delivery', *Proceedings of the National Academy of Sciences*, 102(13), pp. 4688–4693. doi: 10.1073/pnas.0501176102.

Kelly, S. M., Jess, T. J. and Price, N. C. (2005) 'How to study proteins by circular dichroism'. doi: 10.1016/j.bbapap.2005.06.005.

Kelly, S. M. and Price, N. C. (2000) 'The Use of Circular Dichroism in the Investigation of Protein Structure and Function', *Current Protein and Peptide Science*, 1, pp. 349–384. Available at: http://ctrstbio.org.uic.edu/manuals/kelly.pdf (Accessed: 7 March 2018).

Kessler, S. W. (1975) 'Rapid isolation of antigens from cells with a staphylococcal protein A-antibody adsorbent: parameters of the interaction of antibody-antigen complexes with protein A.', *Journal of immunology (Baltimore, Md. : 1950)*. American Association of Immunologists, 115(6), pp. 1617–24. Available at: http://www.ncbi.nlm.nih.gov/pubmed/1102604 (Accessed: 24 July 2019).

Khormaee, S. (2009) *The use of a biopolymer for mammalian cell membrane encapsulation and cryopreservation*. University of Cambridge.

Khormaee, S. *et al.* (2010) 'The Influence of Aromatic Side-Chains on the Aqueous Properties of pH-Sensitive Poly(L-lysine iso-phthalamide) Derivatives', *Journal of Biomaterials Science, Polymer Edition*. Taylor & Francis Group , 21(12), pp. 1573–1588. doi: 10.1163/092050609X12519805626194.

Khormaee, S. *et al.* (2013) 'Endosomolytic anionic polymer for the cytoplasmic delivery of siRNAs in localized in vivo applications', *Advanced Functional Materials*. doi: 10.1002/adfm.201201945.

Kline, S. R. (2006) 'Reduction and analysis of SANS and USANS data using IGOR Pro', *Journal of Applied Crystallography*. International Union of Crystallography, 39(6), pp. 895–900. doi: 10.1107/S0021889806035059.

Kopeček, J. (2013) 'Polymer–drug conjugates: Origins, progress to date and future directions', *Advanced Drug Delivery Reviews*, 65(1), pp. 49–59. doi: 10.1016/j.addr.2012.10.014.

Korzh, V. and Strähle, U. (2002) 'Marshall Barber and the century of microinjection: from cloning of bacteria to cloning of everything', *Differentiation*. Elsevier, 70(6), pp. 221–226. doi: 10.1046/J.1432-0436.2002.700601.X.

Kroeze, W. K., Sheffler, D. J. and Roth, B. L. (2003) 'G-protein-coupled receptors at a glance.', *Journal of cell science*. The Company of Biologists Ltd, 116(Pt 24), pp. 4867–9. doi: 10.1242/jcs.00902.

Kumaki, J., Sakurai, S. and Yashima, E. (2009) 'Visualization of synthetic helical polymers by high-resolution atomic force microscopy', *Chemical Society Reviews*. The Royal Society of Chemistry, 38(3), p. 737. doi: 10.1039/b718433f.

Langer, R. (1998) 'Drug delivery and targeting.', *Nature*, 392(6679 Suppl), pp. 5–10. Available at: http://www.ncbi.nlm.nih.gov/pubmed/9579855 (Accessed: 24 December 2018).

Langer, R. and Tirrell, D. A. (2004) 'Designing materials for biology and medicine', *Nature*, 428(6982), pp. 487–492. doi: 10.1038/nature02388.

Langeveld-Voss, B. M. W. *et al.* (1996) 'Circular Dichroism and Circular Polarization of

Photoluminescence of Highly Ordered Poly{3,4-di[(S)-2-methylbutoxy]thiophene}'. American Chemical Society. doi: 10.1021/JA9600643.

Lau, W. L. *et al.* (2004) 'Oligomerization of Fusogenic Peptides Promotes Membrane Fusion by Enhancing Membrane Destabilization', *Biophysical Journal*, 86(1), pp. 272–284. doi: 10.1016/S0006-3495(04)74103-X.

Lee, E. S., Na, K. and Bae, Y. H. (2005) 'Doxorubicin loaded pH-sensitive polymeric micelles for reversal of resistant MCF-7 tumor', *Journal of Controlled Release*. Elsevier, 103(2), pp. 405–418. doi: 10.1016/J.JCONREL.2004.12.018.

Leite, P. E. C., Pereira, M. R. and Granjeiro, J. M. (2015) 'Hazard effects of nanoparticles in central nervous system: Searching for biocompatible nanomaterials for drug delivery', *Toxicology in Vitro*. Pergamon, 29(7), pp. 1653–1660. doi: 10.1016/J.TIV.2015.06.023.

Li, P. *et al.* (2010) 'Evaluating the impacts of osmotic and oxidative stress on common carp (Cyprinus carpio, L.) sperm caused by cryopreservation techniques.', *Biology of reproduction*. Society for the Study of Reproduction, 83(5), pp. 852–8. doi: 10.1095/biolreprod.110.085852.

Liseth, K. *et al.* (2005) 'The viability of cryopreserved PBPC depends on the DMSO concentration and the concentration of nucleated cells in the graft.', *Cytotherapy*, 7(4), pp. 328–33. doi: 10.1080/14653240500238251.

Lu, R. Z. *et al.* (2003) 'Polymerizable Fab' antibody fragment targeted photodynamic cancer therapy in nude mice', *S.T.P. Pharma Sciences*. Editions de Sante, 13(1), pp. 69–75. Available at: https://utah.pure.elsevier.com/en/publications/polymerizable-fab-antibody-fragment-targeted-photodynamic-cancer- (Accessed: 24 December 2018).

Luo, Y., Li, W.-M. and Wang, W. (2008) 'Trehalose: Protector of antioxidant enzymes or reactive oxygen species scavenger under heat stress?', *Environmental and Experimental Botany*. Elsevier, 63(1–3), pp. 378–384. doi: 10.1016/J.ENVEXPBOT.2007.11.016.

Lv, H. *et al.* (2006) 'Toxicity of cationic lipids and cationic polymers in gene delivery', *Journal of Controlled Release*, 114(1), pp. 100–109. doi: 10.1016/j.jconrel.2006.04.014.

Lynch, A. L. *et al.* (2010) 'Biopolymer mediated trehalose uptake for enhanced erythrocyte cryosurvival', *Biomaterials*, 31(23), pp. 6096–6103. doi: 10.1016/j.biomaterials.2010.04.020.

Lynch, A. L., Chen, R. and Slater, N. K. H. (2011) 'PH-responsive polymers for trehalose loading and desiccation protection of human red blood cells', *Biomaterials*. Elsevier Ltd, 32(19), pp. 4443–4449. doi: 10.1016/j.biomaterials.2011.02.062.

Maeder, M. L. and Gersbach, C. A. (2016) 'Genome-editing Technologies for Gene and Cell Therapy', *Molecular Therapy*. Cell Press, 24(3), pp. 430–446. doi: 10.1038/MT.2016.10.

Martin, M. E. and Rice, K. G. (2007) 'Peptide-guided gene delivery', *The AAPS Journal*. Springer-Verlag, 9(1), pp. E18–E29. doi: 10.1208/aapsj0901003.

Mayor, S. and Pagano, R. E. (2007) 'Pathways of clathrin-independent endocytosis', *Nature Reviews Molecular Cell Biology*, 8(8), pp. 603–612. doi: 10.1038/nrm2216.

Mays, L. E. and Wilson, J. M. (2011) 'The Complex and Evolving Story of T cell Activation to AAV Vector-encoded Transgene Products', *Molecular Therapy*. Cell Press, 19(1), pp. 16–27. doi: 10.1038/MT.2010.250.

Meacham, J. M. *et al.* (2014) 'Physical Methods for Intracellular Delivery', *Journal of*

Laboratory Automation, 19(1), pp. 1–18. doi: 10.1177/2211068213494388.

van Meer, G., Voelker, D. R. and Feigenson, G. W. (2008) 'Membrane lipids: where they are and how they behave', *Nature Reviews Molecular Cell Biology*, 9(2), pp. 112–124. doi: 10.1038/nrm2330.

Melechko, A. V *et al.* (2003) 'Large-scale synthesis of arrays of high-aspect-ratio rigid vertically aligned carbon nanofibres', *Nanotechnology*. IOP Publishing, 14(9), pp. 1029–1035. doi: 10.1088/0957-4484/14/9/318.

Mercado, S. A. *et al.* (2016) 'The intracellular fate of an amphipathic pH-responsive polymer: Key characteristics towards drug delivery', *Materials Science and Engineering: C*, 69, pp. 1051–1057. doi: 10.1016/j.msec.2016.08.004.

Mercado, S. A. (2016) *The use of a biopolymer for mammalian cell membrane encapsulation and cryopreservation*. University of Cambridge.

Mercado, S. A. and Slater, N. K. H. (2016) 'Increased cryosurvival of osteosarcoma cells using an amphipathic pH-responsive polymer for trehalose uptake', *Cryobiology*. Academic Press, 73(2), pp. 175–180. doi: 10.1016/J.CRYOBIOL.2016.08.002.

Midoux, P. and Monsigny, M. (1999) 'Efficient Gene Transfer by Histidylated Polylysine/pDNA Complexes'. American Chemical Society. doi: 10.1021/BC9801070.

Mishra, P. K. *et al.* (2009) 'Regulation of isocyanate-induced apoptosis, oxidative stress, and inflammation in cultured human neutrophils Isocyanate-induced neutrophils apoptosis', *Cell Biol Toxicol*, 26, pp. 279–291. doi: 10.1007/s10565-009-9127-9.

Miyahara, T., Nakatsuji, H. and Sugiyama, H. (2013) 'Helical Structure and Circular Dichroism Spectra of DNA: A Theoretical Study', *The Journal of Physical Chemistry A*. American Chemical Society, 117(1), pp. 42–55. doi: 10.1021/jp3085556.

Mondal Roy, S. and Sarkar, M. (2011) 'Membrane fusion induced by small molecules and ions.', *Journal of lipids*. Hindawi Publishing Corporation, 2011, p. 528784. doi: 10.1155/2011/528784.

Montixi, C. *et al.* (1998) 'Engagement of T cell receptor triggers its recruitment to low-density detergent-insoluble membrane domains', *The EMBO Journal*. John Wiley & Sons, Ltd, 17(18), pp. 5334–5348. doi: 10.1093/emboj/17.18.5334.

Mousavi, S. A. *et al.* (2004) 'Clathrin-dependent endocytosis.', *The Biochemical journal*, 377(Pt 1), pp. 1–16. doi: 10.1042/BJ20031000.

Mukherjee, S., Ghosh, R. N. and Maxfield, F. R. (1997) 'Endocytosis', *Physiological Reviews*, 77(3), pp. 759–803. doi: 10.1152/physrev.1997.77.3.759.

Mura, S., Nicolas, J. and Couvreur, P. (2013) 'Stimuli-responsive nanocarriers for drug delivery', *Nature Publishing Group*, 12. doi: 10.1038/NMAT3776.

Nakano, T. and Okamoto, Y. (2001) 'Synthetic Helical Polymers: Conformation and Function'. doi: 10.1021/cr0000978.

Neises, B. and Steglich, W. (1978) 'Simple Method for the Esterification of Carboxylic Acids', *Angewandte Chemie International Edition in English*. Hüthig & Wepf Verlag, 17(7), pp. 522–524. doi: 10.1002/anie.197805221.

Nguyen, L. A., He, H. and Pham-Huy, C. (2006) 'Chiral drugs: an overview.', *International journal of biomedical science : IJBS*. Master Publishing Group, 2(2), pp. 85–100. Available at: http://www.ncbi.nlm.nih.gov/pubmed/23674971 (Accessed: 19 December 2018).

Packer, J. E., Slater, T. F. and Willson, R. L. (1979) 'Direct observation of a free radical interaction between vitamin E and vitamin C', *Nature*. Nature Publishing Group, 278(5706), pp. 737–738. doi: 10.1038/278737a0.

Pasternack, R. F. (2003) 'Circular dichroism and the interactions of water soluble porphyrins with DNA?A minireview', *Chirality*. Wiley Subscription Services, Inc., A Wiley Company, 15(4), pp. 329–332. doi: 10.1002/chir.10206.

Penfold, J. and Thomas, R. K. (2014) 'Neutron reflectivity and small angle neutron scattering: An introduction and perspective on recent progress', *Current Opinion in Colloid & Interface Science*. Elsevier, 19(3), pp. 198–206. doi: 10.1016/J.COCIS.2014.01.002.

Pralle, A. *et al.* (2000) 'Sphingolipid–Cholesterol Rafts Diffuse as Small Entities in the Plasma Membrane of Mammalian Cells', *The Journal of Cell Biology*. Rockefeller University Press, 148(5), pp. 997–1008. doi: 10.1083/jcb.148.5.997.

Ram-Liebig, G. *et al.* (2015) 'Regulatory challenges for autologous tissue engineered products on their way from bench to bedside in Europe', *Advanced Drug Delivery Reviews*. BioMed Central, 82–83(3), pp. 181–191. doi: 10.1016/j.addr.2014.11.009.

Redmann, S. M. and Rhodes, W. (1979) 'Circular dichroism of helical polynucleotides calculated by the linear response method', *Biopolymers*. Wiley Subscription Services, Inc., A Wiley Company, 18(2), pp. 393–409. doi: 10.1002/bip.1979.360180215.

Resh, M. D. (1999) 'Fatty acylation of proteins: new insights into membrane targeting of myristoylated and palmitoylated proteins.', *Biochimica et biophysica acta*, 1451(1), pp. 1–16. Available at: http://www.ncbi.nlm.nih.gov/pubmed/10446384 (Accessed: 24 December 2018).

Richard, J. P. *et al.* (2003) 'Cell-penetrating peptides. A reevaluation of the mechanism of cellular uptake.', *The Journal of biological chemistry*. American Society for Biochemistry and Molecular Biology, 278(1), pp. 585–90. doi: 10.1074/jbc.M209548200.

Rietveld, A. *et al.* (1999) 'Association of sterol- and glycosylphosphatidylinositol-linked proteins with Drosophila raft lipid microdomains.', *The Journal of biological chemistry*, 274(17), pp. 12049–54. Available at: http://www.ncbi.nlm.nih.gov/pubmed/10207028 (Accessed: 24 December 2018).

Roy, A.-M. M. *et al.* (2000) 'Early Stages of Influenza Virus Entry into Mv-1 Lung Cells: Involvement of Dynamin', *Virology*, 267(1), pp. 17–28. doi: 10.1006/viro.1999.0109.

Rudolph, A. S. and Crowe, J. H. (1985) 'Membrane Stabilization during Freezing: The Role of Two Natural Cryoprotectants, Trehalose and Proline', *Cryobiology*, 22, pp. 367–377.

Rust, M. J. *et al.* (2004) 'Assembly of endocytic machinery around individual influenza viruses during viral entry', *Nature Structural & Molecular Biology*, 11(6), pp. 567–573. doi: 10.1038/nsmb769.

Sampaio, J. L. *et al.* (2011) 'Membrane lipidome of an epithelial cell line', *Proceedings of the National Academy of Sciences*, 108(5), pp. 1903–1907. doi: 10.1073/pnas.1019267108.

Seeman, P., Cheng, D. and Iles, G. H. (1973) 'Structure of membrane Holes in Osmotic and Saponin Hemolysis', *The Journal of Cell Biology*, 56(2). Available at: http://jcb.rupress.org/content/56/2/519.long (Accessed: 25 June 2017).

Sengupta, D. *et al.* (2008) 'Toroidal pores formed by antimicrobial peptides show

significant disorder', *Biochimica et Biophysica Acta (BBA) - Biomembranes*. Elsevier, 1778(10), pp. 2308–2317. doi: 10.1016/J.BBAMEM.2008.06.007.

Shalek, A. K. *et al.* (2010) 'Vertical silicon nanowires as a universal platform for delivering biomolecules into living cells', *Proceedings of the National Academy of Sciences*, 107(5), pp. 1870–1875. doi: 10.1073/pnas.0909350107.

Shiah, J. G. *et al.* (2001) 'Combination chemotherapy and photodynamic therapy of targetable N-(2-hydroxypropyl)methacrylamide copolymer-doxorubicin/mesochlorin e(6)-OV-TL 16 antibody immunoconjugates.', *Journal of controlled release : official journal of the Controlled Release Society*, 74(1–3), pp. 249–53. Available at: http://www.ncbi.nlm.nih.gov/pubmed/11489502 (Accessed: 24 December 2018).

Singer, S.J.; Nicolson, G. L. (1972) 'The Fluid Mosaic Model of the Structure of Cell Membranes', *Science*, 175(4023), pp. 720–731. Available at: https://idiscover.lib.cam.ac.uk/primo-explore/fulldisplay?docid=TN_jstor_archive_231733071&context=PC&vid=44CAM_PROD&lang=en_US&search_scope=default_scope&adaptor=primo_central_multiple_fe&tab=default_tab&query=any,contains,The fluid mosaic model of the s (Accessed: 30 June 2019).

Singh, R. D. *et al.* (2003) 'Selective Caveolin-1–dependent Endocytosis of Glycosphingolipids', *Molecular Biology of the Cell*, 14(8), pp. 3254–3265. doi: 10.1091/mbc.e02-12-0809.

Spector, A. A. and Yorek, M. A. (1985) 'Membrane lipid composition and cellular function', *Journal of Lipid Research*, 26, pp. 1015–1035.

Stewart, M. P., Langer, R. and Jensen, K. F. (2018) 'Intracellular Delivery by Membrane Disruption: Mechanisms, Strategies, and Concepts', *Chemical Reviews*. American Chemical Society, 118(16), pp. 7409–7531. doi: 10.1021/acs.chemrev.7b00678.

Subbarao, N. K. *et al.* (1987) 'The pH-dependent bilayer destabilization by an amphipathic peptide', *Biochemistry*. American Chemical Society, 26(11), pp. 2964–2972. doi: 10.1021/bi00385a002.

Sun, D., Forsman, J. and Woodward, C. E. (2015) 'Current Understanding of the Mechanisms by which Membrane-Active Peptides Permeate and Disrupt Model Lipid Membranes.', *Current topics in medicinal chemistry*, 16(2), pp. 170–86. Available at: http://www.ncbi.nlm.nih.gov/pubmed/26265353 (Accessed: 11 December 2018).

Swanson, J. A. (2008) 'Shaping cups into phagosomes and macropinosomes', *Nature Reviews Molecular Cell Biology*, 9(8), pp. 639–649. doi: 10.1038/nrm2447.

Swierczewska, M., Lee, K. C. and Lee, S. (2015) 'What is the future of PEGylated therapies?', *Expert Opinion on Emerging Drugs*. Taylor & Francis, 20(4), pp. 531–536. doi: 10.1517/14728214.2015.1113254.

Tampo, Y. *et al.* (2003) 'Oxidative Stress–Induced Iron Signaling Is Responsible for Peroxide-Dependent Oxidation of Dichlorodihydrofluorescein in Endothelial Cells', *Circulation Research*, 92(1).

Tappel, A. L. (1962) 'Vitamin E as the Biological Lipid Antioxidant', in *Vitamins & Hormones*, pp. 493–510. doi: 10.1016/S0083-6729(08)60732-3.

Tatone, C. *et al.* (2010) 'Cryopreservation and oxidative stress in reproductive cells', *Gynecological Endocrinology*. Taylor & Francis, 26(8), pp. 563–567. doi: 10.3109/09513591003686395.

Timothy E. McKnight, *,†,‡,§ *et al.* (2004) ‘Tracking Gene Expression after DNA Delivery Using Spatially Indexed Nanofiber Arrays’. American Chemical Society . doi: 10.1021/NL049504B.

Van Tonder, A., Joubert, A. M. and Cromarty, A. D. (2015) ‘Limitations of the 3-(4,5-dimethylthiazol-2-yl)-2,5-diphenyl-2H-tetrazolium bromide (MTT) assay when compared to three commonly used cell enumeration assays’, *BMC Research Notes*, 8(47). doi: 10.1186/s13104-015-1000-8.

Tortora, G. J. and Nielsen, M. T. (Mark T. (2012) *Principles of human anatomy*. John Wiley & Sons.

Varga, C. M. *et al.* (2005) ‘Quantitative comparison of polyethylenimine formulations and adenoviral vectors in terms of intracellular gene delivery processes’, *Gene Therapy*, 12(13), pp. 1023–1032. doi: 10.1038/sj.gt.3302495.

Villalobos, A. *et al.* (2006) ‘Gene Designer: a synthetic biology tool for constructing artificial DNA segments’, *BMC Bioinformatics 2006 7:1*. BioMed Central, 7(1), p. 285. doi: 10.1186/1471-2105-7-285.

Vistica, D. T. *et al.* (1991) ‘Tetrazolium-based Assays for Cellular Viability: A Critical Examination of Selected Parameters Affecting Formazan Production’, *Cancer Research*, 51(10). Available at: http://cancerres.aacrjournals.org/content/51/10/2515.short (Accessed: 24 August 2017).

Wang, H. H. *et al.* (2009) ‘Programming cells by multiplex genome engineering and accelerated evolution’, *Nature*. Nature Publishing Group, 460(7257), pp. 894–898. doi: 10.1038/nature08187.

Wang, M. *et al.* (2017) ‘Left or Right: How Does Amino Acid Chirality Affect the Handedness of Nanostructures Self-Assembled from Short Amphiphilic Peptides?’, *Journal of the American Chemical Society*. American Chemical Society, 139(11), pp. 4185–4194. doi: 10.1021/jacs.7b00847.

Weinberger, A. *et al.* (2013) ‘Gel-Assisted Formation of Giant Unilamellar Vesicles’, *Biophysical Journal*, 105(1), pp. 154–164. doi: 10.1016/j.bpj.2013.05.024.

Weis, W. *et al.* (1988) ‘Structure of the influenza virus haemagglutinin complexed with its receptor, sialic acid’, *Nature*, 333(6172), pp. 426–431. doi: 10.1038/333426a0.

White, J., Helenius, A. and Gething, M. J. (1982) ‘Haemagglutinin of influenza virus expressed from a cloned gene promotes membrane fusion.’, *Nature*, 300(5893), pp. 658–9. Available at: http://www.ncbi.nlm.nih.gov/pubmed/6815542 (Accessed: 3 December 2018).

Wilczewska, A. Z. *et al.* (2012) ‘Nanoparticles as drug delivery systems’, *Pharmacological Reports*. BioMed Central, 64(5), pp. 1020–1037. doi: 10.1016/S1734-1140(12)70901-5.

Williams, D. F. (1999) *Williams Dictionary of Biomaterials*. Liverpool University Press.

Williams, D. F. (2014) *The Williams Dictionary of Biomaterials*. Ebsco Publishing.

Wolkers, W. F. *et al.* (2001) ‘Human Platelets Loaded with Trehalose Survive Freeze-Drying’, *Cryobiology*, 42(2), pp. 79–87. doi: 10.1006/cryo.2001.2306.

Wu, C. *et al.* (2017) ‘Co-delivery of multiple drug resistance inhibitors by polymer/inorganic hybrid nanoparticles to effectively reverse cancer drug resistance’, *Colloids and Surfaces B: Biointerfaces*, 149, pp. 250–259. doi: 10.1016/j.colsurfb.2016.10.029.

Yang, J. and Kopeček, J. (2017) ‘The Light at the End of the Tunnel-Second Generation HPMA Conjugates for Cancer Treatment.’, *Current opinion in colloid & interface science*. NIH Public Access, 31, pp. 30–42. doi: 10.1016/j.cocis.2017.07.003.

Yashima, E. *et al.* (2009) ‘Helical Polymers: Synthesis, Structures, and Functions’, *Chem. Rev.*, 109, pp. 6102–6211. Available at: http://pubs.acs.org/doi/pdf/10.1021/cr900162q (Accessed: 13 July 2017).

Yashima, E. (2010) ‘Synthesis and structure determination of helical polymers’, *Polymer Journal*. Nature Publishing Group, 42(1), pp. 3–16. doi: 10.1038/pj.2009.314.

Yashima, E. and and Katsuhiro, M. (2007) ‘Chirality-Responsive Helical Polymers’. American Chemical Society. doi: 10.1021/MA071453S.

Yue, Y. *et al.* (2011) ‘Revisit complexation between DNA and polyethylenimine — Effect of uncomplexed chains free in the solution mixture on gene transfection’, *Journal of Controlled Release*. Elsevier, 155(1), pp. 67–76. doi: 10.1016/J.JCONREL.2010.10.028.

Yue, Z., Eccleston, M. E. and Slater, N. K. H. (2005) ‘Modulation of the pH-responsive properties of poly(l-lysine iso-phthalamide) grafted with a poly(ethylene glycol) analogue’, *Biomaterials*. Elsevier, 26(32), pp. 6357–6366. doi: 10.1016/J.BIOMATERIALS.2005.03.035.

Zasloff, M. (2002) ‘Antimicrobial peptides of multicellular organisms’, *Nature*, 415(6870), pp. 389–395. doi: 10.1038/415389a.

Zhang, D. *et al.* (2015) ‘ROS-induced oxidative stress and apoptosis-like event directly affect the cell viability of cryopreserved embryogenic callus in Agapanthus praecox’, *Plant Cell Reports*, 34(9), pp. 1499–1513. doi: 10.1007/s00299-015-1802-0.

Zhang, H. and Deng, J. (2016) ‘Helical Polymers Showing Inverse Helicity and Synergistic Effect in Chiral Catalysis: Catalytic Functionality Determining Enantioconfiguration and Helical Frameworks Providing Asymmetric Microenvironment’, *Macromolecular Chemistry and Physics*, 217(7), pp. 880–888. doi: 10.1002/macp.201500522.

Zheng, L. *et al.* (2015) ‘Fumarate induces redox-dependent senescence by modifying glutathione metabolism’, *Nature Communications*, 6. doi: 10.1038/ncomms7001.